UC Berkeley
UC Berkeley Electronic Theses and Dissertations

Title

Dynamics of Coordination Complexes in Ground and Excited States

Permalink

https://escholarship.org/uc/item/8cv0j414

Author

Hill, Adam Doherty

Publication Date

2013

Peer reviewed|Thesis/dissertation

Dynamics of Coordination Complexes in Ground and Excited States

By

Adam Doherty Hill

A dissertation submitted in partial satisfaction of the

requirements for the degree of

Doctor of Philosophy

in

Chemistry

in the

Graduate Division

of the

University of California, Berkeley

Committee in charge:

Professor Charles B. Harris, Chair
Professor Phillip L. Geissler
Professor Robert W. Dibble

Spring 2013

Dynamics of Coordination Complexes in Ground and Excited States

Copyright © 2013

by

Adam Doherty Hill

Abstract

Dynamics of Coordination Complexes in Ground and Excited States

by

Adam Doherty Hill

Doctor of Philosophy in Chemistry

University of California, Berkeley

Professor Charles B. Harris, Chair

Metal coordination complexes represent the chief reusable tools of chemical transformation. Their flexibility and controllability are responsible for the success of numerous fields, from production of feedstock chemicals to medicine to solar energy conversion. Here, several aspects of the behavior of coordination complexes are explored, including the relationship between ligand design and spectroscopic properties. First, the mechanism of vibrational population transfer in trincarbonyl(η^4-diene)iron "piano stool" complexes is explored via temperature-dependent 2D-IR spectroscopy and density functional theory (DFT). The "wagging" motion of the carbonyl ligands is characterized, differentiating it from chemical exchange. Second, the structure and energy of hydroxypyridinone-based (HOPO) MRI contrast agents were explored via DFT. This understanding of medicinal metals could allow for directed synthesis of promising future contrast agent candidates. Finally, the dynamics of electronically excited cobalt-zirconium heterobimetallic complexes were investigated with time-resolved IR spectroscopy and DFT. A short-lived singlet metal-to-metal charge transfer state was characterized that mitigated the original goal of the complex: catalytic CO_2 reduction chemistry. Together, these experiments expand the knowledge of important coordination complex behavior in ground and excited states.

To my parents.

Table of Contents

Acknowledgements

First and foremost, I'd like to thank my advisor and P.I., Professor Charles B. Harris for his knowledge and support as I pursued my Ph.D. On even the most miserable and frustrating days, he was there to help: there was no looming problem he couldn't make evaporate. Perhaps just as importantly, he gave me the liberty to pursue the topics that entranced me most. Through Charles, I learned that good management is about support, rather than micromanagement, and that learning cannot happen if students are not free to make their own mistakes.

Dr. Piper Klemm has been a constant source of support and advice throughout my graduate career. Her brilliant business acumen and clever tactics inspired me, and taught me the true importance of networking. My knowledge of the broader world, and particularly the realm of medical and quantitative biology, would not be the same without her.

My work would never have been possible without the help of my undergraduate students, Molly Ryan and Sally Jeon. They kept me honest and, through their own educations, taught me more about being a scientist than any lecture. (And they always forgave my gaps in bio-knowledge.) Watching their steps into the wider world of science makes me enormously proud.

My favorite chemist/cryptophysicist, Brendan Abolins, was always there for me with an open mind and a tolerance of my long scientific tangents. Many a lunch was improved by his AMO knowledge and wild forays into particle physics. When it came time for a reality check, I knew there was no better source.

I also want to thank the Harris Group for their knowledge and help throughout my time at Berkeley. James Cahoon, Karma Sawyer, Jacob Schlegel, and Matt Zoerb taught me everything I know about ultrafast spectroscopy, and Son Nguyen and Justin Lomont were the best coworkers anyone could ask for. James Johns, Eric Muller, Ben Caplins, David Suich, and Alex Shearer were always ready to talk about science in two *or* three dimensions.

I would also like to thank the many other students and faculty with whom I've collaborated and discussed science in the past: Miriam Bowring, for teaching me the arcane art of air-free synthesis; Stephen Elkind and Martin Head-Gordon, for discussions on the finer points of density functional theory and transition state structures; Kenneth Raymond and his group, for the opportunity to contribute to the field of medicinal metals; and Christine Thomas and her group at Brandeis, for their knowledge and their heterobimetallic compounds.

The Berkeley Science Review's staff has made an enormous impact on the way that I communicate science to the public. The BSR also gave me the opportunity to act as the Blog Editor, where I had the opportunity to further practice both writing and leadership.

1 Introduction

The world faces an array of challenges: a looming energy crisis, environmental devastation, and threats to human health. Through chemistry, we can understand the world around us, and through chemistry we have the opportunity to solve global problems while expanding human knowledge. Chemistry has two complementary and overlapping goals: one that pursues the practical challenges of synthesizing and characterizing novel compounds, and the second that focuses on using chemical experimentation to better understand chemistry itself. In this latter school, physical chemistry has led a charge towards experimental and computational characterization of ever-more-fundamental processes and ever-more-complex systems.

The goal of the chemical spectroscopist is to make the geometry, motion, and energy of every moiety at every moment of a reaction accessible. Across many timescales and classes of compound, this goal has largely been fulfilled. The academic, then, has taken on the role of curator, studying the odd and important edge cases where chemical intuition breaks down, or where twisting simple approximations produces important results. Coordination complexes represent a class of compound in which deep understanding of fundamental behavior can lead to myriad improvements in practical applications. These metal-ligand combinations have, over a century of scientific investigation, displayed an almost fantastical capacity to shepherd chemical transformations in ways both subtle and overt. Changing the identity of a ligand or metal can achieve that "just right" reactivity and selectivity; when lanthanides or multiple metals are involved, an even broader variety of chemistry is accessible.
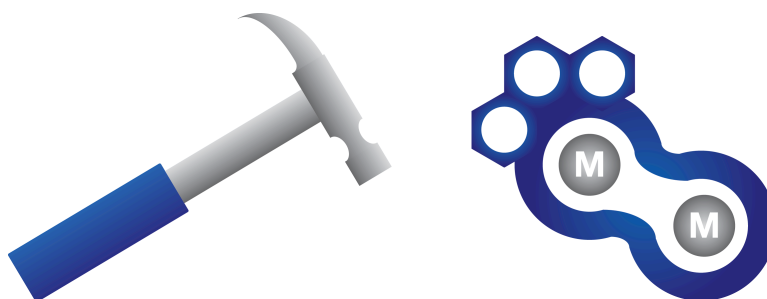

Figure 1.1 The coordination complex as molecular tool: a useful metaphor. In both, metal does the work while ligands/handles provide control.

From this basis, I draw the metaphor of coordination complex as a nanoscale tool—a central metal atom or atoms whose orbitals perform transformative chemistry, and ligand "handles" that mediate the interactions.

In studying these complexes, I invoke a tripartite experimental sequence of synthesis, analysis, and theory. Though individual components of the cycle are often the provenance of collaborative efforts, one source of the Harris group's success stems from its capacity to work successfully in each milieu.
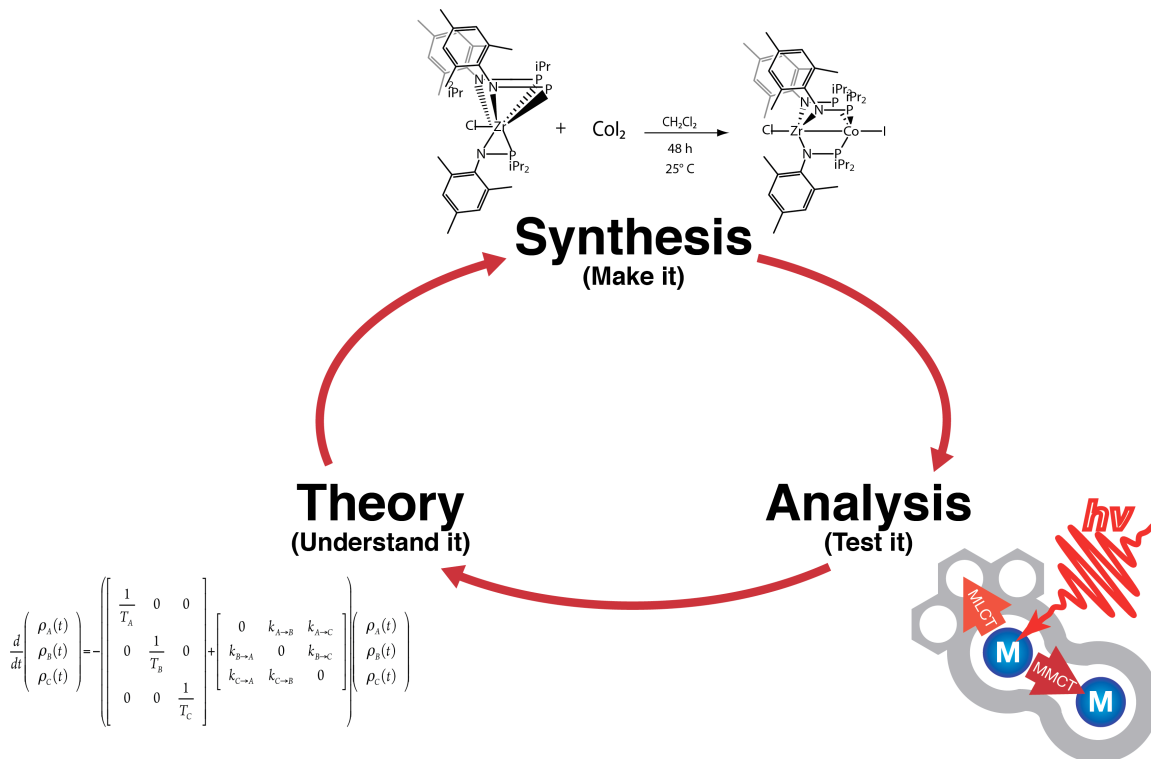
Figure 1.2   General workflow for optimizing chemical compounds.

In this thesis, I explore several aspects of the chemistry of coordination complexes using all three techniques. The capacity to directly address experimental concerns in any area offers a degree of flexibility and insight that would not be available in a more limited context. In particular, a practical and useful understanding of the computer code that is involved in running experimental apparatuses, analyzing data, and simulating dynamics has been absolutely indispensible. This work has lead to important conclusions in three distinct areas:

The fundamental motions of metal complexes with applications in catalysis remain controversial even after decades of study. The relationship of chemical motion to the interactions of vibrational states in tricarbonyl(η^4-diene)iron complexes has been significantly debated. The application of air-free synthesis, temperature-dependent 2D-IR, and density functional theory together produce a unique insight into the fundamental nature of the complexes' spectral behavior (Chapter 4). Ultimately, intramolecular vibrational redistribution coupled to the torsional motion of the carbonyl ligands is the source.

The structure of metal complexes become far more interesting in the case of lanthanide complexes, where the rich chemistry of f-orbitals produces behavior somewhat unlike that of transition metals. In particular, the high spin multiplicities of f-block elements have made them popular choices for modifying the behavior of hydrogen nuclei in magnetic fields. The practical application of this phenomenon has been found in the field of magnetic resonance imaging (MRI), where differences in pathological tissue can be diagnosed more effectively with the aid of gadolinium complexes. However, the large number of relevant electrons and the large size of the chelating moieties make high-level computations a challenge. My work is the first to use DFT to characterize contrast agents based on HOPO (hydroxypyrodinone) ligands popularized by Prof. Kenneth N. Raymond's group (Chapter 5). In particular, the previously ambiguous water coordination number was quantified.

Finally, I addressed the challenges of developing a CO_2 reduction catalyst using heterobimetallic complexes. By using multiple, heterogeneous metals, the precise reactivity of a metal complex can be selectively tuned. In collaboration with Christine Thomas's group at Brandeis University, a cobalt-zirconium catalyst candidate has been developed. Completing the catalytic cycle will require removal of a highly stable carbonyl ligand. My application of time-resolved, visible-pump, IR-probe ultrafast spectroscopy identified the metal-to-metal charge transfer state responsible for quenching the excitation and protecting the carbonyl (Chapter 6). Controlling the character of other ancillary ligands can vary the transfer of charge between metal centers.

With these studies, I have explored the behavior of several classes of coordination complexes and reaffirmed the importance of a three-fold synthesis/spectroscopy/theory approach to solving chemical problems. The results point to both the usefulness and future challenges of metal coordination complexes.

2   Background

2.1   Coordination complexes and relevant applications

Metal coordination complexes consist of a central metal atom with one or more ligands surrounding it. While the metal center typically performs the majority of the actual chemistry, the ligands provide stability, solubility, and mediation of these interactions.[1] Though coordination complexes are critical in a variety of applications, there are two fields that would look quite different without metal systems: homogeneous catalysis and medical imaging. In addition to their intrinsic use, many coordination complexes serve as effective models of more complex systems from fields like heterogeneous catalysis and bioinorganic chemistry.[2] This broad set of applications, and the catalytic nature of many metal complexes, means that small improvements in the understanding of coordination chemistry can have vast implications. As such, significant study has been devoted to understanding their behavior.
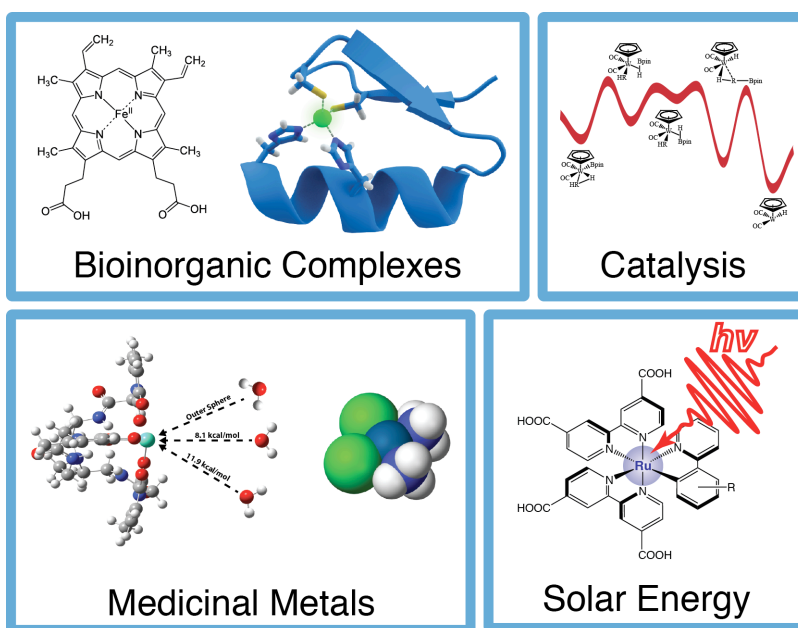
Figure 2.1   An overview of some fields in which coordination complexes play a critical role. From the chemistry of the human body to large-scale industrial processes, metal complexes fulfill integral chemistry.[3]

In their general role as catalysts, the activity of coordination complexes is cyclical. Reactant molecules bind to the metal center, the adduct undergoes some transformation reaction, and the now-modified product molecule dissociates from the metal center, returning the complex to its initial state. If this final step does not occur, the metal center is poisoned and can do no further work—the adduct becomes the final product. Though this is critical in the synthesis of new metal systems, it is anathema to catalytic processes.
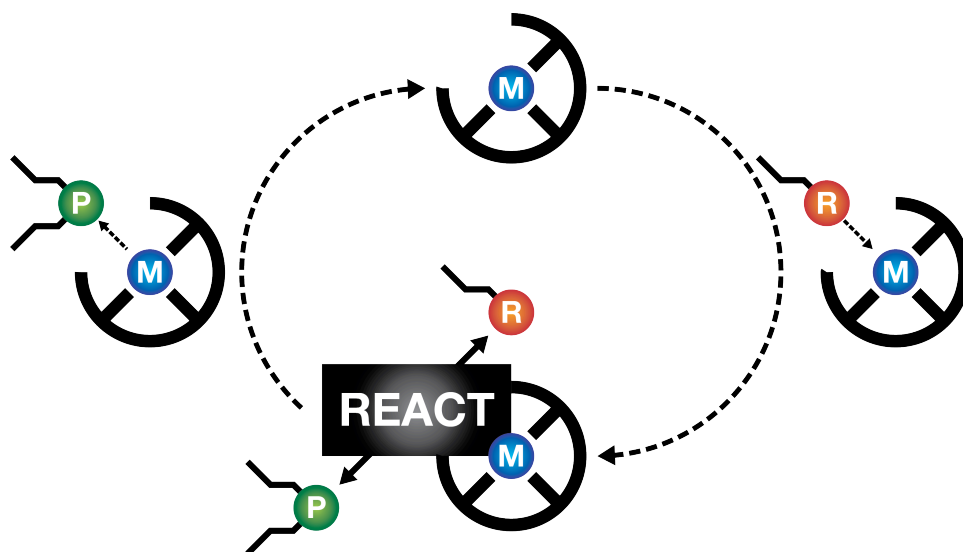
Figure 2.2 Schematic representation of a simple catalytic cycle. The catalyst forms an adduct with a guest molecule, and facilitates the transformation of that molecule. To complete the cycle, the modified guest molecule must dissociate from the center. This dissociation often occurs in concert with coordination of a new guest.

Though the kinetic rate laws that govern the complete catalytic cycle maybe be sophisticated in their functional form, the individual steps of the reaction are often simple and reasonably studied. Perhaps most critically to my own work, the transformations of the adduct are often unimolecular, and thus display simple rate laws. The reactivity of this system is controlled by the barrier to this rearrangement, as expressed in either the Eyring or Arrhenius equation:[4,5]

$$k_{Eyring} = \frac{k_B T}{h} e^{\frac{-\Delta G}{k_B T}} \qquad (2.1)$$

$$k_{Arrhenius} = A e^{\frac{-E_A}{k_B T}} \qquad (2.2)$$

This means that the rates of both the adduct's reaction, and of the subsequent dissociation of the modified guest molecule, have fairly simple dependence on

temperature of the system and the barrier heights involved. By controlling the former, the information on the later is revealed. As a physical inorganic chemist, I extract the maximum of information by investigating the relationship between timescale and barrier.
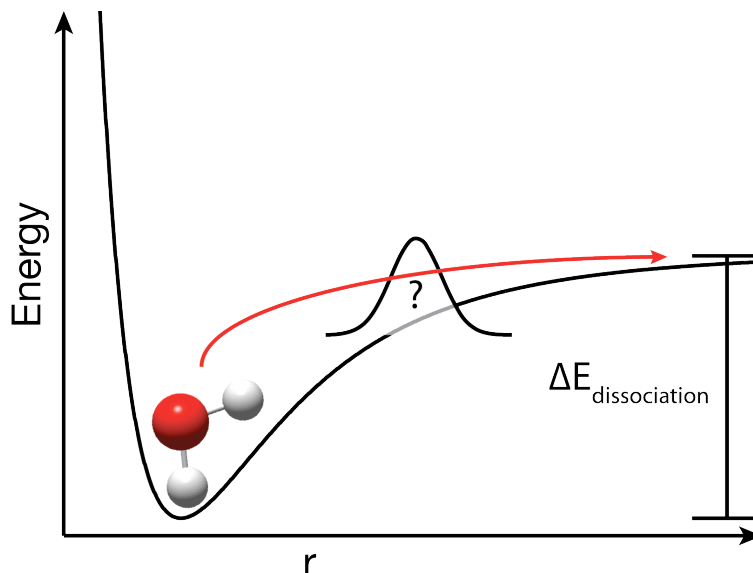
Figure 2.3   Thermal dissociation of a guest molecule from the inner sphere of a complex. There is often an effective barrier to this process in the liquid phase as a result of the solvent reorganization energy necessary to accommodate a new molecule.

2.1.1 Model coordination complexes

Over the course of my work, I have studied compounds that fall into approximately three classes. The first are so-called model reactions. These are studies of the behavior of complexes that are so simple that they do not show interesting catalytic activity, but that otherwise bear structural similarity to important catalysts. Simple intramolecular rearrangements are termed "fluxional."[1] They serve as a proving ground for future techniques that can someday be applied to more sophisticated processes.
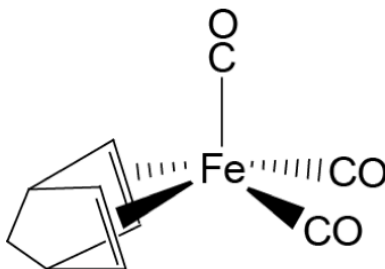
Figure 2.4 Tricarbonyl(1,5-norbornadiene)iron(0), an organometallic compound that undergoes fluxional exchange of its carbonyl ligands. This functions as a model of more complicated rearrangements.

Studying even these simple processes can present a challenge, as they occur at thermal equilibrium—thus there is no easily measured "start" point as in a photochemical or mixing experiment.[6] As I will show, two-dimensional infrared spectroscopy is a highly sensitive probe of their behavior. As discussed in chapter 4, these complexes can also occasionally pose interesting spectroscopic enigmas when their fluxional processes occur quickly enough.

2.1.2 Contrast agents for medical imaging

The model catalytic cycle (Figure 2.2) intentionally leaves the nature of the adduct's behavior ambiguous. Though catalytic chemical transformations are perhaps the most obvious use of metal complexes as "tools," there is an alternate class in which the guest is not changed chemically by its interaction, but is nonetheless modified in an important way. An obvious example is the behavior of hemoglobin, which binds and releases oxygen for the purpose of transporting it around the body.[2] This process is reversible, and would be largely impossible without the coordinated metal center, but nonetheless leaves the oxygen molecule chemically identical. The role of many metal complexes used in the clinic is similar—important, reusable, but not directly performing chemistry.

Perhaps one of the most fascinating cases of this is in the field of magnetic resonance imagine (MRI). MRI images the body in three dimensions using radio waves, and is thus far safer than imaging techniques that use ionizing radiation (e.g. CT scans). Every year, more than 22 million scans are performed in the United States alone, and 45% of those scans utilize an injectable contrast agent to provide improved or targeted imagining (Figure 2.5).[7-10]
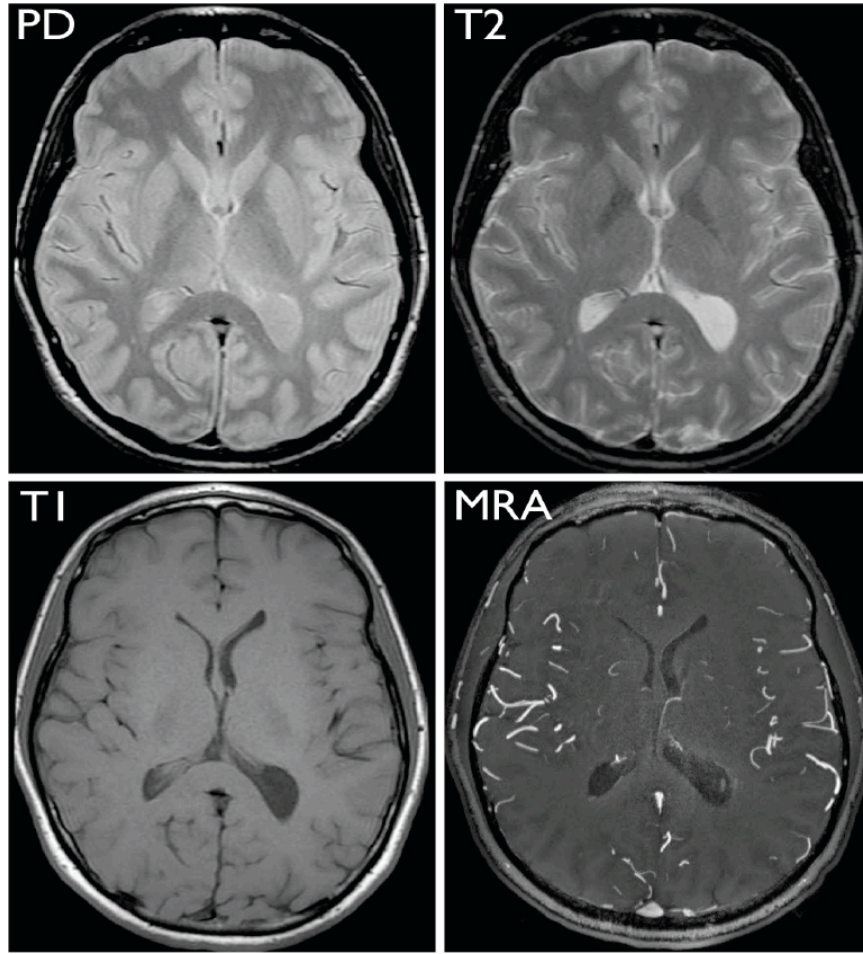
Figure 2.5 MRI scans obtained of proton density (top left), T₂ mode (top right), T₁ mode (bottom left), and magnetic resonance angiography (MRA) (bottom right).[7] Note that different types of tissue illuminated in each.

Contrast agents increase or differentiate the signal of water protons near them by changing their T₁ or T₂ relaxation times. This ability to change relaxation rates is referred to as "relaxivity," and the factors influencing it are described by the Solomon-Bloembergen-Morgan equations:[11-14]

$$(1/T_1) = qP_m[1/(T_{1m} + \tau_m)]$$

$$\frac{1}{T_{1m}} = \frac{2}{15} \frac{\gamma^2 g^2 \mu_B^2 S(S+1)}{r^6} \left[\frac{3\tau_{c1}}{(1+\omega_I^2 \tau_{c1}^2)} + \frac{7\tau_{c2}}{(1+\omega_S^2 \tau_{c2}^2)} \right]$$

$$1/\tau_{ci} = 1/\tau_R + 1/T_{ie} + 1/\tau_m \text{ with } i = 1,2$$

r_i = relaxivity (inner-sphere)	T_{im} = relaxation time of bound water
q = number of bound solvent nuclei	τ_c = correlation time
P_m = mole fraction of bound water	τ_R = rotational correlation time
τ_m = mean water residence time	T_{ie} = electronic longitudinal relaxation time

(2.3)

Many of the parameters of this equation are directly accessible and modifiable to the coordination chemist. The change in relaxation time of the bound water is proportional to the spin multiplicity of the metal center; as such, gadolinium, with its eleven unpaired electrons, is the metal of choice for the majority of commercial contrast agents.[15]
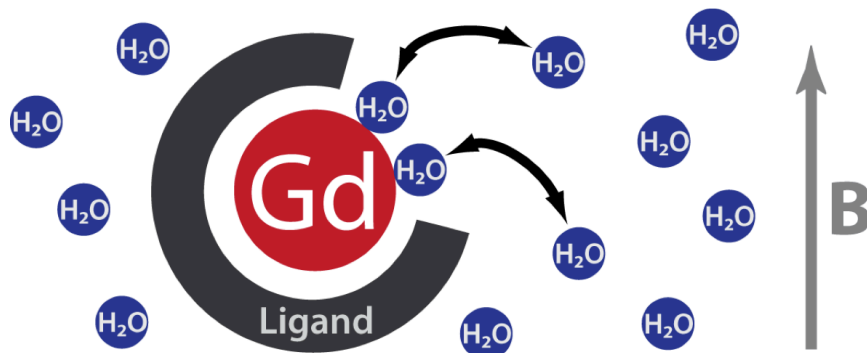
Figure 2.6 Gadolinium contrast agents operate by rapidly exchanging multiple solvent molecules between the inner coordination sphere and the bulk. When polarized by an external magnetic field, the metal center alters the relaxation timescale of protons with which it interacts.

However, the parameters typically modified to improve the relaxivity of commercial agents are the water exchange rate and the number of coordinated waters (the q value). The values can not only be determined by ^{17}O-NMR, but also predicted via structure calculations.[16-18]

Given that the majority of commercial MRI contrast agents use highly multidentate ligands (Figure 2.7) with a large number of degrees of freedom, it was previously not feasible to perform high level structure calculations to determine these values.[9,19] Molecular mechanics approaches typically yielded approximate structures and q values, but ultimately struggled to provide accurate water exchange energies that could aid in the rational design of new contrast agents. Computational advances of the past decade now mean that DFT structure optimizations are now becoming feasible. I leveraged the supercomputing power of the National Energy Research Scientific Computing center at Lawrence Berkeley National Laboratory to perform the first DFT calculations of HOPO-based oxygen donor chelators as developed by UC Berkeley's Raymond group.
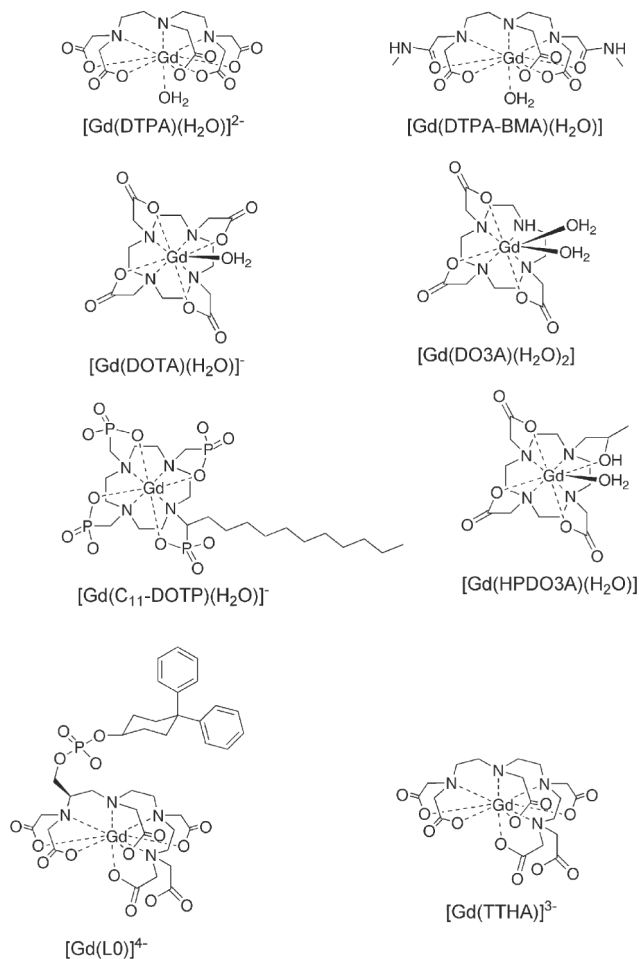
Figure 2.7 Current, commercially available gadolinium-based MRI contrast agents. Note the use of flexible, multi-dentate ligands and open sites for water exchange.[7]

The reasons for optimizing MRI contrast agents, and for the application of theoretical techniques in guiding this optimization, are several. First, there is the general goal of reducing the necessary amount of a drug that must be manufactured and injected into a patient. Second, there are concerns in certain patients with compromised renal systems that the current high doses may be dangers. Finally, the increasing field strengths of modern MRI instruments actually weakens then efficacy of current contrast agents; for them to remain relevant, they must be re-optimized for these new higher-MHz instruments.[7]

2.1.3 Catalytic systems for artificial photosynthesis

In addition to model systems and method development, I have investigated practical concerns in the development of new catalysts. Among the most pressing challenges is the development of an effective catalyst for what it termed "artificial photosynthesis."[3,20-22] Photosynthetic organisms use photons, water, and carbon dioxide to produce chemical energy in the form of sugars (as well as oxygen.) Though very efficient with low amounts of light, biological photosynthesis has low total throughput. Increasing the photosynthetic capacity of the biosphere to offset the increased carbon load and the increased fuel requirements of global industrialization would require large amounts of arable land that are simply not available.[23-25]

Instead, chemists seek a manmade equivalent. This field constitutes two parallel photochemical challenges: (1) splitting water into H_2 and O_2, and (2) splitting CO_2 into O_2 and CO. The combination of H_2 and CO is called syngas, and the engineering necessary to convert it to synthetic natural gas is well established.[3,26,27]
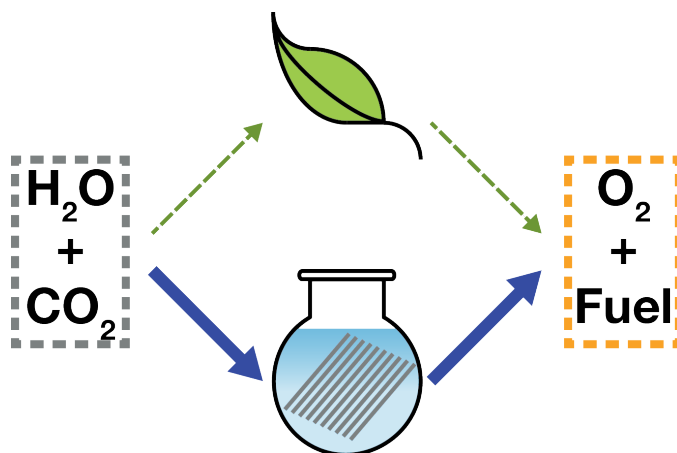
Figure 2.8 The goal of artificial photosynthesis is to replicate the behavior of plants with dramatically higher throughput.

Effective catalysts for water splitting currently exist, and the field is generally better developed. The reduction of CO_2, on the other hand, has posed a fairly large challenge. New ideas are very important here, and a variety of approaches are being considered—either as direct solutions, or as models that could be transmuted into more large-scale solutions.[28]

Many of the current successful catalysts use expensive metals—particularly ruthenium. However, the use of multiple metal centers with different reduction potentials can simulate the behavior of a single, more expensive metal. At the forefront of this heterobimetallic catalysis has been the Christine Thomas group at Brandeis University.[29-32] They have developed a series of highly durable homogenous catalysts (Figure 2.9) that can effectively split CO_2 into CO and an oxo bridge that can later be chemically altered.
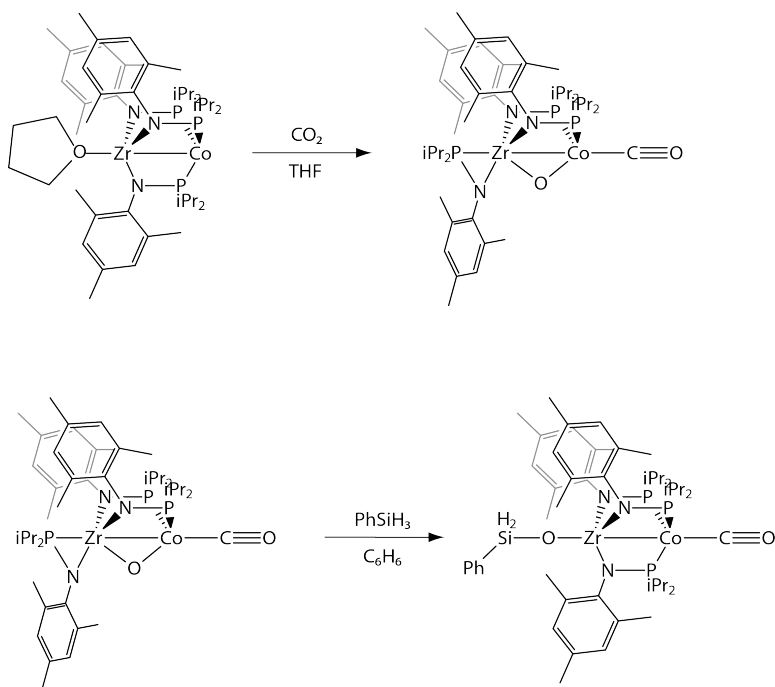
Figure 2.9 Carbon dioxide fixation can be carried out by this cobalt-zirconium complex, a potential catalyst.[31,33] However, further efforts have great difficulty removing the subsequent carbonyl ligand and completing the catalytic cycle.

However, removing the resulting carbonyl has proven extremely difficult, and the inability to do so threatens the future of this otherwise promising catalytic system. The insights presented by time-resolved IR spectroscopy can be used to reveal the underlying behavior hampering further reactivity.

2.2 Ultrafast spectroscopy

In the past twenty years, the advent of titanium-doped sapphire lasers and ultrafast spectroscopy has revealed previously unreachable timescales—down to the most fundamental motions of nuclei. Just as with the various pulses used in NMR spectroscopy to examine varieties of coupling between nuclei, photons at other frequencies can also be used to determine the time dynamics of chemical processes.[34,35]

Though a variety of pulse sequences and geometries can be used, all experiments in the Harris group are so-called "pump-probe" experiments (Figure 2.10). In these experiments, an initial pulse of light (the "pump") tags an ensemble of molecules—either by exciting vibrations, or initiating some photochemistry. After a waiting time (T_w), the state of the system is interrogated via a "probe" pulse. By varying the waiting time, a "molecular movie" can be produced that details the evolution of the system.[35-37]
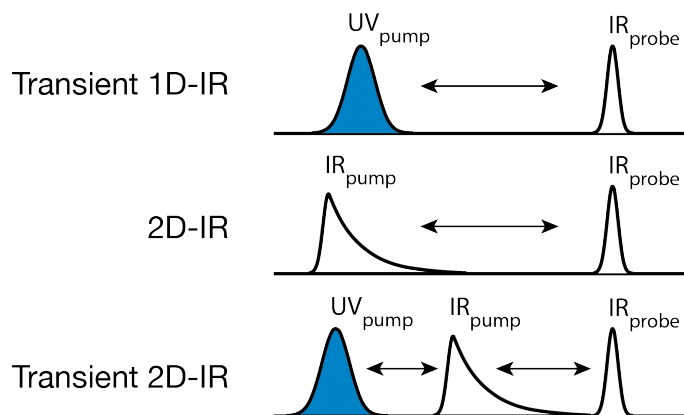
Figure 2.10 The instrument can produce a variety of relevant pump/probe pulse sequences, each of which reveals different information about the behavior of the system in solution.

However, the majority of the molecules will be left unchanged by the initial pulse; to study only those in the ensemble that have been influenced by the pump pulse, we subtract the spectrum of the pumped molecules from that of the unpumped.[38]

$$\Delta A = A_{pumped} - A_{unpumped} \qquad\qquad (2.4)$$

The resulting spectrum is called a difference spectrum. Unlike linear spectra produced by common laboratory spectrophotometers, a difference spectrum has both positive and negative peaks (Figure 2.11). The negative peaks, called bleaches, correspond to species whose concentration has been reduced as a result of the pump pulse. Positive product peaks correspond to enhanced species. In complicated spectra, it is often possible to compare the growth and decay of bleach and product peaks to determine the progression of multiple states through time.[39,40]
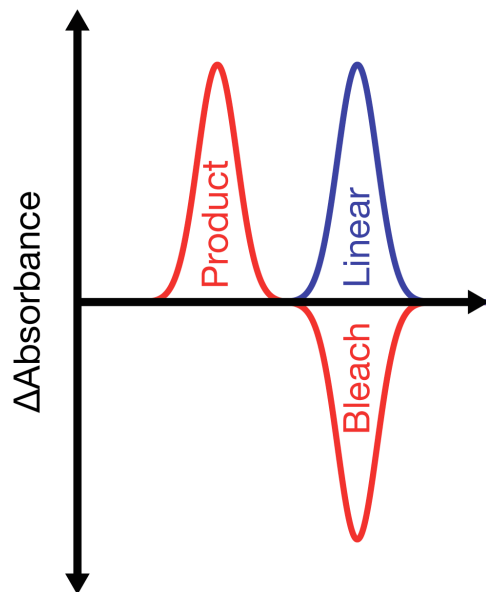
Figure 2.11 Comparison of a transient absorption spectrum (red) and a linear spectrum (blue) for a species. Note the parent bleach at the location of the original absorption, as well as the presence of a product peak at a new frequency.

The resulting spectrum records only the higher-order responses of the system.[41] This utility means that the applications of ultrafast difference spectroscopy are broad and range across a variety of fields. Depending on the sorts of rotations, vibrations, electronic excitations, or core ionizations to be studied, a variety of light frequencies are leveraged. Transient ultraviolet and visible spectroscopy has long been an excellent choice to achieve a basic understanding of the photophysics of a species, but ultimately is hampered by broad absorptions that cannot always be differentiated.[42] Identifying and separating states can be challenging. X-ray techniques can provide a higher degree of specificity, but require X-ray sources that, as of the early 21st century, are not yet available on the tabletop with sufficient photon fluxes to facilitate the study of third-order processes routinely.[43,44] By combining the necessary time resolution (far faster than NMR) and specificity (far more sensitive than transient absorption), IR probe experiments provide an invaluable tool in probing the kinetics and dynamics of metal complexes.

2.3   Vibrational spectroscopy

The development of multipass optimal parametric amplifiers has made routine generation of low-noise mid-infrared light facile. This light is superb for use in ultrafast experiments for several reasons. From a practical standpoint, it resides in a "window" in the atmosphere free of interference from common gases, including CO_2 and H_2O; as a result, experiments can be performed at ambient conditions without the need to purge the area around the instrument.[45] From a molecular standpoint, mid-IR light exists in a region where only molecular

vibrations can be excited. There is no ambiguity that electronic or rotational levels could potentially be excited, as in the far- and near-IR ends of the spectrum respectively.

In the context of metal complexes, the mid-IR corresponds closely to the frequencies associated with stretching modes of a variety of common ligands, including the carbonyl (CO), cyano (CN), and nitrosyl (NO). These ligands share the property of being pi-acceptor ligands—that is, there is overlap between the d orbitals of the metal center and the π^* orbitals of the ligand. The resulting bond with the metal center is not only strong, but also exceptionally sensitive to the geometry of the ligand, relative to the metal. Subtle rearrangements can result in significant shifts in the vibrational frequencies of these ligands. As a result, these chromophores can function as local probes of oxidation state, geometry, temperature, and dynamics.[46-49]
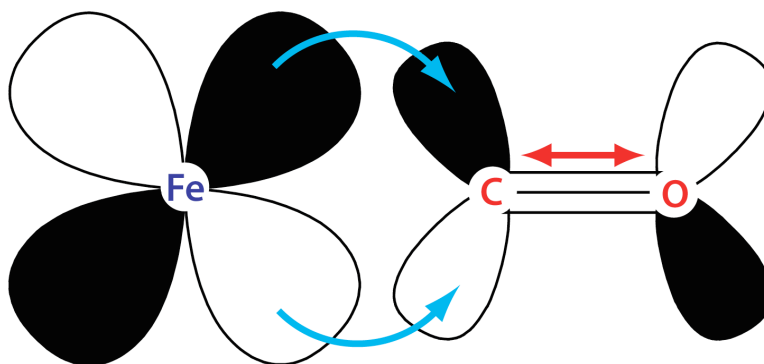
Figure 2.12 In pi-accepting ligands, metal and ligand orbitals overlap to transfer electron density to the antibonding MO of the carbonyl. This makes the carbonyl's stretching frequency dependent on the degree of this overlap.

Though mid-IR light interacting with carbonyl ligands has served as a foundation for all of my spectroscopic experiments, the pump pulses have varied enormously. The time-resolved experiments used UV or visible light; the conceptual interpretation of these is relatively facile.[34]

Two-dimensional IR experiments, on the other hand, are drastically more sophisticated both in their potential for insight, as well as in the methods necessary to understand the resulting data. The correlation between various vibrational modes at different times can yield deep insights into thermal motion.[50-53]

To understand the 2D-IR experiment conceptually, it can be helpful to begin with the description of the light involved. The output of the OPA is always a broad, approximately Gaussian distribution of light, the center frequency of which can be adjusted by tuning mixing crystals within the system. From this source, I utilize a Fabry-Pérot interferometer to shape the pulse. Only allowed frequencies pass through the shaper, resulting in a spectally-narrow pulse (Figure 2.13) that will excite only one vibrational mode of the system.
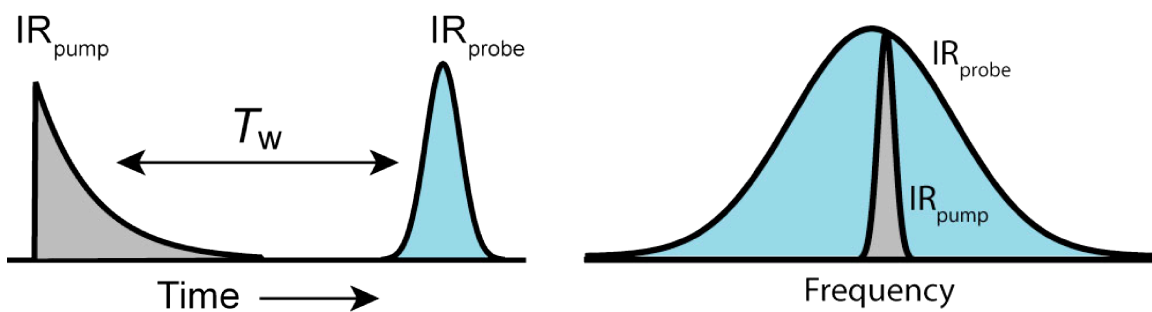
Figure 2.13 Time- and frequency-domain views of pulses for the double-resonant 2D-IR experiment.

The broad probe pulse then records the state of every relevant vibrational mode, effectively following that initial vibrational excitation as it couples to other modes. Conceptually, this is the "vibrational label" that travles throughout the molecule. By taking multiple pump slices for each vibrational mode, a complete 2D-IR spectrum can be assembled that describes the coupling of vibrational energy from any mode to any other mode (Figure 2.14). The finite width of the pump pulse means that the vertical (pump) axis of the spectrum is stretched.[6]
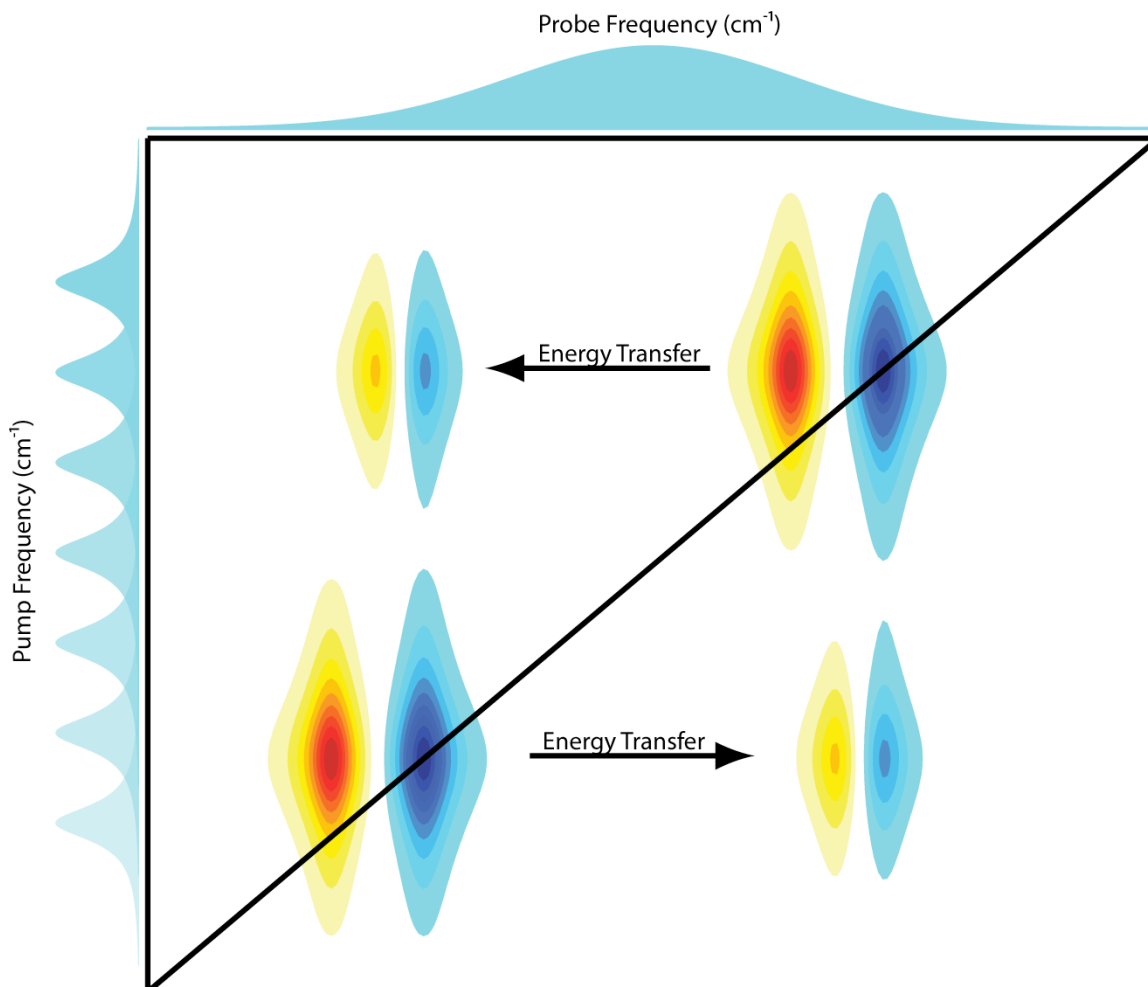
Figure 2.14 Simulated 2D-IR spectrum of a species with two vibrations. Along the diagonal are the n=0-1 bleaches in blue; shifted slightly to the red is a positive peak associated with the n=1-2 transition of each oscillator. If energy moves from one mode of the system to the other, this results in the appearance of a cross-peak.

A great deal of information can be determined from a 2D-IR spectrum; the 2D-lineshapes alone mean that substantial information can be determined without invoking time dynamics.

However, the apparatus developed in the Harris group sacrifices precision measurement of lineshapes in favor of the capacity to very quickly, and very accurately, measure the time dynamics of the vibrational populations associated with a given peak. This ultimately means that, after fitting, lineshape information can be discarded.
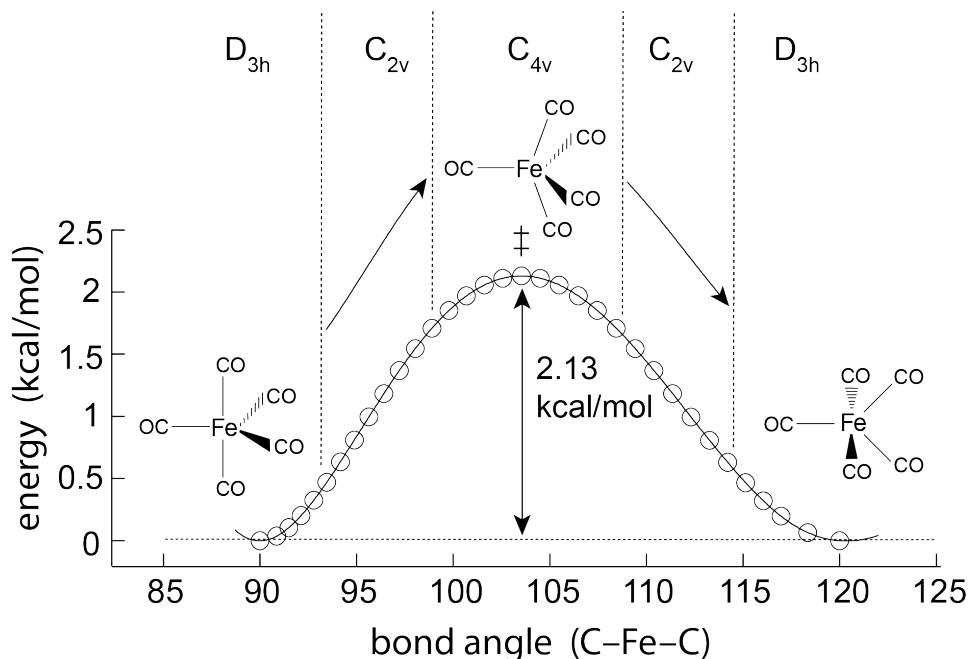
Figure 2.15 The motion of a complex undergoing a fluxional rearrangement can be quantified by tracking the spread of vibrational population between modes. This was previously applied in the case of $Fe(CO)_5$, where the Berry pseudorotation mechanism was found to control rearrangement of the carbonyls.[6]

      The kinetics data associated with each peak can be compared to Monte Carlo simulations of vibrational population transfer. These patterns are ultimately mechanism-specific, and can be used (as in the previous *Science* paper[6]) to separate hypothetical rearrangement mechanisms of a molecule (Figure 2.15). As I shall show, this approach is actually far more general, and capable of far greater insight, than has previously been appreciated.

      Metal complexes have a variety of applications, and are critically important as "molecular tools" to facilitate reactions. Ultrafast spectroscopy presents the opportunity to directly measure the motions associated with these reactions; perhaps no method is more sensitive and precise than IR spectroscopy.[54-64]

3   General methods

A broad set of techniques is necessary to confront the challenges of modern coordination chemistry. The spectroscopic experiments described this thesis each have three components: (1) synthesis and preparation of experimental samples, (2) ultrafast spectroscopy, either time-resolved or 2D infrared, and (3) use of density functional theory and Monte Carlo models to produce a theoretical description. The specifics of each experiment are discussed in greater detail in the appropriate section.

3.1   Synthesis and sample preparation

The chemical compounds used in the following experiments were not commercially available. In most cases, this was due to their low stability on a month-to-year timescale; in other cases, it was as a result of their novel formulation. Though the syntheses conducted for the purposes of this thesis are not themselves novel, there was nonetheless significant challenge in producing and purifying significant quantities for spectroscopic interrogation.

All experimental compounds were produced using a Schlenk line and air-free techniques. Described briefly, a vacuum line and an inert gas line are used in concert to carefully control the atmosphere above a reaction mixture. Many of the ligands in the coordination complexes are labile enough to be displaced by atmospheric gases (given the significant excess of those an open-air sample would encounter), or alternately could be protonated by the presence of water. Additionally, many of the reactants and products (e.g. $Fe(CO)_5$) are somewhat toxic; the same protocols that protect the molecules from air also protect me from the molecules.
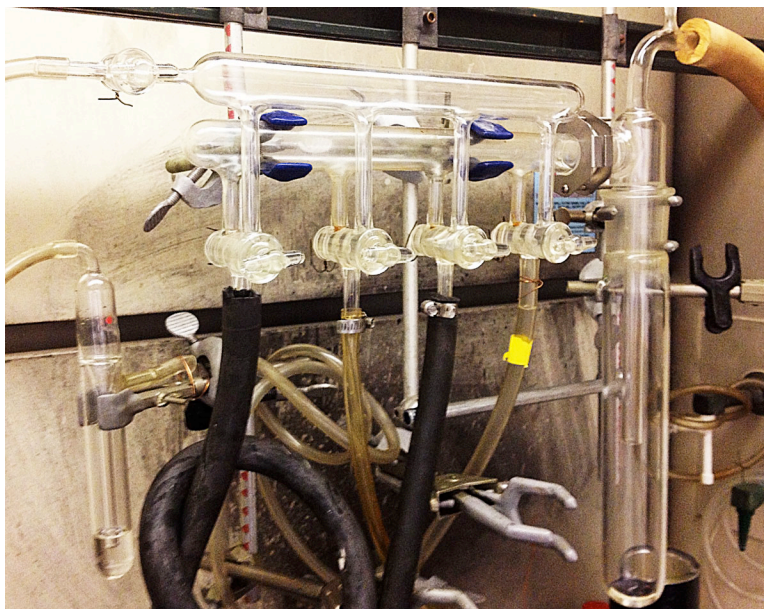
Figure 3.1 Schlenk line, featuring argon and vacuum lines, as well as a solvent trap at right.

For synthesis of tricarbonyl η^4-diene iron complexes, nitrogen was used as the inert gas. However, given its similarity to air, a high degree of care is required when transferring and purifying compounds. To mitigate some of the complications that can result, work for the heterobimetallic project was accomplished using argon gas. As its density is significantly greater than air, handling is made facile.

Purification of the resulting compounds was accomplished using silica columns under 10" in length. Progress was tracked using thin-layer chromatography under UV illumination. Following purification, products and intermediates were typically characterized using the UC Berkeley NMR Facility's 400 Mhz NMR, the AVB-400, in deuterated solvents including chloroform and benzene.

Experimental compounds were stored under nitrogen in a -20 ºC freezer. Solutions of these compounds for spectroscopic experiments were made using dry solvents in a Vacuum Atmospheres M040-1 nitrogen glove box to concentrations of ~1 mM, resulting in a peak optical density of ca. 0.7 at a path length of 0.5 mm, as determined by a Thermo-Fischer Nicolet 6700 FTIR. It should be particularly noted that this glove box underwent a complete overhaul in March 2011, when the gloves, a cracked panel, and the inoperable atmospheric processing unit were completely replaced. In particular, damage to the original atmospheric processing unit was such that regeneration of the catalyst was impossible; as such, the quality of samples produced in the box prior to spring 2011 was significantly degraded (if they exhibited significant air sensitivity.) Following the upgrade/overhaul, regular regeneration of the catalyst provided a far superior operating environment.

3.2 Spectroscopy

The design and construction of the ultrafast apparatus and much of its sample handling accessories have been described in great detail in earlier theses, including those of James Cahoon and Karma Sawyer.[65-67] I provide here a schematic overview, as well as an in-depth explanation of my own work in developing the hardware necessary to conduct temperature-dependent experiments over a broad range of values.

3.2.1 Ultrafast, time-resolved instrumentation

The ultrafast apparatus uses a Spectraphysics Spitfire Ti:Sapph regenerative amplifier, producing 1.06 W of 800 nm, 90-fs pulses at a 1 kHz repetition rate. The amplifier is seeded by a Ti:Sapph Tsunami oscillator and pumped by a 1 kHz Nd:YLF Spectraphysics Empower pump laser.

The output of the commercial system is sent to two of three lines: The first is a third-harmonic generation line, using two BBO crystals to produce 400 nm and 267 nm light. These pulses are stretched using a 25 cm fused silica rod to ca. 1 ps to prevent two-photon absorptions. This light is used for TR-IR (UV pump, IR probe) experiments. The other two lines are home-built OPAs (optical parametric amplifiers), incorporating two passes through a BBO, and mixing the resulting beams in a $AgGaS_2$ crystal; this produces tunable mid-IR light from 3.0 to 6.0 μm with a bandwidth of ~200 cm^{-1} and a pulse duration of ca. 100 fs.[68] One OPA is used in all experiments to produce probe and reference lines ("Odin"). The other is used to produce the pump pulse for 2D-IR experiments ("Thor"). After the OPA, the system is arranged in a conventional frequency-domain 2D-IR pump-probe geometry that has been described elsewhere.[36] To summarize: the mid-IR light is sent through an 84-16 beam splitter. A high-finesse tunable Fabry-Pérot interferometer is used to shape the majority of the light into the pump pulse. This pump has a spectral width of approximately 14 cm^{-1} and duration ca. 1 ps. This beam is sent through an achromatic CdS/CdSe half-wave plate mounted on a Newport RGV100 rotation stage. For these experiments, the pump pulse was set to the magic angle (54.7°) to remove the effects of rotational diffusion. A Newport delay stage in the pump line allows for adjustment of the time delay (T_w) between pulses. A mechanical chopper (New Focus) runs at 500 Hz, blocking every-other pump pulse from reaching the sample.

The remaining 16% of each pulse is sent through a 50-50 beam splitter to produce probe and reference lines. Critically, this beam splitter features two faces that are slightly angled relative to one another. Early work determined that a rectangular-cross-sectioned splitter would produce a second, "ghosted" pulse that disrupts the kinetics data.
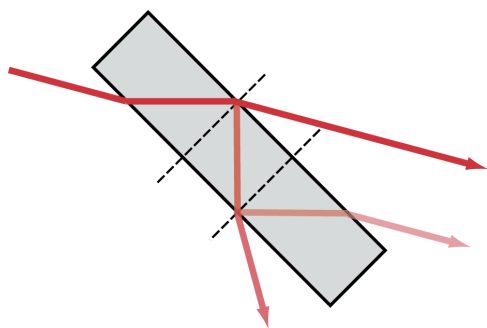
Figure 3.2 A beam splitter with parallel faces produces a second ("ghost") pulse that interferes with kinetics data.

T_w (ps)
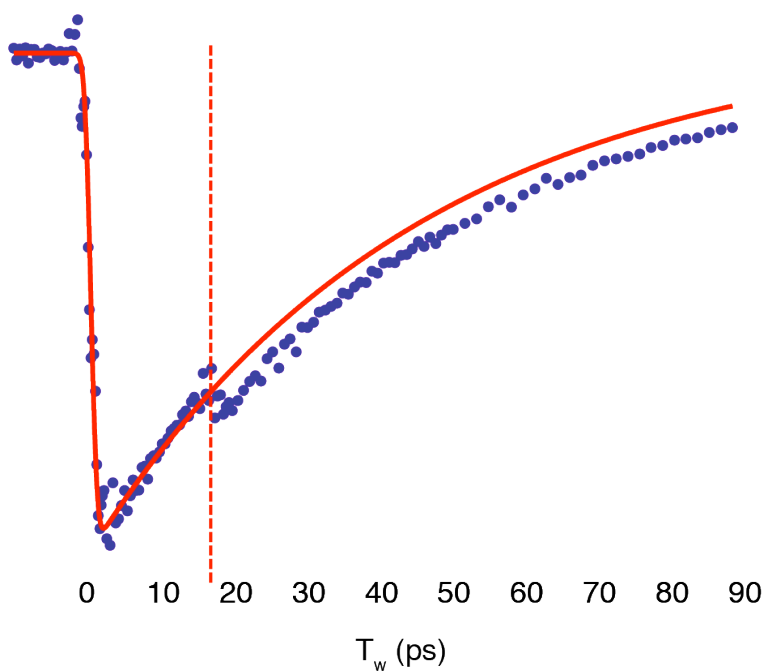
Figure 3.3 Kinetics data with original beam splitter incorporated. Note the additional population caused by the arrival of the "ghost pulse" at ca. 18 ps.

The probe and pump are sent to the sample via a 10-cm focal length, gold-coated, off-axis parabolic mirror (Janostech) to produce an overlap spot size ca. 200 μm. After interaction with the sample, the probe line carries the response information of the molecule-solvent system. The probe and reference lines are focused, sent through 40 μm slits, and spectrally dispersed by a grating (Acton Research Corporation SpectraPro 150) onto a 2x32-element MCT detector (Infrared Associates), yielding ~3 cm^{-1} of spectral resolution. Data is integrated by a high-speed signal acquisition system and associated software from Infrared Systems Development Corp. Each spectrum is the averaged result of 20,000 shots. It should be noted that this value is easily adjusted on-the-fly.
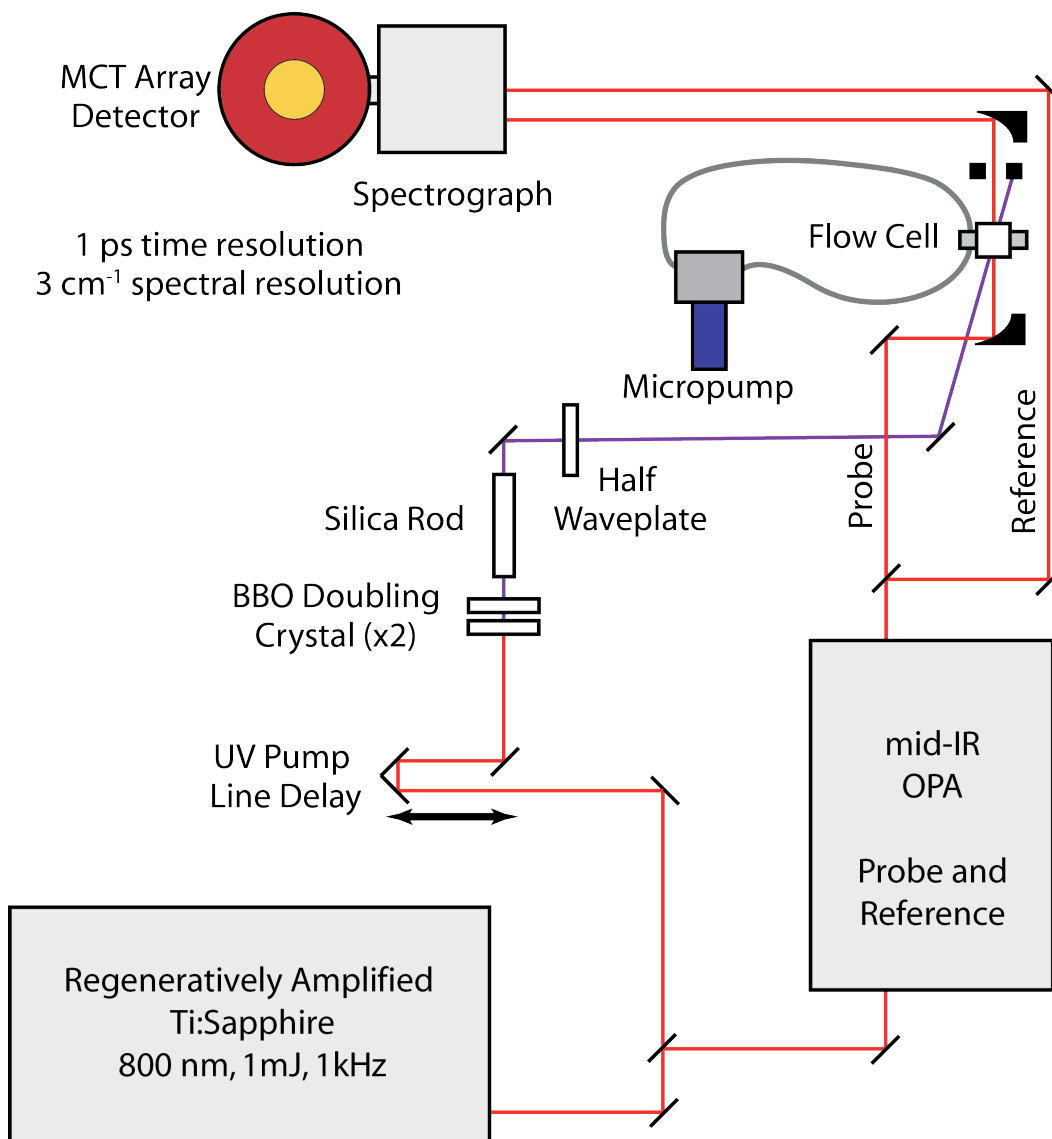
Figure 3.4 Schematic of the ultrafast apparatus as configured for TR-IR experiments.
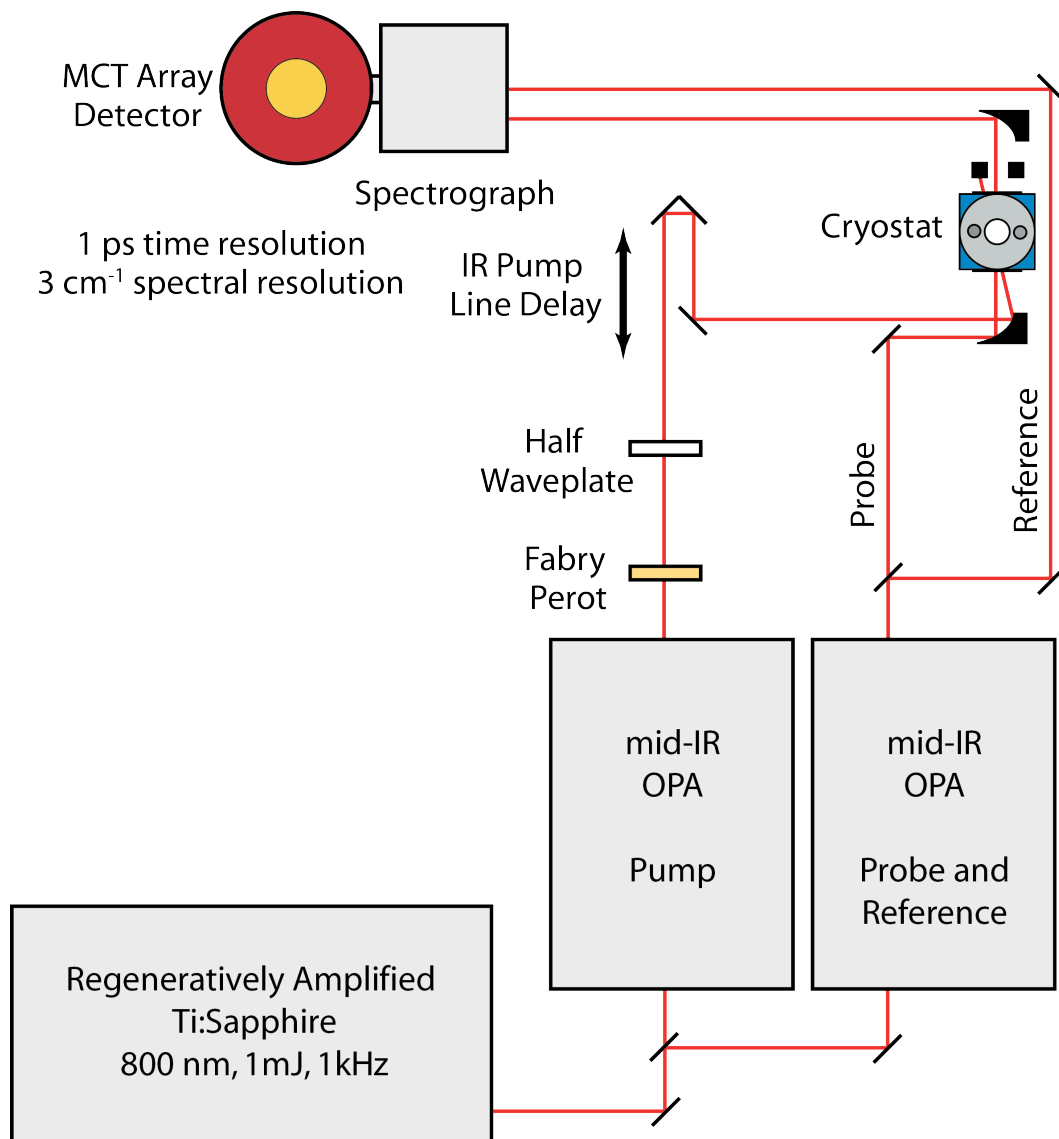
Figure 3.5 Schematic of the ultrafast apparatus as configured for 2D-IR experiments.

The instrument is controlled using software in Labview v.8.2. All resulting data is averaged, fit, and plotted using MATLAB R2010a. The double-resonant 2D-IR experimental design means that 2D spectra are composed of slices of the probe spectrum for a particular pump frequency. Full two-dimensional spectra are assembled from these slices.

3.2.2 Temperature control systems

Significant attention was paid to the design of sample holders, to facilitate the array of experimental approaches. For TR-IR experiments, the sample solution was flowed using a Micropump pump to prevent degradation in a manner described in detail in the thesis of Karma Sawyer.[66] For the 2D-IR experiments, a broad range of temperatures was required. In these cases, simply cooling the experimental solution is not acceptable; significant condensation from external air is problematic. Instead, the sample solution is held in a 0.5 mm-pathlength CaF_2 liquid cell contained in a liquid N_2 cryostat with CaF_2 windows (Specac VT Cell), allowing accurate temperature control and monitoring. The cryostat is suspended in the path of the laser by a combination of a three-dimensional translation stage (designed specifically for holding high-mass objects) and a custom-machined bracket (see Appendix D).
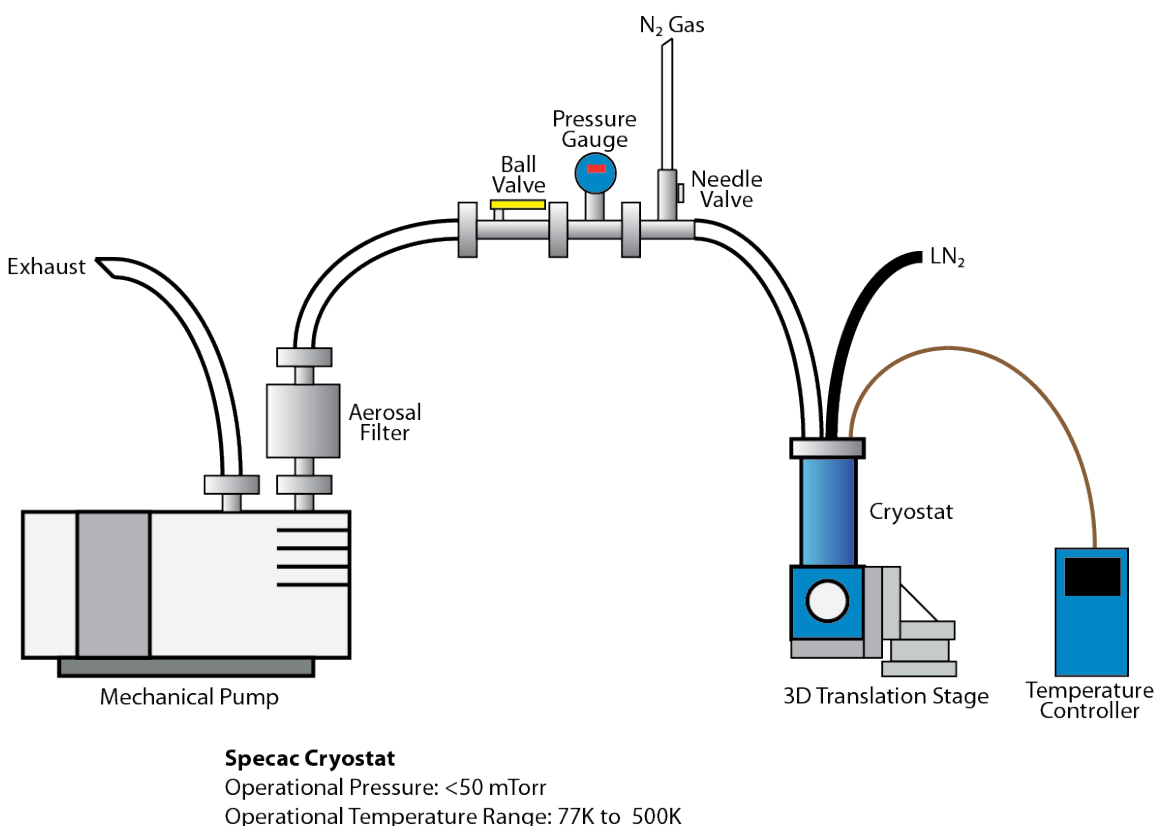
Figure 3.6 Design of the cryostat and associated vacuum systems as implemented.

The cryostat is serviced by a custom vacuum manifold. In functional application, this simple vacuum system could provide operating pressures inside the cryostat of under 30 mTorr, sending exhaust to a hood through 30 m of 1" diameter tubing. A needle valve running to house nitrogen provides backfilling

capacity; thus, opening the cryostat for sample changing does not risk condensation on the windows due to atmospheric water. Much of the tubing used is PVC, as it provides the necessary durability and strength; installation of these components required a break-in period during which volatile organics outgassed from much of the tubing.

The cryostat itself relies on an insulating mushroom piston to regulate interaction between the liquid nitrogen reservoir and the heated block around the sample. The original design of the reservoir assumed the operator would simply fill the reservoir directly from a Dewar over the course of an experiment. Testing of the loiter times associated with this design indicated that the small reservoir would not be sufficient to allow for a full 2D-IR kinetics run without disrupting the system.
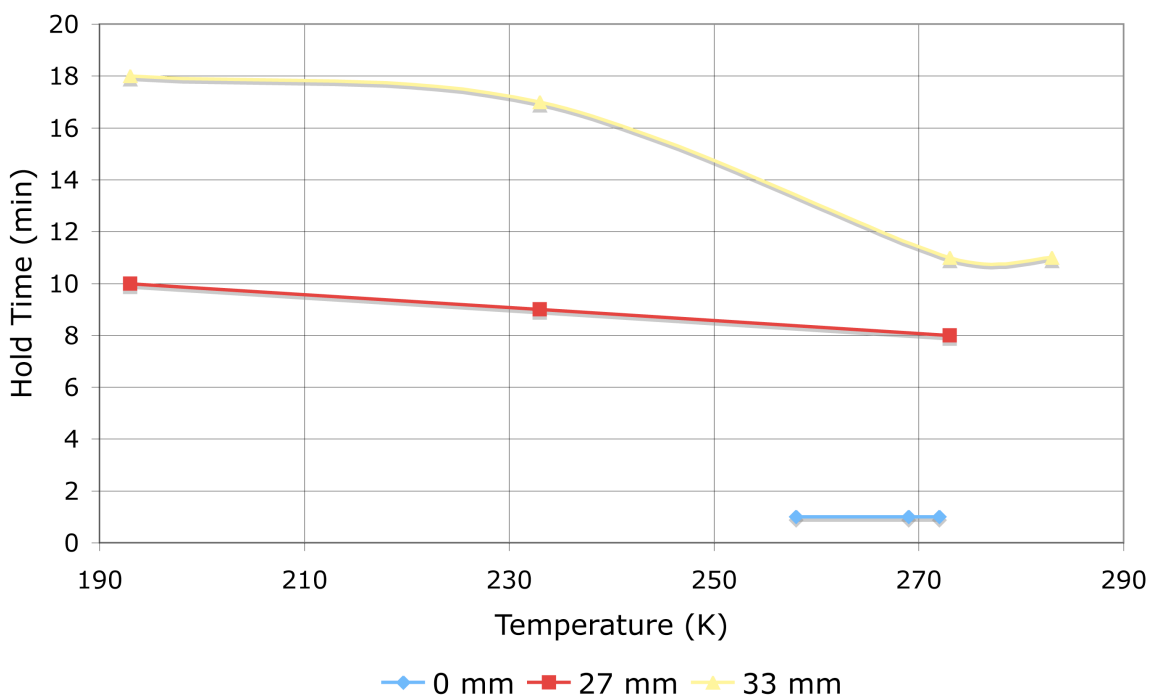
Figure 3.7   Cryostat low-temperature hold times, as determined by mushroom piston thickness. (Hold times decrease with temperature increase because the heating block works harder against the cold sink.) The thickest plunger possible was deemed optimal.

In light of this deficiency, I designed and machined a new plug for the liquid nitrogen reservoir. This PTFE plug added two stainless steel tubes, permitting flow of liquid nitrogen directly from a 40 L Dewar. With this upgrade in place, hold times in excess of twelve hours have been achieved. Calibration of liquid nitrogen flow rate is accomplished via a needle valve control nitrogen gas backpressure.
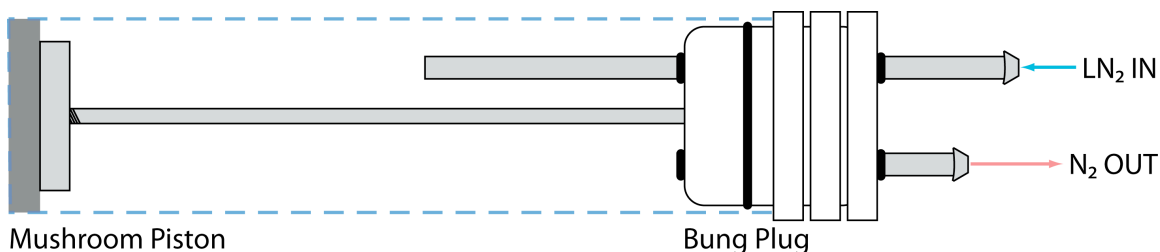
Figure 3.8 Schematic of improved PTFE bung plug design, with added tubing for LN_2 flow. Rubber tubing connected to each provided both supply, as well as an output for cold gas removed from the optics table.

The final challenge in preparing the cryostat apparatus was to ensure that a 2D-IR spectrum could be taken in spite of its thicker, vacuum-resistant windows. Though it provides no interesting cross-peaks (due to the degeneracy of CO stretching modes), $Cr(CO)_6$ is an excellent calibration standard (and is used in calibrating the frequency of the MCT detector.) Initial spectra of the compound in hexanes at low temperature produced effective spectra and confirmed the capacity of the cryostat system to work within required parameters. In particular, the absence of correlated noise due to transient grating effects was a relief. Transient grating effects, though often desired in their own experimental light, pose a significant challenge to 2D-IR experiments where the frequency of pump and probe light matches.[69-72]
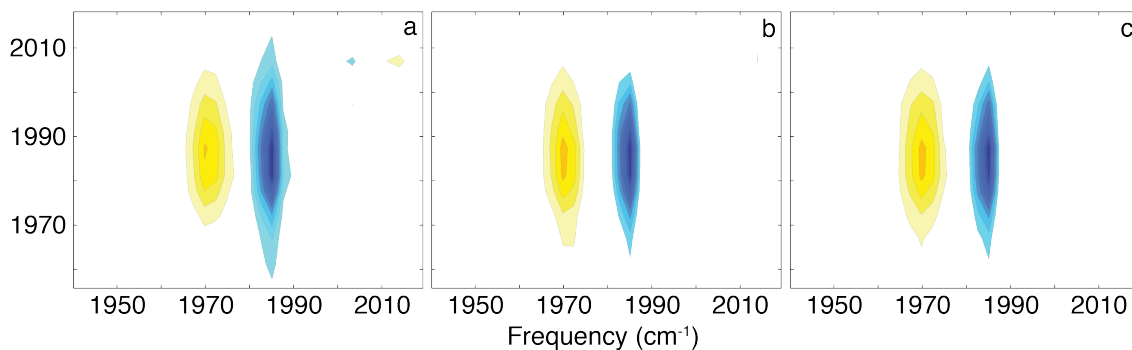
Figure 3.9 Spectra of $Cr(CO)_6$ in hexane at 223 K. Waiting times are (a) 2 ps, (b) 4 ps, and (c) 7 ps, showing an absence of transient grating effects at all times.

These initial tests of the mechanical, thermal, and spectral stability of the cryostat system as integrated into the existing apparatus indicated that it would function more than satisfactorily. The temperature-dependent 2D-IR experiments that took advantage of it indicated that this was indeed the case. Practical application of the cryostat system for actual experimentation later showed the degree to which its use it as much art as science. Balancing LN_2 flow rates with the needle valve is nontrivial, as is passing through the quenching/blowback phase of cooling.

Ultimately, however, the cryostat works effectively for providing a broad range of temperature control. In either TR-IR or 2D-IR configurations, the apparatus provides the necessary time and spectral resolution to make important conclusions on the behavior of coordination complexes. Interpretation of the resulting spectra, however, mandates an understanding of the expected peaks that is provided optimally by calculation. Only in this context can the output from this instrument be truly understood.

3.3   Calculations

A variety of calculations were necessary for these experiments. They fall into several approximate categories: (1) data processing code, (2) data fitting code, (3) classical master equation simulations, or (4) DFT structure calculations. Though the details of these calculations are considered in the relevant chapters focusing on particular experiments, several general points about each should be considered.

3.3.1 Data analysis and fitting

The data output from Labview 8.2 has undergone basic background subtracting and computation to produce a difference spectrum, but is otherwise presented as a text file containing frequencies, delay times (T_w), and absorbance intensities. Data can be recorded with a varying number of repetitions, and averaged at the level of either Labview or the later MATLAB R2010a averaging software. The data is subjected to statistical tests to remove outliers, as well as cases where the laser recorded no data. This analysis then takes advantage of MATLAB's internal plotting methods to render 1-D and 2-D spectra of that data.

The resulting spectral data are still excessive for the majority of analyses; the optimal values to correlate with theory are the kinetics traces for each species in solution. As such, it is necessary to determine the volume of each observed peak. Though previous experiments in the group simply integrated the area under a given curve, this approach is ultimately unacceptable for cases where there is significant overlap between peaks.[49,61,73] I instead adapted fitting code used by Eric Muller and the Surface Side; this code leverages the simps fitting algorithm to fit multiple Voigt lineshapes to a given spectrum. Not only does this approach increase the precision in fits, it also increases the accuracy of the resulting values—a challenge for which a simple integration has no recourse.

With kinetics data in hand, the transfer and lifetime rates associated with each peak must be calculated. However, as many experimental systems studied in this thesis undergo forward and backward reactions at the same rate, it is necessary to fit at a more accurate level than simple exponential decay. Rather, a Monte Carlo simulation of the master equation governing coupling between modes was established. This so-called Gillespie Algorithm is far more accurate, but does require significantly more computational time to fit a kinetics curve.[74]

3.3.2 Structure determination via density functional theory

The resulting kinetics data are compared with ground and transition state geometries, as well as vibrational frequencies, calculated using DFT. All DFT calculations were done using the Gaussian09 software package[75] as run on the National Energy Research Scientific Computing Center's (NERSC) computers. Two systems were used: Jacquard, a LinuxNetworkx Linux Cluster of 712 2.2 GHz Opteron processors, or Carver, an IBM iDataPlex of 1,202 Nehalem and Westmere 2.67 and 2.00 GHz processors.

Structures and their vibrational frequencies were calculated using the BP86 or UB3LYP density functionals, with the 6-31+g(d,p) basis set for H, C, and O atoms,[76-85] and the LANL2DZ basis set and effective core potential for iron atoms.[86-88] In the case of the Gd complex, calculations utilized the Stuttgart potential and ECP with 53 core electrons incorporated into the pseudopotential. In order to describe the effects of the outer solvent shell molecular cavity on the energy and geometry of each complex, all calculations for MRI systems included a polarizable continuum model of water, $\varepsilon = 78.3553$. Transition state structures were determined by direct transition state optimizations. When studying dissociation processes, values for $r = \infty$ were computed from separate calculations of solvent and solute molecules.

4 Temperature-dependent 2D-IR of tricarbonyl diene iron systems

4.1 Introduction

Ultrafast 2D infrared spectroscopy (2D-IR), as pioneered by Hochstrasser and coworkers, presents the opportunity to directly observe the dynamics of complexes at thermal equilibrium.[34,51,53] Organometallic systems, due to their relevance to a wide range of chemical transformations, are critically important spectroscopic subjects.[6,59-61] These systems are particularly exciting in 2D-IR because the rates of vibrational population transfer can be correlated with the geometry and energy of the transition state for exchange processes.[89-91] Most notably, we have previously applied this 2D-IR approach to the molecule $Fe(CO)_5$ and determined its method of fluxional rearrangement to be the Berry pseudo-rotation.[6]

However, competing dynamics can interact to produce important effects that are a challenge to effectively measure.[52,53,92] Multicarbonyl systems present a 2D-IR hurdle: population transfer from both chemical exchange and intramolecular vibrational redistribution (IVR) can occur simultaneously and at similar rates. Differentiating the transfer mechanism is difficult as the faster mechanism will ultimately dominate transfer and obscure the other.[39] To resolve this, we exploit the different temperature dependence of most IVR relative to exchange processes. Temperature-dependent 2D-IR is a mechanism-sensitive measure of vibrational coupling to a more advanced degree than a single temperature can provide.[93,94] We use this technique to reveal the symmetry-breaking "wagging" motion in tricarbonyl(η^4-diene)iron complexes (Figure 1).
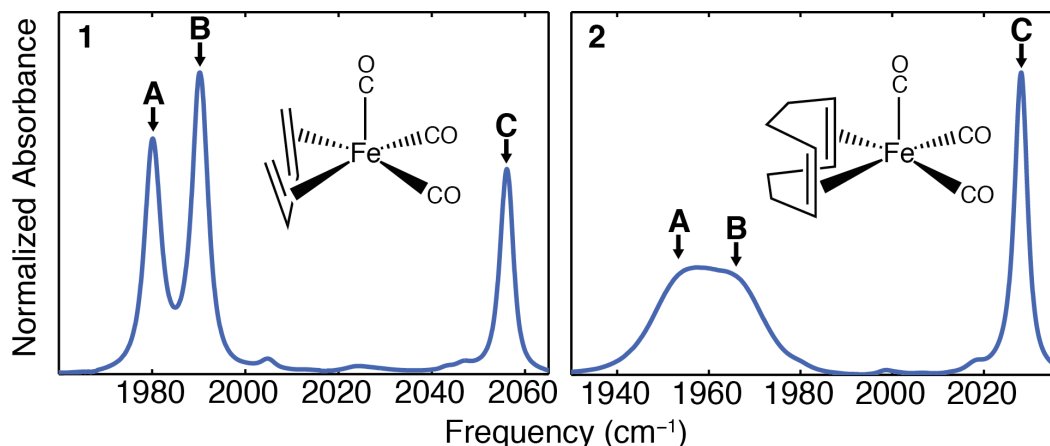
Figure 4.1 Room temperature FTIR spectra and associated structures for Fe(CO)$_3$(1,3-butadiene) (**1**) and Fe(CO)$_3$(1,5-cyclooctadiene) (**2**) complexes; note that only in the latter complex are peaks A and B coalesced.

This approach presents unique opportunities to elucidate the details of ambiguous phenomena that have otherwise eluded a definitive experimental assignment. The spectral behavior of the carbonyl stretching modes of tricarbonyl(η^4-diene)iron complexes (Figure 4.1) have proven controvertible.[95-99] Though several of these complexes have been shown to undergo a fluxional exchange of CO ligands, the timescales associated with this exchange vary significantly. Some members of this family show chemical exchange on the hundred-nanosecond timescale that results in coalescence in NMR spectra (e.g. butadiene complex **1**);[100] their IR spectra show three well-resolved peaks across all temperatures.[101] Studies of these compounds showed that this exchange follows a so-called "turnstile" mechanism, in which the three CO groups rotate in concert to exchange positions (Figure 4.2).[102]
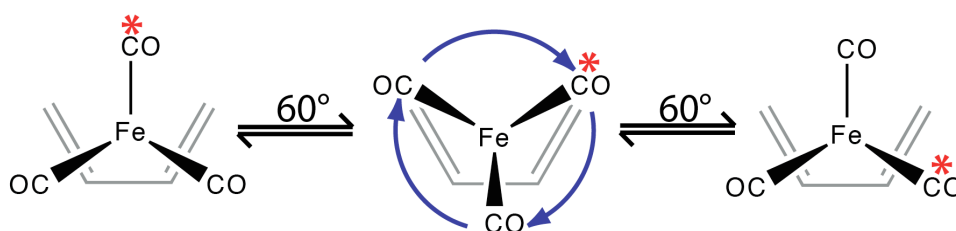
Figure 4.2 Turnstile rotation mechanism.

31

A minority of the complexes (e.g. cyclooctadiene complex **2**) show temperature-dependent coalescence in IR spectra.[95,96,103] In these complexes, a single broad peak will resolve into two sharp CO stretching modes (A and B) at low temperatures (Figure 4.1). Though the temperature-dependence of the spectra clearly show that the motions of the system have slowed, the relationship of those motions with spectral features remains ambiguous.[97]

In previous work, the optical Bloch equations were used to simulate the effects of a turnstile rotation on IR spectra, and a barrier height for rotation of the CO groups in cyclooctadiene compound **2** was calculated to be in the 1.0-1.5 kcal/mol range.[96,99] However, Strauss and co-workers have noted that a low-frequency, intrawell wagging motion along the same torsional reaction coordinate would result in coalescence behavior even in the absence of a barrier crossing (Figure 4.3).[97,104-106] This interpretation means that the effects of this one-well motion would render the optical Bloch equations unreliable in predicting IR spectra when the experimental timescales involved are on the order of nuclear motion. Though further experiments confirmed the fast exchange of the carbonyl ligands, even faster intrawell motion could still overwhelm fluxionality as the source of vibrational coupling. Despite further experiments, the spectral behavior of these complexes at thermal equilibrium nonetheless remains somewhat ambiguous.[99]
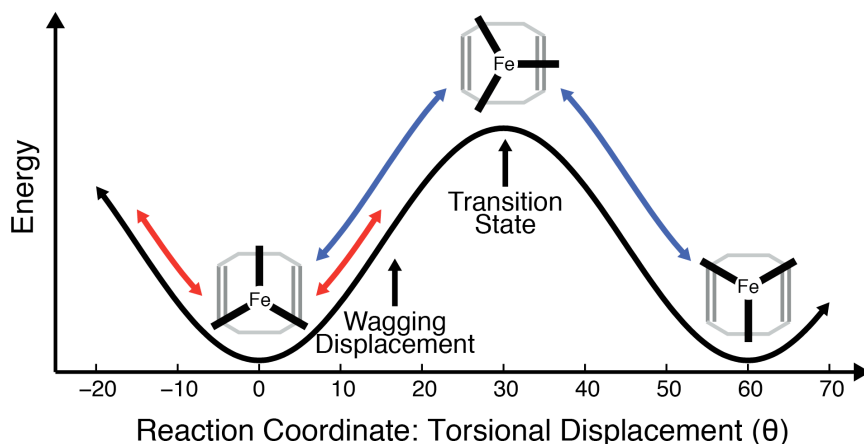
Figure 4.3 The reaction coordinate for CO exchange in tricarbonyl(1,5-cyclooctadiene)iron (**2**); note that the wagging motion described by Strauss (in red) is on the same coordinate as exchange (blue).

This family of piano stool complexes offers the opportunity to explore the full capacity of temperature-dependent 2D-IR to differentiate differing sources of vibrational coupling. Simultaneously, we shed light on the validity of previous descriptions of tricarbonyl(η^4-diene)iron complexes. In these piano stool systems, there are two possible sources of vibrational coupling that 2D-IR can differentiate (Figure 4.4): (I) quantum-mechanical IVR (possibly coupled to the wagging motion of the ligands),[107,108] and (II) chemical exchange via a turnstile motion.

Time-Dependent Sources of Vibrational Coupling:

Intramolecular Vibrational Redistribution   Geometric Perturbaton

(I) Torsion-Coupled IVR   (II) Turnstile Exchange
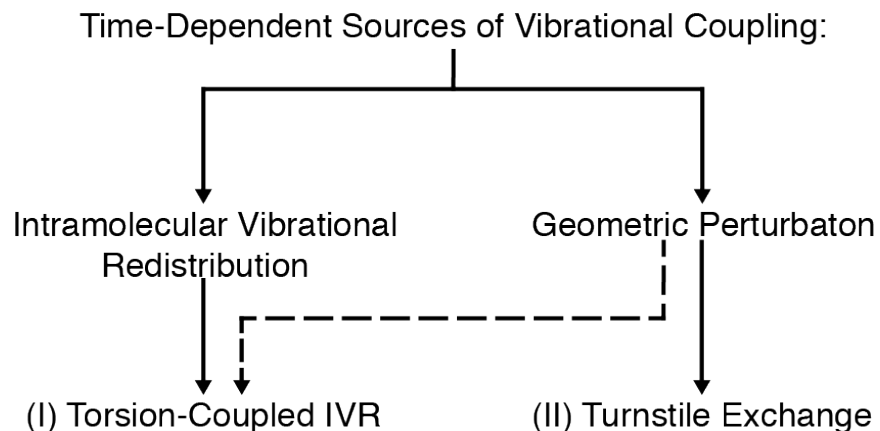
Figure 4.4 Relevant sources of vibrational coupling in tricarbonyl(η^4-diene)iron complexes.

The study of the butadiene complex (**1**) will characterize the rate and temperature dependence of vibrational population transfer via solely IVR (I), as the NMR-determined turnstile exchange rate is far too slow to produce vibrational coupling. These results provide a context for examination of vibrational population transfer in $Fe(CO)_3$(1,5-cyclooctadiene) (**2**), a compound in which both IVR (I) and turnstile exchange (II) are possible explanations. Our analysis demonstrates both the additional insight that temperature-dependent 2D-IR provides, as well as the remaining challenges of spectroscopically interrogating similar coordination complexes. We show that a wagging motion breaks the symmetry of the complex, facilitating population transfer.

4.2   Methods

4.2.1 Synthesis of Fe(CO)$_3$(η^4-diene) complexes

The synthesis of Fe(CO)$_3$(1,3-butadiene) (**1**) and Fe(CO)$_3$(1,5-cyclooctadiene) (**2**) were both accomplish according to previously published literature protocols.[109-111] Briefly, the following methods were used (Figure 4.5):

To synthesize the butadiene complex **1**, Fe(CO)$_5$ and butadiene from Aldrich were dissolved in n-pentane (Fisher Scientific) under N$_2$. The reaction vessel was irradiated for 14 hours by a 450 W medium pressure Hg lamp (Hanovia). The product was purified via vacuum distillation.

To synthesize the cyclooctadiene complex **2**, Fe(CO)$_5$ and cyclooctadiene were dissolved in benzene (Aldrich) under N$_2$. Photolysis was carried out with the same 450 W Hg lamp for 44 hours; the temperature of the reaction vessel was kept at 20°C by a Neslab ULT-80DD circulating bath. As noted in the literature, it would appear that either remaining starting material or side-products of the reaction quickly break down the desired product (in a matter of hours.) The complex was purified by crystallization, silica column, and extraction to n-pentane.
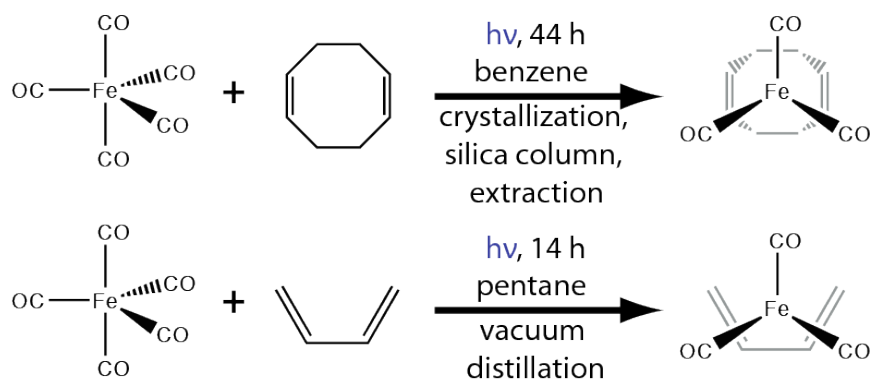
Figure 4.5 Synthesis of piano stool complexes for TD-2D-IR interrogation.

Following synthesis, both compounds were characterized by ^{1}H-NMR and ^{13}C-NMR (Figure 4.6); both showed spectral peaks associated in the literature with the expected products.[110,111]
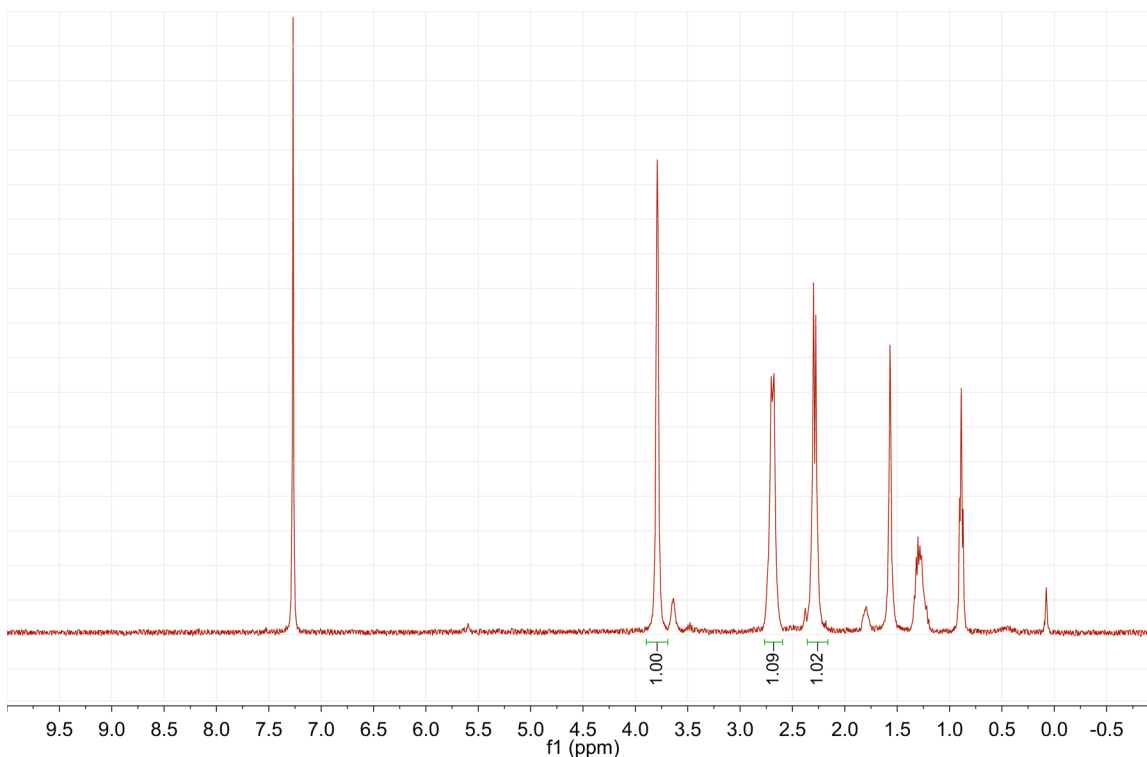
Figure 4.6 ^{1}H-NMR spectrum of the 1,5-cyclooctadiene complex, matching literature values. ^{13}C-NMR spectra also replicated literature values.

Resulting infrared spectra of the compounds showed carbonyl stretching peaks at positions matching literature values.[101,109] The stability of these compounds in solution when exposed to air is extremely sensitive to the success of the purification. Both samples can be stable in hexane under ambient atmosphere and temperature for upwards of three days if sufficiently pure; prior to purification, the cyclooctadiene complex **2**, in particular, will decompose in ca. 10 hours under nitrogen in a -80°C freezer.

Both compounds were stored under N_2 at -20°C. Spectroscopic solutions were prepared in hexane (Fisher) to concentrations of ~1 mM, resulting in a peak optical density of ca. 0.7 at a path length of 0.5 mm, as determined by a Thermo-Fischer Nicolet 6700 FTIR.

4.2.2 Temperature-dependent, ultrafast 2D-IR spectroscopy

The ultrafast apparatus follows the standard pump-probe 2D-IR design. A liquid nitrogen cryostat (Specac VT Cell) provided inert atmosphere and temperature control. Further details of the spectroscopic system are found in Chapter 3.

4.2.3 Density functional theory calculations

All calculations were done using the Gaussian09 software package[75] as run on the National Energy Research Scientific Computing Center's (NERSC) Jacquard computer, a LinuxNetworkx Linux Cluster of 712 2.2 GHz Opteron processors. Structures and their vibrational frequencies were calculated using the BP86 density functional, with the 6-31+g(d,p) basis set for H, C, and O atoms,[76-85] and the LANL2DZ basis set and effective core potential for iron atoms.[86-88] Transition state structures were determined by direct transition state optimizations.

4.3 Results and discussion

To determine the chief underlying mechanism of vibrational population transfer, we use 2D-IR to measure the rate of transfer between normal modes of the system at different temperatures. The off-diagonal cross peaks are indicative of vibrational population moving between modes of the system over the course of the experiment. The rate at which this transfer occurs, and dependence of this rate on temperature, are indicative of the underlying behavior of the system.[39,92] Two chief mechanisms can be responsible for the time-dependent growth of the cross peak: The first is a change in the geometry of the system. When this occurs, there is a shift in the frequency at which the oscillator appears in an infrared spectrum: a cross peak.[112,113] The second process, intramolecular vibrational redistribution (IVR), is a quantum-mechanical phenomenon that results from the non-ideal nature of molecular vibrations.[114-116] Molecular vibrations, unlike the idealized harmonic oscillators of chemical group theory, are not truly orthogonal, but rather coupled and capable of exchanging population. This population transfer thus produces cross peaks in the 2D-IR spectrum in the absence of chemical exchange. Both processes may occur simultaneously, and on similar timescales, in tricarbonyl(η^4-diene)iron complexes.

To differentiate the two mechanisms, we correlate the observed patterns in relative rates and temperature dependencies to theoretical models of the two possible mechanisms.
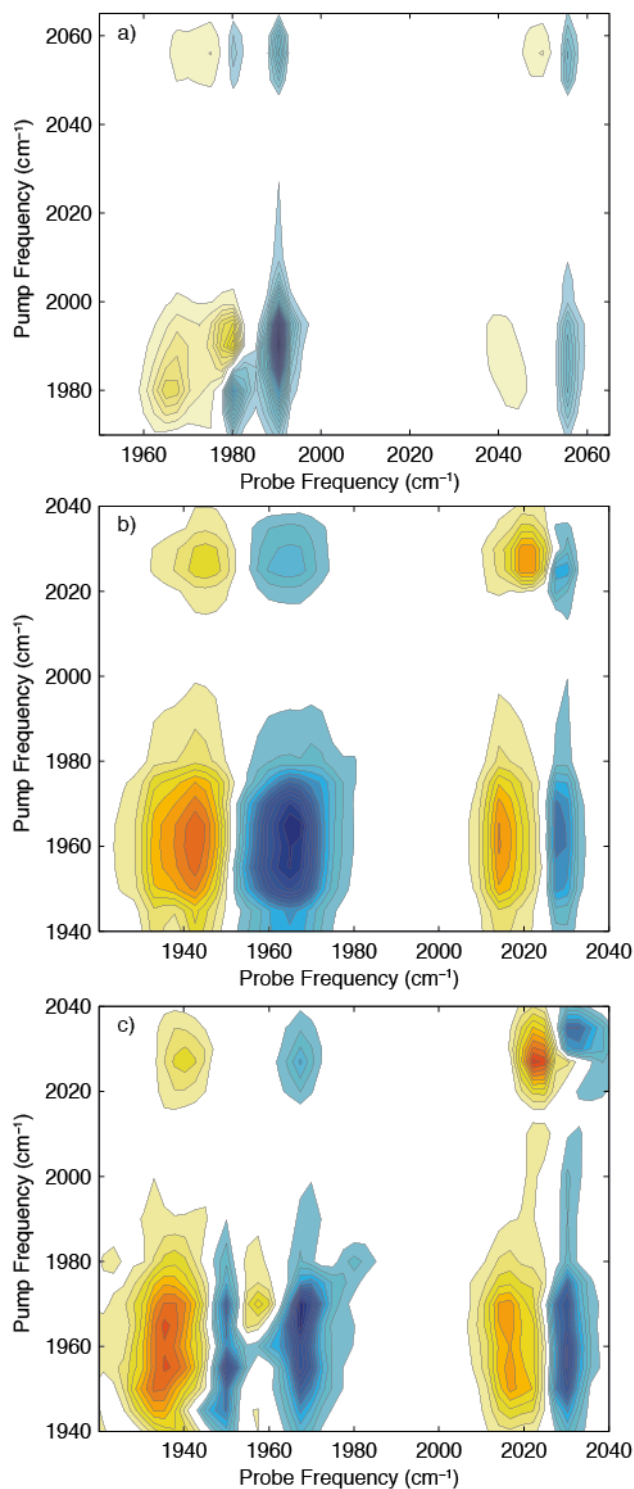
Figure 4.7 TD-2D-IR spectra, T_w = 2 ps: a) butadiene complex **1** at 288 K (low temperature spectra are qualitatively identical); b) cyclooctadiene complex **2** at 288 K; note the highly coalesced peaks in the region of 1960 cm⁻¹; c) complex **2** at 198 K; previously coalesced peaks are now well resolved.

4.3.1 Extracting vibrational kinetics from 2D-IR spectra

Each complex has three carbonyl ligands. The stretching modes of these ligands form three normal modes, which we name modes A, B, and C. The frequencies and symmetries of the modes are listed in Table 4.1.[117]

Mode	Complex: Symmetry	1 $Fe(CO)_3(C_4H_4)$ Frequency (cm^{-1})	2 $Fe(CO)_3(C_8H_{12})$ Frequency (cm^{-1})
A	a"	1980	1953
B	a'	1990	1965
C	a'	2056	2027

Table 4.1 Frequencies and symmetries of CO stretching modes in relevant piano stool complexes.

That the cross peaks observed involving each of these modes appear at the same frequency in 2D-IR spectra as in FTIR spectra means that we can discard anharmonic coupling as a significant source of cross-peak intensity. DFT calculations of the anharmoncities of the three modes confirm that the values are less than 3 cm^{-1} for each.

The double-resonant 2D-IR experimental design means that 2D spectra are composed of slices of the spectrum for a particular pump frequency. Full two-dimensional spectra are assembled from these pump slices. In a 2D-IR spectrum, each vibrational mode of the system has *two* transitions near the diagonal. The transition from the ground to the first (n=0-1) vibrationally excited state appears as a blue, negative peak. Redshifted off the diagonal is the orange, positive peak associated with the transition from the first to second (n=1-2) vibrationally excited state of the mode. Analysis of spectroscopic data (Figure 4.7) requires careful consideration of the phenomena contributing to the nonlinear signal; failure to account for these can result in the appearance of anomalous and misleading kinetics.[92]

To extract peak areas from each spectrum, we fit three positive and three negative Voigt peaks at each pump slice. Extracting information on the kinetics of vibrational coupling between the respective carbonyl stretching modes of each molecule requires accurate fitting of the individual positive (orange) and negative (blue) peaks. The shape of each peak follows a Kubo lineshape, which includes broadening over the first few picoseconds of the experiment as the solvent molecules rearrange.[92] This broadening will not be relevant to our analysis of the transfer of population between modes. Fitting six Voigt-profile peaks to each time slice (three negative peaks for the n=0-1 transitions, and three positive peaks for the n=1-2 transitions) effectively removes the effects of this broadening from the kinetics. For a given time slice, only the area of each mode is preserved.

I n the portion of each spectrum near 1955 and 1990 cm^{-1}, respectively, spectra at many temperatures showed significant overlap between the n=0-1

transition of the lower-frequency mode (A) and the redshifted n=1-2 transition of the higher-frequency mode (B). We avoid this region and instead measure the vibrational populations via the "outer" modes: the 1-2 transition of the lower-frequency peak (A) and the 0-1 transition of the higher-frequency mode (B) (Figure 4.8).
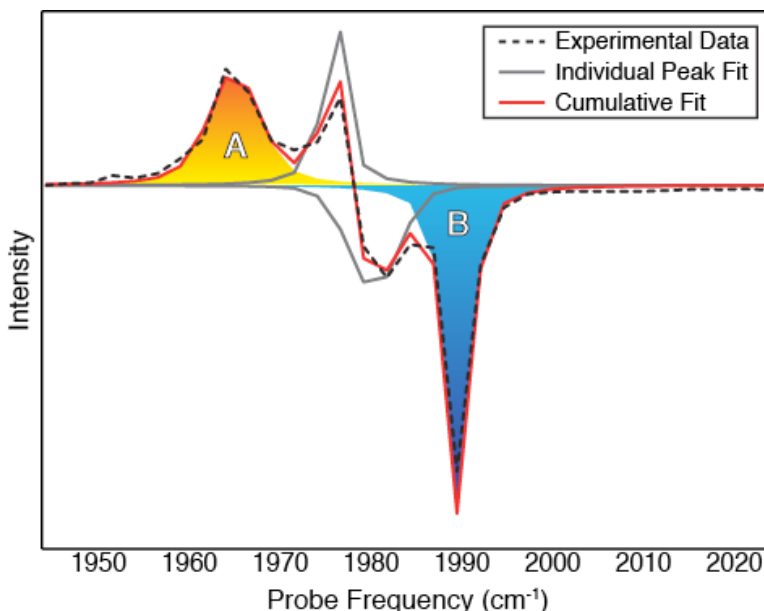
Figure 4.8 A portion of the 2D-IR spectrum of butadiene complex **1** at 288 K and T_w=10 ps following excitation centered at 1980 cm^{-1}. Note the two peaks overlapped in the center (in gray). The solid peaks at 1965 and 1990 cm^{-1} correspond to modes A and B, respectively, that are used to follow the vibrational population of each state.

The data resulting from this fitting describe the area under each peak as a function of waiting time, T_w, and are then made proportional to the vibrational population by dividing by their oscillator strengths (as determined using FTIR). Each curve is normalized by the maximum intensity of the pumped mode.

The pump pulse results in almost-immediate nonzero intensity in all modes of the system; two issues are responsible for this phenomenon: Given that the spectral width of the pump pulse is similar to the splitting between vibrational modes, some intensity in multiple modes is expected. Additionally, the three normal modes of each molecule share the same CO local modes, resulting in a partial distribution of the initial vibrational excitation to all normal modes of the system. Despite these two phenomena, the initial energy distribution is non-equilibrium, and thus vibrational population transfer dynamics are still observable.[118]

4.3.2 Fitting vibrational kinetics data

The frequency-domain 2D-IR technique reveals only populations resulting from the initial pump pulse. The excitation of a mode of the system to the n=1 state acts as a "vibrational label." The change in the population of each mode (due to either IVR or exchange) is equivalent to the vibrational label moving between modes. The n=1 excited states of modes A, B, and C form a three-state system.

The system can be described as a three-element vector, with each term containing the percentage of the initial vibrational label currently in that mode of the ensemble. Though a variety of processes can facilitate population transfer between states (*vide supra*), our initial treatment is mechanism-agnostic. The individual populations of these states also decay over time due to population relaxation, which couples each mode to the surrounding bath. The time evolution of this vector is described by a three-state classical master equation,[4]

$$\frac{d}{dt}\begin{pmatrix} \rho_A(t) \\ \rho_B(t) \\ \rho_C(t) \end{pmatrix} = -\left(\mathbf{T} + \mathbf{k}_{coupling}\right)\begin{pmatrix} \rho_A(t) \\ \rho_B(t) \\ \rho_C(t) \end{pmatrix} \tag{4.1}$$

Where the $\mathbf{T}$ matrix describes population relaxation and the $\mathbf{k}_{coupling}$ matrix describes population transfer between states of the system:

$$\mathbf{T} = \begin{bmatrix} \dfrac{1}{T_A} & 0 & 0 \\ 0 & \dfrac{1}{T_B} & 0 \\ 0 & 0 & \dfrac{1}{T_C} \end{bmatrix} \tag{4.2}$$

$$\mathbf{k}_{coupling} = \begin{bmatrix} 0 & k_{B \to A} & k_{C \to A} \\ k_{A \to B} & 0 & k_{C \to B} \\ k_{A \to C} & k_{B \to C} & 0 \end{bmatrix} \tag{4.3}$$

The population relaxation times, **T**, place an inherent limit on the timescale of the dynamics that can be observed and quantified: noise in the system increases as the vibrational label decays. The lifetimes of all CO stretching modes of butadiene (**1**) and cyclooctadiene (**2**) systems exhibit very similar lifetimes at all temperatures of 33 ps and 27 ps, respectively (Table 4.2).

Temp (K)	Molecule/Mode Lifetime (ps)					
	Buta A	Buta B	Buta C	COD A	COD B	COD C
288	34±4	35±4	34±4	27±3	27±3	28±3
273	30±3	30±3	31±3	27±4	28±5	27±3
253	34±2	34±2	33±2	28±2	28±2	28±2
233	33±4	34±4	33±4	28±2	28±2	29±3
213	32±3	32±3	32±3	28±2	28±2	28±2
198	34±2	34±2	34±2	28±3	27±3	28±4

Table 4.2 Vibrational Lifetimes of Iron Complexes at Experimental Temperatures

The equivalent lifetimes of the vibrations mean that a ratio of an individual kinetics curve over the sum of all curves (i.e. the fraction of the remaining overall population in that particular mode) will remove the direct effects of population relaxation and isolate the changes to the system due to population transfer (Figure 4.9).
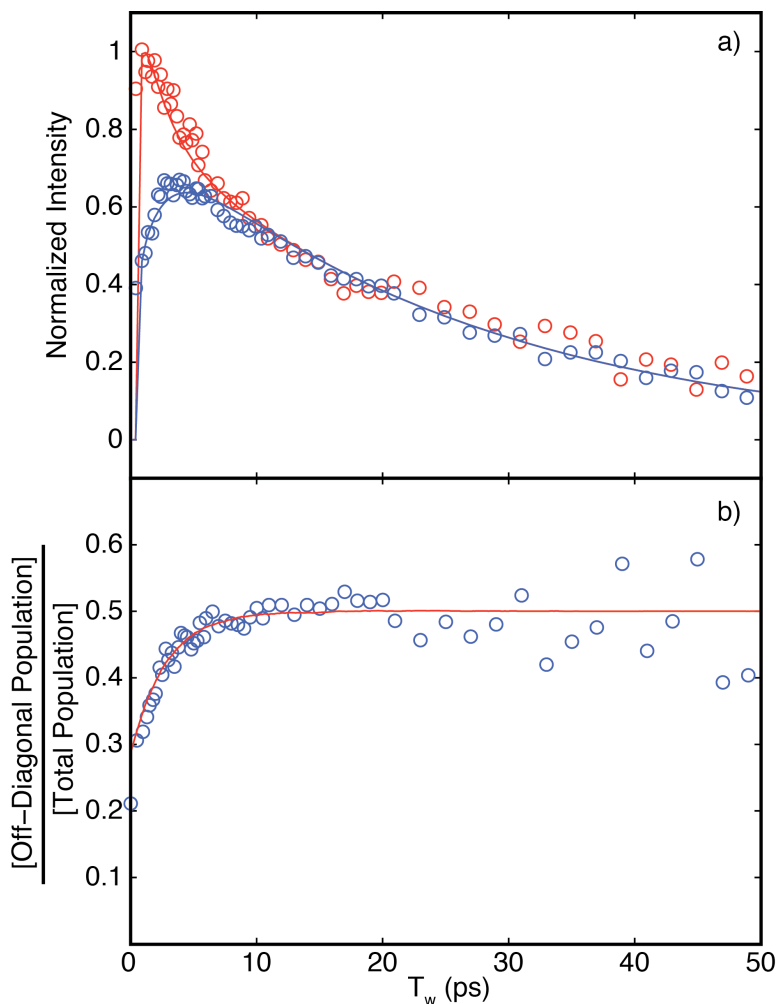
Figure 4.9 a) Kinetics data for modes A (red) and B (blue) of 1,5-cyclooctadiene complex **2** at 288 K. b) The corresponding ratio of off-diagonal population to total population as a function of time at 288 K. The red line is simulated data from equation 5. The timescale for this population transfer is 4.4 ps. Corresponding data for other temperatures appears qualitatively similar.

In the case of both systems **1** and **2**, the population of mode C established by the pump pulse shows virtually no change in magnitude due to exchange; we can deduce that only lifetime decay contributes significantly to its dynamics.[119] Thus these ratios reveal that the rates of population transfer between mode C and both modes A and B cannot be occurring faster than the order of magnitude of population relaxation (Figure 4.10).
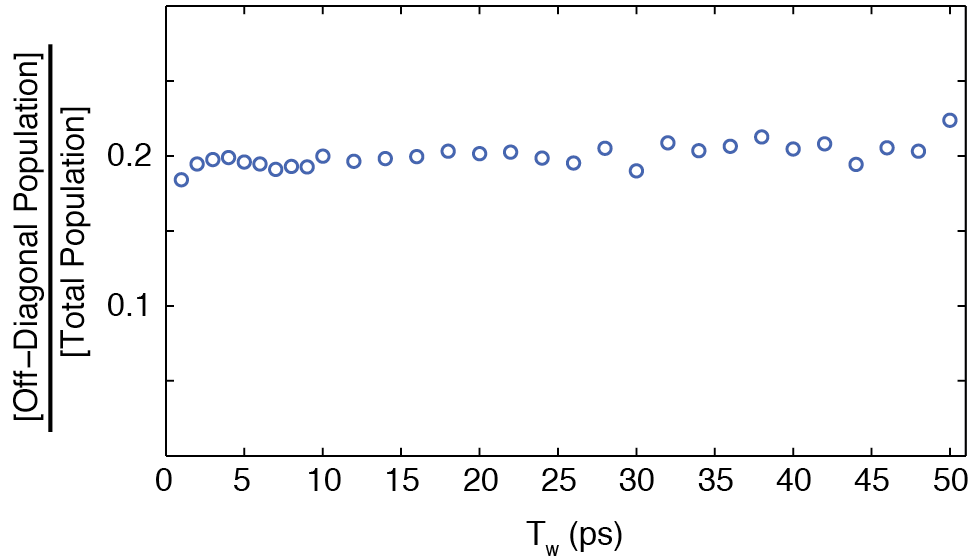
Figure 4.10 Coupling to Mode C does not occur past the first picosecond of the experiment, thus further simulations need not incorporate this behavior.

This rate is too slow to be confidently measured and too slow to contribute meaningfully to the experiment. This means that the three-state model describing the system can be simplified considerably by neglecting coupling to and from mode C.[120]

$$
\begin{bmatrix}
\dfrac{1}{T_A} & k_{B\to A} & k_{C\to A} \\[2ex]
k_{A\to B} & \dfrac{1}{T_B} & k_{C\to B} \\[2ex]
k_{A\to C} & k_{B\to C} & \dfrac{1}{T_C}
\end{bmatrix}
\approx
\begin{bmatrix}
\dfrac{1}{T_A} & k_{B\to A} & 0 \\[2ex]
k_{A\to B} & \dfrac{1}{T_B} & 0 \\[2ex]
0 & 0 & \dfrac{1}{T_C}
\end{bmatrix}
\tag{4.4}
$$

Taking the ratio of an individual population over the total population removes the effects of population relaxation; the remaining coupling between modes A and B (consistent with data in Figure 4.9) is described by this much-simplified two-state equation:

$$
\frac{d}{dt}
\begin{pmatrix} \rho_A(t) \\ \rho_B(t) \end{pmatrix}
= -
\left[
\begin{pmatrix}
0 & k_{B\to A} \\
k_{A\to B} & 0
\end{pmatrix}
\right]
\begin{pmatrix} \rho_A(t) \\ \rho_B(t) \end{pmatrix}
\tag{4.5}
$$

The population of each state at t_o is determined from experimental values. The vector is propagated using Gillespie's stochastic algorithm to produce simulated kinetics for each mode.[4,6,74] The ratio of mode intensities in the

43

theoretical system is calculated and compared with experimental ratio values. The k values are adjusted to achieve the best fit to the experimental kinetics data (Figure 4.9b). For all molecules and temperatures, the rate constants for the forward and back reactions are identical; they are summarized in Table 4.3. The master equation approach effectively replicates the observed kinetics data.

| Temp (K) | Exchange Timescale (ps) | |
	Complex 1	Complex 2
288	7±2	4.4±0.7
273	11±3	7±1
253	14±4	7±2
233	20±6	7±2
213	22±6	6±2
198	50±20	7±2

Table 4.3: Timescales for vibrational population transfer between modes of iron diene tricarbonyl systems.

4.3.3 Correlating dynamics with the temperature dependence of kinetics data

Determining these rates from the 2D-IR spectra abstracts away information and reveals the rate of population transfer between modes of the system for a given temperature. To understand each molecule's underlying behavior, we correlate the trends in vibrational coupling rates with the expected trends associated with likely coupling mechanisms.

Given the timescales of population transfer observed at room temperature, two principle phenomena could be responsible for kinetics occurring on these timescales: intramolecular vibrational redistribution (IVR) or chemical exchange (turnstile rotation). The underlying coupling mechanisms in each case are different, resulting in significantly different temperature dependencies. The temperature dependence of chemical exchange is related to the energy required for the process to occur, the activation energy, E_a. Coupling resulting from this mechanism will show exponential temperature scaling.[121] The coupling rate should then vary with temperature as:[4]

$$k_{Arrhenius} \propto e^{-E_a/k_B T}$$

(4.6)

By contrast, IVR is the quantum mechanical coupling of vibrational modes with slightly mismatched energies. Matching phonons or low frequency vibrations in the solvent account for the energy mismatch between the modes, facilitating population transfer.[122,123] As such, the rate of IVR coupling will dependent upon the availability of phonons at the splitting energy, E_p:[124]

$$k_{IVR} \propto \frac{1}{(e^{E_p/k_BT})-1}$$ (4.7)

The temperature dependences of the coupling described in equations 6 and 7 can be depicted in and extracted from an Arrhenius plot.[125] This plot of ln(k) vs. 1/(Temperature) (Figure 4.11) is expected to produce effectively linear behavior for both Arrhenius-type and IVR behavior over this temperature range. Given the possible range of E_a (>1 kcal/mol) values and the splitting between modes A and B ($E_p < 20$ cm^{-1}), the slope of a set of rates with Arrhenius-like temperature dependence should be steeper. Though the E_a values are almost an order of magnitude different between compounds **1** and **2**, the E_p for each is virtually the same.
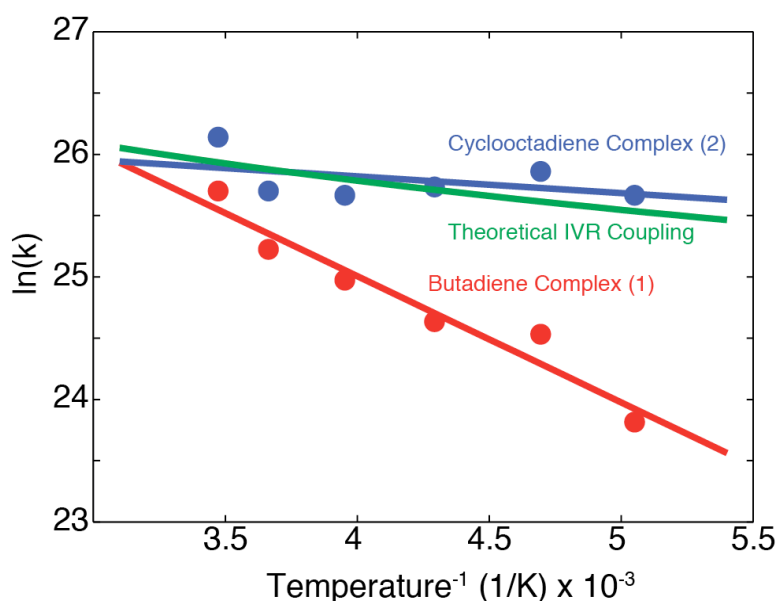
Figure 4.11 Arrhenius plots of compounds **1** and **2** depict the temperature dependence of population transfer rates for each species. Neither data set shows temperature dependence consistent with a turnstile rotation as the source of vibrational coupling.

Upon examining the Arrhenius plot, we see immediately that both compounds, as expected, show linear behavior. As we will now show, this plot also allows us to exclude chemical exchange as the mechanism behind vibrational coupling in these complexes:

Recall that butadiene complex **1** can only undergo time-dependent vibrational coupling via IVR (mechanism I). When compared with the predicted IVR coupling based purely on the ca. 10 wavenumber splitting between modes (equation 4.7), the slope of the Fe(CO)$_3$(1,3-butadiene) (**1**) complex's population transfer is far steeper. However, its population transfer rates are also too fast to be consistent with the turnstile exchange. The slope correlates with an E_a=1.7±0.5

kcal/mol, while previous isotopic labeling NMR studies agree that the barrier to CO exchange for the butadiene system is in excess of 9 kcal/mol—far too high to be experimentally observed in 2D-IR.[100,102] Turnstile exchange of the CO dipoles could not result in rates fast enough to cause of the observed coupling in this system. Some behavior in the molecule must be producing this abnormally strong temperature dependence.

The slope of the $Fe(CO)_3$(1,5-cyclooctadiene) complex's (**2**) population transfer is E_a = 0.3±0.5 kcal/mol. All previously published studies of the complex agree that the barrier to turnstile exchange is ca. 1.5 kcal/mol.[95-97,99] This temperature dependence does, on the other hand, agree well with the weak dependence predicted by an IVR-based mechanism (I). Based on this evidence, we discard turnstile exchange (II) as the source of vibrational coupling in this molecule.

The source of population transfer in both complexes **1** and **2** is intramolecular vibrational relaxation (IVR). However, we need not stop here; though we have dismissed turnstile exchange as the source of population transfer in both complexes, there is still the temperature dependence of the butadiene complex **1** to explain.

We will now demonstrate a simple model of wagging motion in these complexes accurately predicts two key features of the observed population transfer: (1) The energy scales and temperature dependencies of population transfer between modes A and B. (2) The lack of dynamical coupling to high frequency mode C in each system.

4.3.4 Density functional theory modeling

Our model of each mechanism is based upon density functional theory calculations of the geometries, energies, and torsional motion of each complex. The results from density functional theory calculations are consistent with previous experimental studies of both compounds. The calculated transition state energy for the turnstile rotation of tricarbonyl(1,3-butadiene)iron was found to be 9.3 kcal/mol (versus ca. 9.5 kcal/mol as determined experimentally.)[102] The calculated energy for turnstile transition state energy of tricarbonyl(1,5-cyclooctadiene)iron was found to be 1.0 kcal/mol (versus the ca. 1.5 kcal/mol range resulting from applications of the optical Bloch equations.)[96,99] In both cases, the results agree with experimental values within the errors associated with DFT—particularly given the tendency of DFT to underestimate transition state energies.[126] It is worth noting that the interpretations of both Grevels et. al. and Strauss concur on a ca. 1.5 kcal/mol barrier.
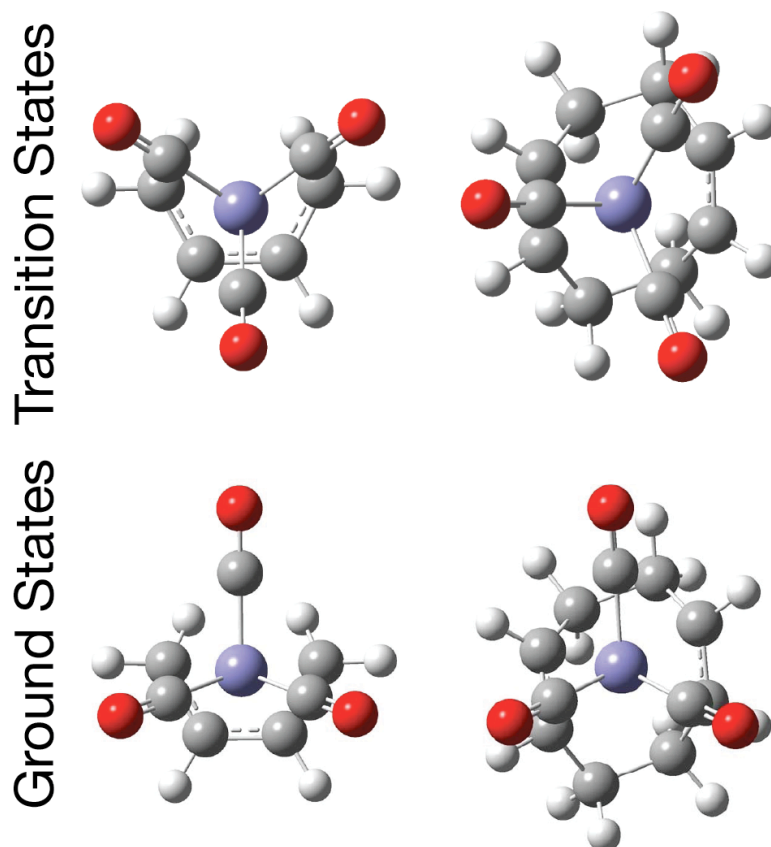
Figure 4.12 DFT calculated structures of tricarbonyl(1,3-butadiene)iron (left) and tricarbonyl(1,5-cyclooctadiene)iron (right) ground and transition state structures.

At this point, we note that the differing symmetries of the diene moieties results in different boundary periodicities. The 1,5-cyclooctadiene ring maintains C_2 symmetry when bonded to the metal center. This difference in symmetry means that the CO ligands of the cyclooctadiene complex (**2**) need only rotate 60° to reach the next global minimum energy geometry. Without this C_2 symmetry relative to the torsional CO motion, tricarbonyl(1,3-butdiene)iron has a lower periodicity to its rotational potential. As a result, the carbonyl ligands of complex **1** must rotate 120° to reach the next minimum energy geometry.

4.3.5 Wagging motion describes the temperature dependence

In previous experiments, the phenomenon of IVR coupled to low-frequency torsional motions has been described.[107,108] The lowest-frequency torsion in this family of piano stool complexes is the wagging motion of the carbonyls previously emphasized by Strauss as the source of coalescence behavior.[97] Torsionally coupled vibrational population transfer results from the overlap between the modes of the system in the perturbed geometry. As such, we expect the energy scale of that perturbation to agree with energy scale of the observed temperature dependence.[6,99]

Strauss described a simple model of the wagging motion that, on the timescale of picoseconds, perturbs the energy of the system.[97,104-106] He described this motion with the torsional Hamiltonian,

$$H_T = \frac{1}{2}I\dot{\theta}^2 + \frac{1}{2}E_{TS}(1 - \cos(m\theta)) \tag{4.8}$$

Where I is the moment of inertia of the $Fe(CO)_3$ moiety, E_{TS} is the barrier height, and m is the multiplicity of the barrier. This neglects the more subtle distortions of the molecule, but forms a good qualitative description of the system. When the hindered three-CO system is solved, the root mean square deviation from the middle of the potential well can be approximated by,[104]

$$\theta_{RMS} = \sqrt{\frac{\hbar}{4\pi Ic\nu_t}\coth\left(\frac{h\nu_t}{2k_BT}\right)} \tag{4.9}$$

Where ν_t is the frequency of the wagging torsional vibration. The E_{TS} of the system is incorporated into the equation via this frequency, and the mean deviation is the result of calculating the thermal distribution of energy among the modes of the hindered rotor. (Mean deviation, rather than the average position, is calculated because the symmetrical nature of the well means that the average position is at $\theta=0°$ for all temperatures.)

To compare this angular deviation with the slopes from the Arrhenius plot, we use the potential energy portion of the Hamiltonian to approximate the equivalent of E_a for this wagging motion. When we insert the thermally averaged deviation into the potential term of the Hamiltonian, the energy associated with this distortion varies as,

$$E_{RMS} = \frac{1}{2}E_{TS}(1 - \cos(m\theta_{RMS})) \tag{4.10}$$

E_{TS} values are ZPE-adjusted barrier heights from our DFT calculations. The potential energy of the perturbed ("wagged") geometry of each complex is depicted in Figure 4.13.
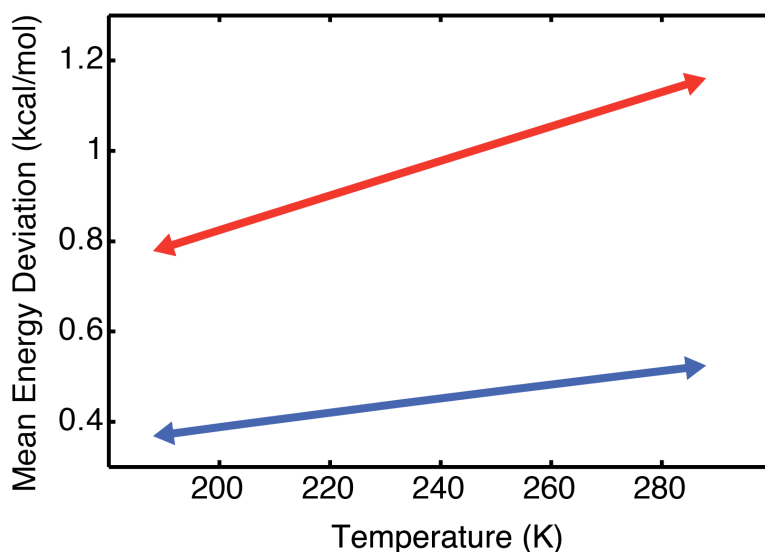
Figure 4.13 Energies associated with structural perturbations due to wagging motions in compounds **1** (top, in red) and **2** (bottom, in blue).

For the purposes of our calculations, the variation in the energy as a result of the temperature is less than the errors in the slope extracted from the Arrhenius plot, and can be safely neglected. This simple description accurately predicts the approximate energy scale of the temperature dependence for both complexes: The butadiene complex **1** exhibits a slope on the Arrhenius plot of ca. 1.7 kcal/mol versus ca. 1 kcal/mol as predicted by this very simple wagging model, and cyclooctadiene complex **2** exhibits a slope ca. 0.3 kcal/mol versus the model's ca. 0.4 kcal/mol.
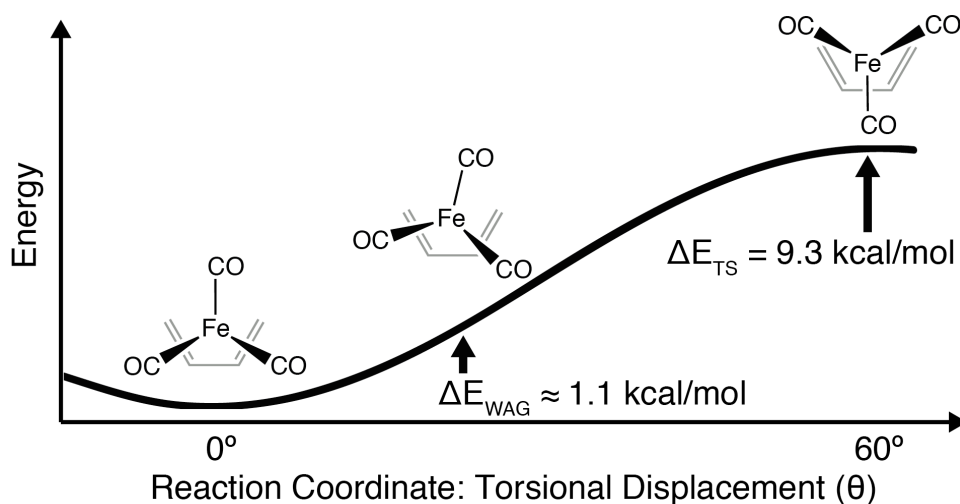
Figure 4.14 Average deviation in wagging displacement of the butadiene complex (**1**) displayed on the potential energy surface, relative to the calculated transition state energy.

This correlation between wagging energy and temperature dependence (Figure 4.14) provides support for the torsionally coupled IVR designation. However, this simple model does not describe the apparent lack of significant population transfer to high-frequency mode C. We next explore the molecular symmetry of the complexes and find the source of this pattern.

4.3.6 Wagging motion describes the coupling pattern

Understanding the observed pattern of population transfer requires a description of the relationship between the normal modes and the geometry of the metal complex. The language of chemical group theory provides a context to do this. For cases in which the system undergoes significant motion on the timescale of the experiment, we expand beyond rigid point groups to consider the molecular symmetry group. This group contains additional symmetries from experimentally-accessible motions within the system.[127] Recall that the wagging motion described by Strauss and the turnstile exchange described by Grevels and Turner are both motions along the same reaction coordinate.[95-99] This motion has the effect of adding a C_3 axis to the vibrations of the carbonyls.

When the CO stretching modes of the system are considered in the context of group theory, the qualitative description matches the observed kinetics data: Mode C is symmetrical with respect to the C_3 axis, and remains a normal mode of the system regardless of any torsional motion the moiety undergoes. Modes A and B, however, cease to be normal modes of the system when the mirror plane of symmetry is broken (Figure 4.15).
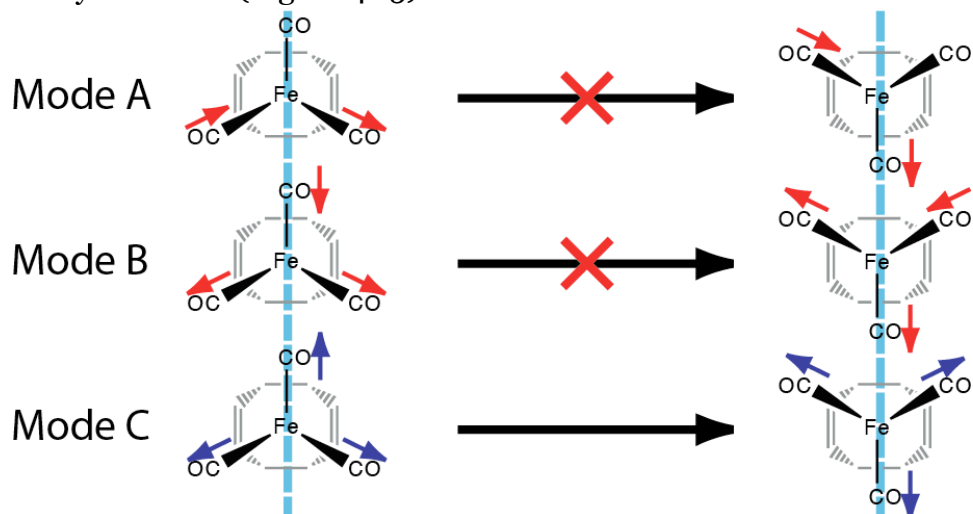
Figure 4.15 Only the high-frequency mode (C) of a piano-stool geometry complex remains unaltered by a torsion that breaks the mirror plane of symmetry.

As the molecule moves away from its ground state, equilibrium geometry, the A and B modes are no longer orthogonal. As a result, population transfer between these modes is enhanced.

To further describe the expected vibrational coupling pattern as a result of distortion to this geometry, we use the mode projection description of coupling due to intramolecular motion.[6,99] The probability of any ground state mode transferring its energy to a perturbed state mode provides the relationship between observed coupling and the rate of the motion:

$$\mathbf{k}_{coupling} = (\mathbf{P}_{coupling} - 1) k_{motion} \tag{4.11}$$

This probability matrix, $\mathbf{P}_{coupling}$, can be calculated by the method of mode projection. This provides the framework necessary to correlate a geometric change with an associated coupling of vibrational modes.[6,99] As the molecule moves away from its ground state, equilibrium geometry, the mirror plane of symmetry in the molecule is broken. The normal modes that that previously characterized the motions of the CO ligands are no longer orthogonal. A new set of normal modes, which consist of a different linear combination of individual CO stretches, will be formed based upon the energy in each local oscillator.

This probability matrix, $\mathbf{P}_{coupling}$, can be calculated by the method of mode projection. A given normal mode of the initial geometry (e.g. mode A) is decomposed into its component local CO vibrations:

$$|A\rangle = \sum_{j=1}^{3} |CO_j\rangle\langle CO_j|A\rangle \tag{4.12}$$

These vibrational amplitudes are projected onto the vibrations of the final geometry:

$$|A\rangle = \sum_{n=1}^{3} |n_f\rangle \sum_{j=1}^{3} \langle n_f|CO_j\rangle\langle CO_j|A\rangle \tag{4.13}$$

$$|n_f\rangle \in \left\{|A\rangle, |B\rangle, |C\rangle\right\} \tag{4.14}$$

The probability of intensity moving from one vibrational normal mode of the initial state to a normal mode of the final state (n_f) via a particular intermediate geometry is calculated:

$$P_{n_f \leftarrow n_i} = \left| \sum_{j=1}^{3} \langle n_f|CO_j\rangle\langle CO_j|n_i\rangle \right|^2 \tag{4.15}$$

Using the ground and transition state geometries calculated by DFT, we perform this calculation to qualify the coupling between normal modes as a result of C_3 motion:

$$\mathbf{P}_{coupling}^{butadiene} = \begin{bmatrix} 0.20 & 0.80 & 0.00 \\ 0.81 & 0.19 & 0.00 \\ 0.00 & 0.00 & 1.00 \end{bmatrix} \tag{4.16}$$

$$\mathbf{P}_{coupling}^{cyclooctadiene} = \begin{bmatrix} 0.25 & 0.74 & 0.01 \\ 0.74 & 0.23 & 0.03 \\ 0.01 & 0.03 & 0.96 \end{bmatrix} \tag{4.17}$$

The experimental kinetics data agree with the results from mode projection: population transfer occurs between modes A and B, but these two modes are not expected to show any significant exchange with high-frequency mode C.

Thus, though the temperature dependence of population transfer rates clearly indicates that chemical exchange is not the mechanism, motion along the same reaction coordinate is responsible for increased coupling between modes A and B. This facilitates IVR between the modes. Though whether IVR in complex **2** is torsionally coupled remains ambiguous, the lack of equivalent coupling to mode C in that system provides some evidence to confirm this hypothesis.

4.4   Summary and conclusions

Temperature-dependent 2D-IR spectra, in conjunction with DFT calculations, have elucidated the behavior of tricarbonyl(η^4-diene)iron complexes. The vibrational population transfer rates and their temperature dependence for tricarbonyl(1,3-butadiene)iron (**1**) were consistent with the mechanism of torsionally-coupled intramolecular vibrational redistribution. The population transfer of the tricarbonyl(1,5-cyclooctadiene)iron complex (**2**) is also consistent with IVR, not chemical exchange, as the mechanism. The degree to which torsional motion plays a role in this process is extrapolated from the behavior of complex **1** and the lack of transfer to high-frequency mode C.

Though 2D-IR could not be used to directly observe chemical exchange in tricarbonyl(1,5-cyclooctadiene)iron, the DFT studies performed indicate that the application of the optical Bloch equations to this system results in an accurate measure of the barrier height associated with chemical exchange of the carbonyl ligands. We expected that turnstile exchange is happening on the picosecond timescale. However, the rate of torsion-coupled IVR is faster, and thus population transfer in 2D-IR spectra is dominated by this term. In light of this result, we recommend that the default assumption should not be that exchange is the only, or even the principle, source of broadening.

Temperature-dependent 2D-IR reveals the wagging motion of the carbonyl ligands, and relative rates make obvious the reaction coordinate associated with that motion. These measurements can be accomplished even when there is effectively no probability of observing the ligands undergoing site exchange. Perturbed geometries, many of which are significantly populated near room temperature, need to be taken into account. Any time the symmetry of the molecule is broken by a low-frequency motion, there is the potential for enhanced vibrational coupling between modes. In a variety of multicarbonyl systems undergoing exchange, this interpretation can mitigate previous discrepancies between temperature dependence and observed population transfer rates. The capacity of temperature-dependent 2D-IR to observe equilibrium fluctuations in small molecules, even in the absence of a barrier crossing, can greatly enhance our knowledge of equilibrium behavior.

5 Theoretical studies of relaxivity in HOPO complexes

5.1 Introduction

Magnetic Resonance Imaging has quickly become one of the most popular medical imaging modalities, in part due to its safety and the absence of ionizing radiation. Many scans rely upon metal complex contrast agents to alter the relaxation time of aqueous protons and ultimately improve signal to noise. This property of altering relaxation rate is called "relaxivity," and it is the chief measure of the quality of a contrast agent. Two kinds of MRI exist: those based on enhancing T_1 relaxation, and those based on modifying T_2. The requirements of effective agents for each mode are different, but they can often be based on a similar underlying ligand structure.[7-9]

These agents scale poorly with increases in field strength that are otherwise very beneficial in the clinic: the move towards 120 MHz MRI leads to a drastic reduction in relaxivity of current contrast agents. Optimization and modification to produce a new generation of agents is necessary.[7] Though the Solomon, Bloembergen, and Morgan equations provide the connection between structure, kinetics, and relaxivity in a general sense,[11-14] the details of structure and dynamics necessary to possess a true understanding of a structure is ambiguous. Behavior that might be relatively facile to characterize in other systems, such as the number of waters coordinated to a metal center, remain up for debate in the realm of contrast agents.[8]

DFT provides the opportunity to produce very accurate descriptions of the inner coordination sphere of the metal complex. Though the collective dynamics of water exchange are most likely much more complicated, we can develop an understanding of the number of coordination sites, energy of solvation, and equilibrium geometry that fulfills three goals:[8,10,17-19,128-131] First, these calculations provide information to contrast with values that could be determined experimentally only with great difficulty. Second, they offer the opportunity to characterize the structure of a compound without the need for a crystal structure that may not be an accurate description of the compound in solution. Finally, they could potentially reveal compounds with water exchange energies low enough to be studied via 2D-IR.

Developing an approach for theoretically treating contrast agents requires a reasonable set of molecules to compare. The compounds studied can be divided into two groups: (1) variants of commercially-available DTPA- and DOTA-based chelators paired with gadolinium(III) centers,[7] and (2) HOPO-based ligands as

developed by the Raymond group, with both Gd(III) and Fe(III) centers for T_1 and T_2, respectively.[132-135]

5.2 Methods

Beginning from an underlying basis of HOPO-and-cap geometry, new variations of ligands are developed in the Raymond group. These structures are then simulated using density functional theory to predict the hydration number and energy, the key characteristics necessary to gauge their usefulness as further targets for development as contrast agents.

5.2.1 Synthesis

DTPA and DOTA chelators were purchased commercially; HOPO ligands were synthesized by my collaborator, Dr. Sylvie Pailloux, following the approximate approach of previous Raymond group syntheses (Figure 5.1). The approach is irrelevant to the ultimate success of the theoretical study, and is thus not explained in detail here. Further description can be found in a variety of Raymond group papers, as the development of the ligands has been in process for two decades.

Described generally, this approach follows the route of producing the six-membered HOPO ring, attaching the ancillary moieties, and then finishing the chelators by attaching three of these ligands together in a tripod geometry using a TREN (tris(2-aminoethyl)amine cap.

Once the chelators was finished, it was complexed over a period of several days at room temperature with the appropriate metal ion salt ($Fe(Cl)_3$ or $Gd(Cl)_3$, respectively) to produce the final product.
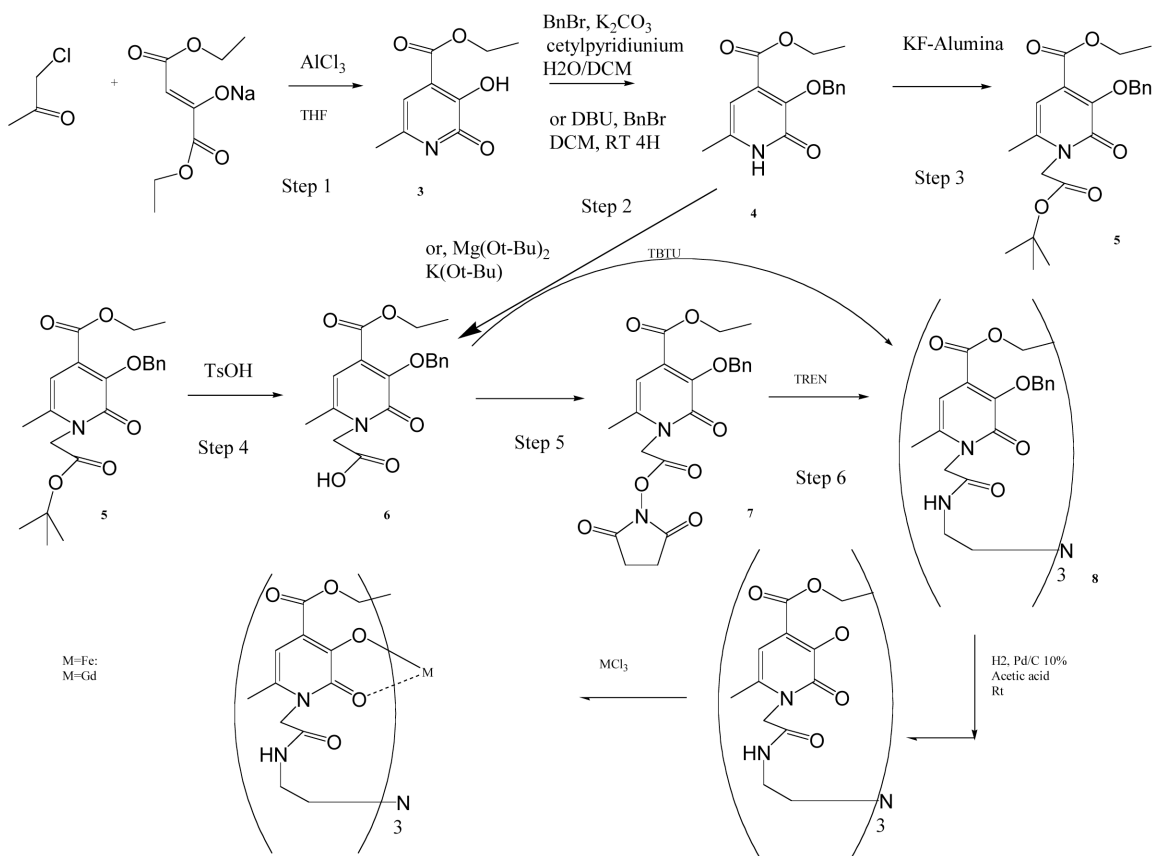
Figure 5.1 Synthetic scheme summarizing the creation of "bottom capped" HOPO chelators. The trio of chelators are synthesized individually, then united by the capping moiety.

5.2.2 Crystallographic characterization

The crystal structures of individual chelating arms (that is, a single HOPO) were characterized, but ultimately proved relatively unrelated to the final structure of the coordinated complex in solution. An individual HOPO molecule, by dint of its highly conjugated structure, is effectively flat. As we shall see, only the orientations of the flat HOPO molecules relative to one another become meaningful.

Crystal structures of the completed chelators, either as a complete metal complex or alone, could not be acquired. Historically, Raymond group complexes are significantly difficult to study via this method. Among other things, this is a source of the motivation to undertake DFT studies.

All further complex characterization was carried out by my Raymond group collaborator, Piper Klemm.

5.2.3 ICP Studies

Confirmation of the complexation of metals can be challenging, as neither mass spectrometry nor NMR are feasible once the high-spin-multiplicity metal center has been added. Instead, exact Gd(III) (or Fe(III)) concentration was determined by Inductively Coupled Plasma-Optical Emission Spectroscopy (ICP-OES). ICP-OES was performed on a Perkin Elmer Optima 7000 DV. Following rinsing to remove any uncomplexed metal salts, samples for analysis were diluted in 2% (v/v) nitric acid in Millipore water. Gd(III), Dy(III), Tb(III), and Yb(III) standards were prepared in 2% (v/v) nitric acid/Millipore water with concentrations between 0.01 and 10 μg/mL.

5.2.4 Relaxivity studies

T_1 and T_2 measurements were performed on a Bruker mq60 minispec relaxometer. T_1 and T_2 were determined at 60 MHz (1.41 T) using an inversion recovery pulse sequence. Temperature controlled at 37 °C using a Julabo F25 circulating water bath. Each sample was normalized against ICP-OES data for exact metal concentration. Relaxivity analyses were performed in triplicate (three samples) and averaged. Samples were vortexed prior to analysis to break up potential aggregation of complexes at 37 °C.

For T_1, the inverse of the longitudinal relaxation time of each sample ($1/T_1$, s⁻¹) was plotted against metal concentration (μM) and fit by linear regression (R² > 0.99).

Instrument Parameters: Scans: 4; Recycle Delay: 18.5 s; Gain: 53; Dummy Shots: 0; Detection mode: real; Bandwidth: Broad, 20,000 kHz; Monoexponential Curve Fitting, Phase Cycling. First Pulse Separation: 5 ms; Final Pulse separation: 18,500 ms, Number of data points for fitting: 20; Delay sample window: 0.05 ms; Sampling Window: 0.02 ms; Time for Saturation Curve Display: 6 s.

T_2 measurements were performed on the same Bruker relaxometer. T_2 was determined at 60 MHz (1.41 T) using an inversion recovery pulse sequence. Temperature controlled at 37 °C. The inverse of the longitudinal relaxation time of each sample ($1/T_1$, s⁻¹) was plotted against metal concentration (μM) and fit by linear regression (R² > 0.99).

Instrument Parameters: Scans: 4; Recycle Delay: 18.5 s; Gain: 53; Dummy Shots: 0; Detection mode: real; Bandwidth: Broad, 20,000 kHz; Monoexponential Curve Fitting, Phase Cycling. Delay sample window: 0.05 ms; Sampling Window: 0.02 ms; Time for Saturation Curve Display: 6 S.Pulse Separation: 1.000 ms. Data Points: 200. Monoexponential Curve Fitting, Phase Cycling.

5.2.3 DFT Studies

Given the difficulty in obtaining crystal structures of these compounds, density functional theory calculations using the Gaussian09 package were instead conducted. Crystal structures of the similar complexes were obtained from the Cambridge Crystallographic Database. These structures were modified and used as the initial estimates for optimization. For both complexes, the UB3LYP hybrid density functional was used with the 6-31g(d,p) basis set for hydrogen, carbon, nitrogen, and oxygen atoms. The metal centers were described by basis sets that include effective core potentials, in order to reduce the computational complexity of the optimizations while retaining the correct geometries and valence electronic structure. In the case of the Fe complex, the LanL2DZ basis set was used, which includes the effective core potential of Hay and Wadt. In the case of the Gd complex, calculations utilized the Stuttgart potential and ECP with 53 core electrons incorporated into the pseudopotential.

In order to describe the effects of the outer solvent shell molecular cavity on the energy and geometry of each complex, all calculations included a polarizable continuum model of water, ε=78.3553.[75-88,126]
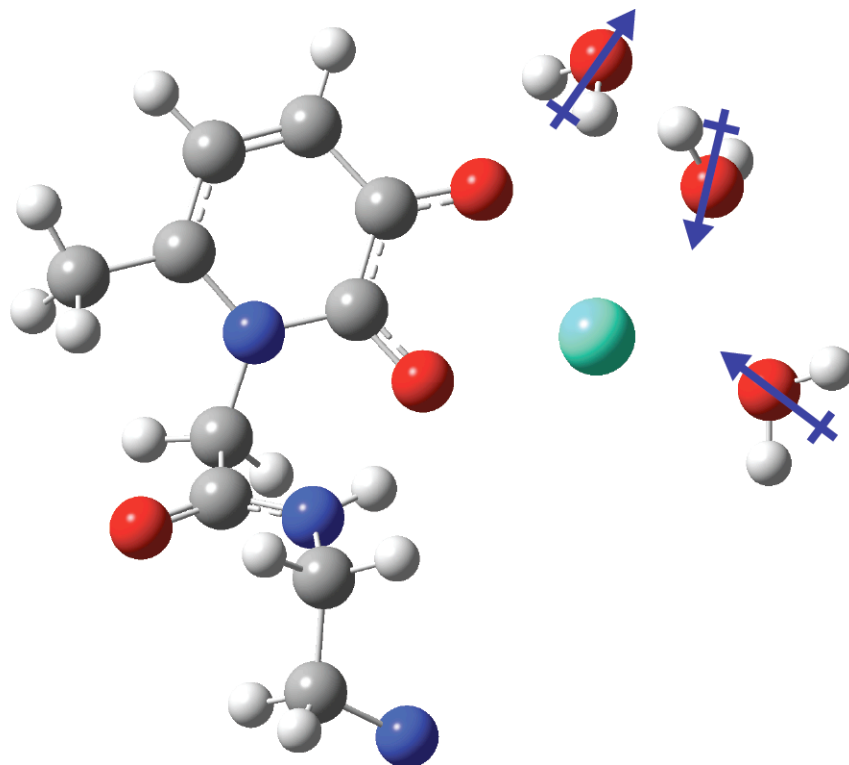
Figure 5.2 Cross-section of Gd-HOPO complex; two of the three chelating arms have been removed. Water molecules (right) are added until they no longer bind to the inner sphere of the metal center (teal) (as determined by the water molecule dipole relative to the metal center). In this figure, the bottom two solvents are complexed to the inner sphere, while the top remains outer-sphere.

To determine the number of inner-sphere waters for each complex, additional water molecules were added to each system, and the geometry reoptimized, until subsequent water molecules exhibited Gd-O and Fe-O distances and dipole orientations consistent with outer-sphere water molecules (Figure 5.2). Most notably, inner-sphere water molecules align to allow donation of their lone pairs to the electron-deficient metal center. Outer-sphere water molecules align 180° opposed, with the electropositive hydrogen molecules attracted to electron-dense metal center.

The energy of the system was then compared with the energy of the system if the water molecule is at infinite distance from the metal center; this comparison yielded the exchange energy.[17,18]

5.3 Results and discussion

Broadly, the work in this experiment can be divided into two categories: creation of a novel MRI contrast agent, and the novel analysis of it using density functional theory and in comparison with current commercially available agents. Discussions of the synthetic details of the study are available elsewhere in the publications of the Raymond group. In considering the details of the theoretical simulation, we study the relaxivity and compare its implied water exchange values with those determined via DFT.

5.3.1 Characterization

Recall that the key value to be optimized is relaxivity per metal center; as each contrast agent in this study has only one metal per molecule, relaxivity is defined by the change in relaxation rate following the addition of the contrast agent, given by the equation:[13]

$$r_i = \frac{\Delta(1/T_i)}{[\text{Contrast Agent}]} \tag{5.1}$$

For further details of the basis of relaxivity, see chapter 2. The relaxivity of an agent can be determined in any NMR, or via a simpler, specialized instrument: the relaxometer.

However, before considering the details of novel compounds, it's first necessary to consider the values associated with currently available, commercial compounds (Table 5.1). In considering these values, recall that the Solomon, Bloembergen, and Morgan equations explicitly include temperature and field strength—and indeed, these considerations are accurate descriptions of clinical phenomena. In spite of this, the standard in the field for many years was to report relaxivity values at low field strengths (10 MHz) and non-physiological temperatures (25°C). As such, the values found in Table 5.1 reflect highly optimistic measurements that do not necessarily reflect the clinical reality.[7]

Commercial Compound	r_1 (mM^{-1}s^{-1})
Gd(DTPA)(H$_2$O)	3.8
Gd(DOTA)(H$_2$O)	10.6

Table 5.1   Relaxivity values for commercial MRI contrast agents at 10 MHz and 25°C; note that these values decrease with increasing field strength and increasing temperature, rendering them impotent at current clinical conditions. DOTA has surpassed DTPA in popularity due to its higher kinetic and thermal stability (not listed) in addition to its relaxivity.[7]

In the past five years, the MRI field has shifted to reporting values at physiological values and clinically relevant field strengths. As such, the values for these compounds are listed at these new conditions. Even an initial glace demonstrates that the HOPO chelators are drastically superior.

Compound	r_1 (mM^{-1}s^{-1})	r_2 (mM^{-1}s^{-1})	Compound	r_1 (mM^{-1}s^{-1})	r_2 (mM^{-1}s^{-1})
Gd-TREN-*tris*-1-(Me)-3,2-HOPO	8.02±0.02	11.9±0.1	Fe-TREN-*tris*-1-(Me)-3,2-HOPO	1.74±0.02	12.69±0.05
Gd-N-TREN-*tris*-6-(Me)-3,2-HOPO-4-(ethyl ester)	8.9±0.9	12.7±0.2	Fe-N-TREN-*tris*-6-(Me)-3,2-HOPO	1.7±0.1	8.5±0.2

Table 5.2   Relaxivity values for relevant Raymond group compounds, measured at 60 MHz and 37.1°C in pH 7.2-7.5 millipore water. Further enhancements in relaxivity are achieved when the chelators are coupled to appropriate macromolecules.

That the Raymond group complexes can routinely surpass clinical contrast agents at the new, more strenuous conditions is attributed principally to two features:[9,132-136] (1) looser water binding that allows for faster exchange, and (2) the ability to directly bind to twice as many waters as clinical agents. Further details of this behavior will be discussed in the theoretical results section.

Though the majority of MRIs performed take advantage of T_1 relaxivity shifts, there has been an increased interest recently in development of T_2 agents for the clinical setting. The key feature in these is not so much a high T_2 relaxivity value (though this is, of course, invaluable), but more particularly both a high T_2 relaxivity and a *low* T_1 relaxivity.[137-141] As such, the high-T_1, Gd-based contrast agents are inappropriate. However, systems based on Fe(III) centers have been found to be relatively effective. In the case of this "bottom-capped" chelator, this is again the case.

Next, the task is to develop DFT models of these many-electron molecules that can accurately replicate the observed behavior, and draw conclusions as to the properties of the molecules from those structures.

5.3.2 Density functional theory results

The relaxivity of paramagnetic compounds is well-described by the Solomon, Bloembergen, and Morgan equations. These equations correlate structural effects with the relaxivity of a system. Given the goal of optimizing the relaxivity and placing the bottom-capped TREN system in a theoretical framework, thorough understanding of the geometry and dynamics of the system in solution is significantly valuable.

The key values to determine, as described previously, are water-proton-to-metal distances and binding energies. Determining water exchange rates is difficult, and requires specialized ^{17}O-NMR techniques.[16] This becomes particularly challenging because many potential contrast agents, particularly in the absence of solubilizing macromolecules (as are frequently used in clinical applications), have low water solubilities that render signal-to-noise a serious concern. Instead, water binding energy is used as a stand-in.

Even more problematically, determining the proton-to-metal distance is effectively impossible, as proton positions cannot be effectively measured using X-ray crystallography without access to extremely high-energy photons. This difficulty is added on top of the general challenge of crystallizing these large complexes, which has proven infeasible in the past.

Therefore, it behooves us to develop a theoretical description of each system that can potentially capture much of the relevant behavior. Though molecular dynamics simulations had previously been used to characterize the structure of MRI contrast agents in solution, this approach is ultimate ineffective for determining inner-sphere binding energies that involve the interaction of a variety of valence electrons that are not explicitly simulated at the MD level. Though DFT suffers in attempting to simulate large volumes of solvent and long-distance interactions, it should be spectacularly effective at determining the inner-sphere interactions that largely dominate T_1 relaxivity effects.

To provide context to the calculations of Raymond group HOPO complexes, I began by calculating (with the same basis sets and density functional) the structures of commercially available agents based on DTPA (diethylene triamine pentaacetic acid) and DOTA (1,4,7,10-tetraazacyclododecane-1,4,7,10-tetraacetic acid).

Top   Side
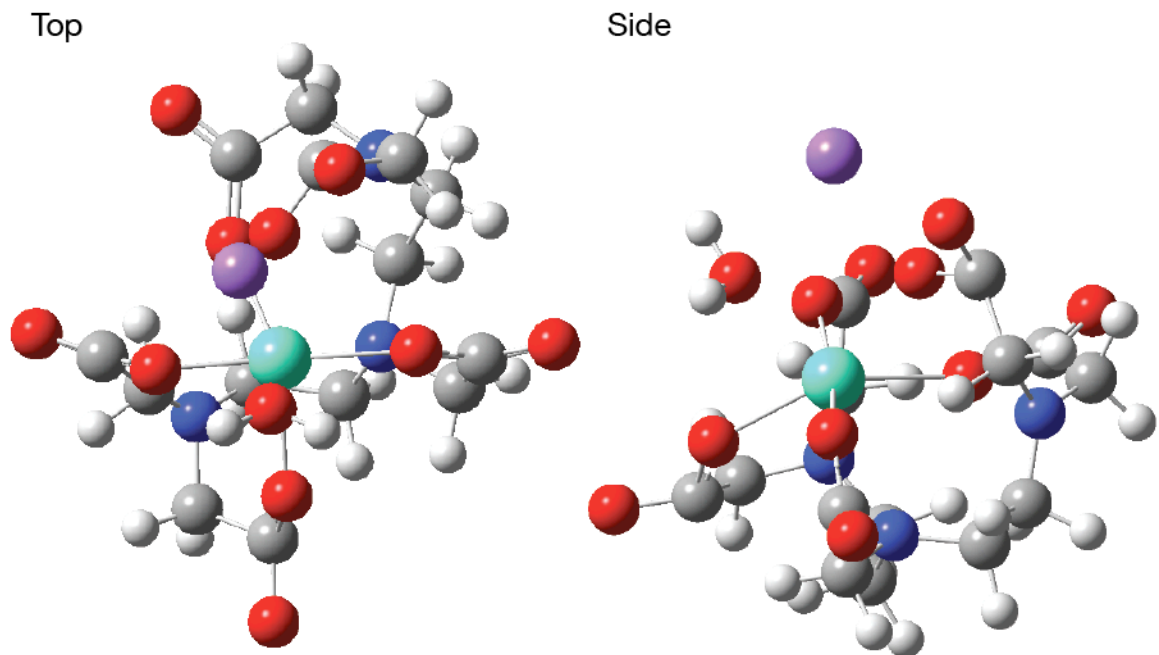
Figure 5.3 Calculated Gd-DTPA structure with inner-sphere water molecule and Na⁺ counterion. Note that DTPA is not a ring- or claw-type chelator, but rather a chain that vaguely resembles a peptide fragment—with an associated lower binding affinity.

The structure of the Gd-DTPA complex displays roughly the "two-tiered" shape expected, with an "inner" tier of nitrogen donors and an "outer" tier of oxygen donors. Though the inner tier has C_3 symmetry, the outer tier has C_4 symmetry. This system is also inherently a weak base, and deprotonates in the buffered solutions of an experiment or the human body. As such, it is accompanied by an additional Na⁺ ion to balance the charge.
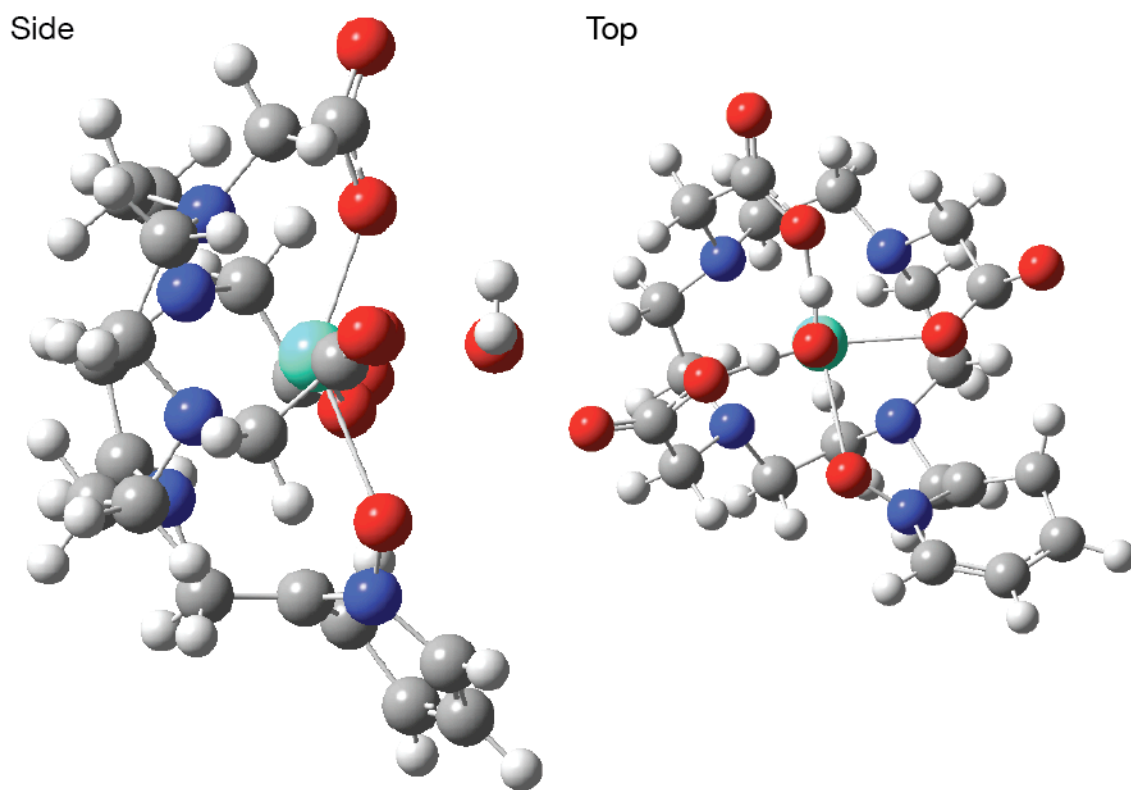
Figure 5.4 DFT structure of Gd-DOTA (with additional ring) contrast agent with inner-sphere water molecule; note the bowl-like pocked for N- and O-donors that grasp the Gd(III) center.

The Gd-DOTA complex, alternately, has C_4 symmetry to both N-donor and O-donor rings, and supports a rigid cavity that is much more carefully selected to the Gd(III) center. Like Gd-DTPA, its q value is 1. Notably, this molecule is so stable that Gd(III) ions are lost from the center with a rate constant on the order of millennia—effectively, so long as the chelator exists, the metal will remain bound.

In the case of both systems, the water binding energies are significantly higher—matching experimental values on near 13 kcal/mol.[7] Water binding distances were typically in line with expected values as well, on the order of 3 Å. These distances, in particular, are expected to fluctuate highly with low-frequency breathing modes of each system. As such, specific values are likely to be imprecise. Likewise, the thermal energy of the system is significantly large, and the inner-sphere waters are perturbed in energy significantly. As such, these values are necessarily approximate.

From this starting point, I moved into calculations of the behaviors of HOPO-based complexes with a higher degree of ambiguity in their behavior. Notably, these molecules are larger than the commercial agents, with far more electrons and many more degrees of nuclear motion (particularly in the TREN linker). In the past, high-level DFT calculations of their structures would have been prohibitively time consuming for the potential knowledge that could be gained.
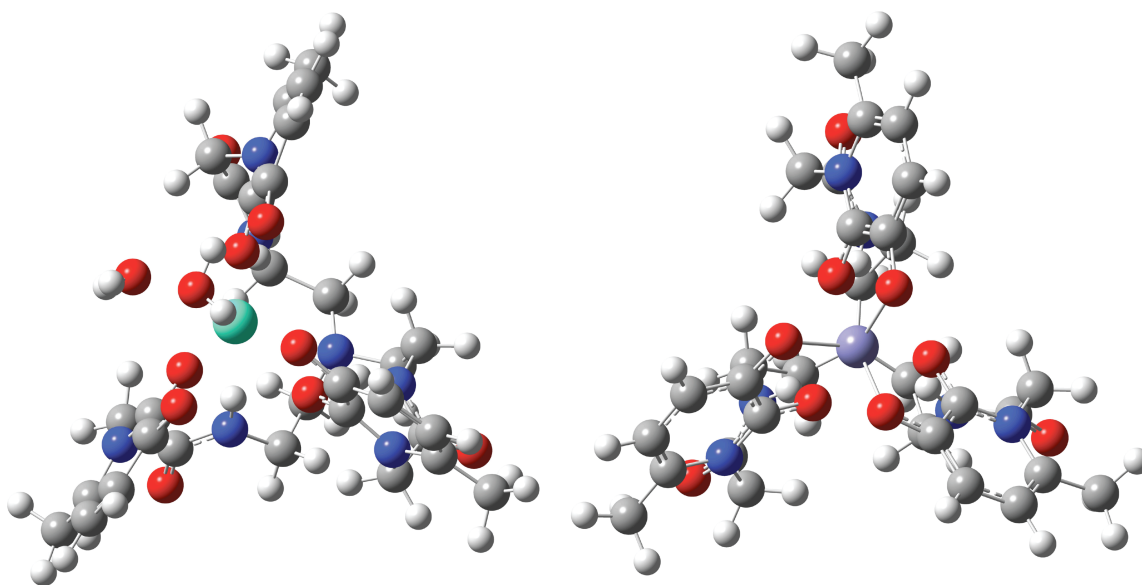
Figure 5.5 Top view of optimized HOPO contrast agent structures. Note that the Gd complex (left) has two inner-sphere water molecules, while the Fe complex (right) has no open coordination sites for solvent. Additionally, note that the C_3 symmetry of the Fe(III) system is absent in the Gd(III) case; a tetra-HOPO chelator could close all binding sites (and result in C_4 symmetry).

As of the time of calculation in 2010-11, however, continued progress in computational hardware development has made detailed density functional theory studies of large Gd-*HOPO* systems feasible in time periods much shorter than would be necessary to achieve a high-quality crystal structure. Additionally, given the critical importance of understanding the interaction between the metal center and the hydrogen atoms of coordinated water molecules, the difficulty in locating electrons via traditional x-ray diffraction is a major barrier to complete understanding of the hyperfine interaction.[19,128,130]

The spin multiplicity of a given metal center is critical to the calculation of the theoretical relaxivity; the unrestricted density functional allows this value to fluctuate freely. The iron system, as might be expected, was found to exist principally in a singlet state, while the gadolinium complex forms an octet. This is likely due to a partial breaking of the orbital symmetry that gadolinium normally exhibits (with 11 unpaired electrons).

Though previous work cast some doubt on the assignment of *q* values of compounds similar to those synthesized in this paper, the results of our calculations allow the definitive assignment of *q*=0 and 2 for the iron and gadolinium complexes, respectively. The Gd-O distances were 2.533 Å and 2.497 Å, respectively, which is consistent with inner-sphere coordination for these complexes. By comparison, the oxygen donors of the HOPO ligands themselves were, on average, at a distance of 1.93 Å in the Fe(III) system and 2.47 Å in the Gd(III) system. In the gadolinium case, the waters clearly take on a geometry that is analogous to that of the HOPO ligands, and provide a roughly equivalent amount of electron density.

There were no reasonable local minima found associated with higher *q* values for either complex. Addition of any further water molecules consistently resulted in the addition of those molecules to the outer coordination sphere, with hydrogen atoms facing the metal center and M-O distances of 3.672 Å and 3.857 Å for iron and gadolinium, respectively; these values are significantly beyond those of inner-sphere water molecules.

By comparing each structure with an additional, independent water molecule (i.e. at r=∞) in a polarizable continuum, the energy of coordination for each inner-sphere water can be ascertained (Figure 5.6). These values were determined to be 11.9 kcal/mol for the first water and 8.1 kcal/mol for the second. (Given the predicted dissociative mechanism of water exchange, this "second water" binding energy is the relevant value; the complex will never simultaneously dissociate both waters.) These values are comparable to the values determined in ^{17}O exchange experiments (8.9 kcal/mol in studies of other Raymond group complexes.) They are also consistent with fast water exchange in many previously published compounds.
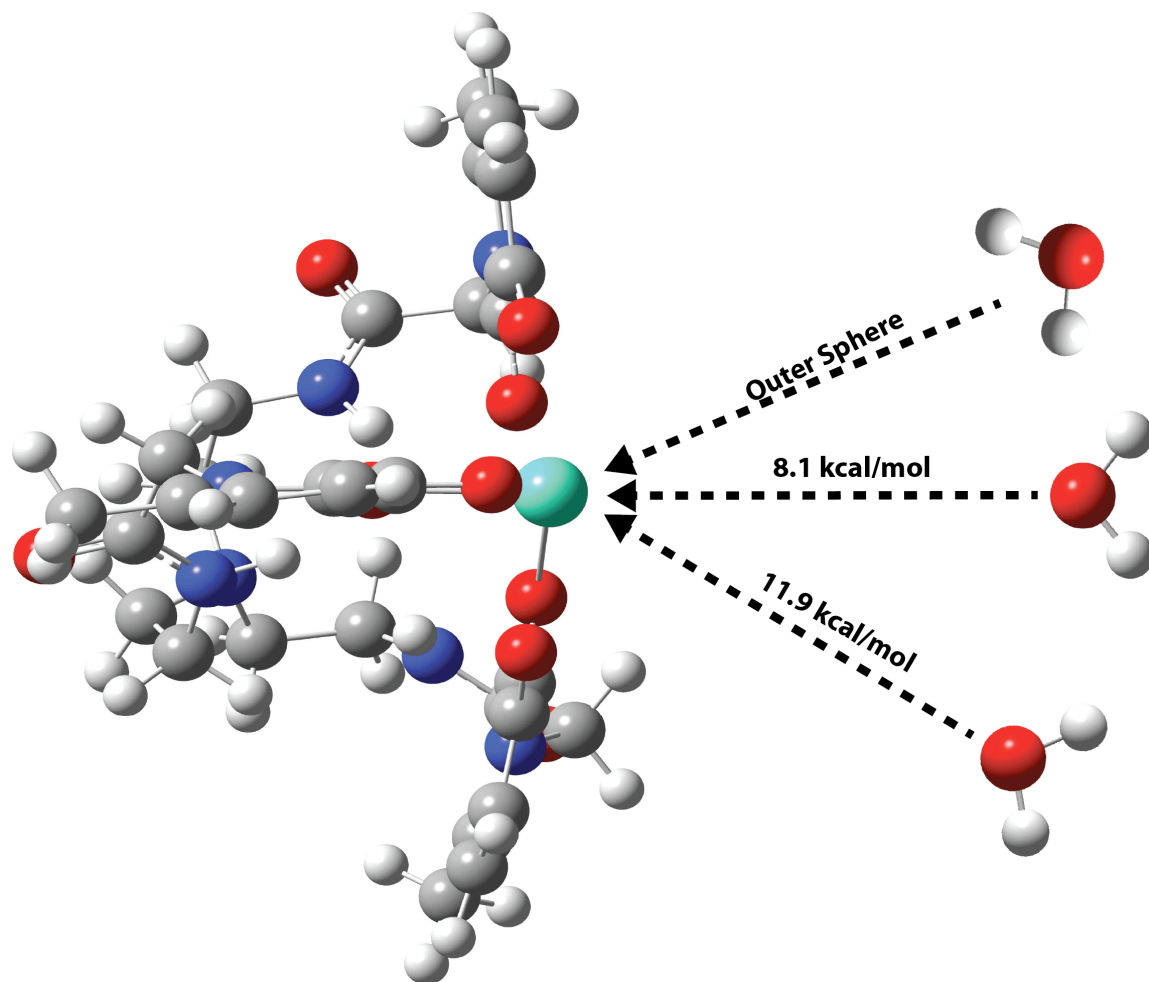
Figure 5.6 Schematic representation of water binding calculation with the converged Gd-HOPO structure from the side. Additional water molecules were added sequentially until they no longer bound to the inner coordination sphere.

Given that all further values for calculation of relaxivity rely on literature values, we can make direct comparisons between the binding distances, numbers, and energies of these systems as a proxy for comparisons of relaxivity. In effect, the Raymond group compounds are expected to exhibit significantly higher relaxivity values due to the larger number of bound waters (q=2), the lower water exchange barrier (8.1 kcal/mol vs. ca. 13 kcal/mol), and the similar metal-to-proton distances.[7]

5.4   Summary and conclusions

The Raymond group successfully synthesized a "bottom-capped," TREN tris-HOPO chelator that dramatically outperforms commercially available MRI contrast agents in measures of relaxivity. This system was characterized using density functional theory, and the water exchange barriers were accurately determined to be lower than those of the commercial agents. This accuracy means that further calculations can be performed in a predictive capacity to determine the potential use of as-yet-unsynthesized contrast agents. Ultimately, this directed synthesis is a critical feature of future investigations due to both the time-consuming nature of ligand synthesis, as well as the environmental concerns associated with unnecessary chemical reactions.

On a somewhat disappointing note, though the water exchange rates of this system are predicted to be on the very fast edge of the NMR timescale, and certainly very much faster than commercial compounds, they are nonetheless three orders of magnitude too slow to be directly observed via 2D-IR spectroscopy. Though fast water exchange of a loosely-bound inner sphere water would be a fascinating process to observe at thermal equilibrium, and certainly a clinically-relevant one in the case of these contrast agents, it nonetheless remains a scientific fantasy.

6 Time-resolved IR of charge transfer states in heterobimetallic systems

6.1 Introduction

Coordination metal complexes are more than homogeneous catalysts; they can also serve as useful models to further the development of more durable heterogeneous systems. Artificial photosynthesis, and particularly the reduction of CO_2 to CO and O_2, has proven to be a particularly challenging problem.[3,20,22,26,142] A single, optimal catalyst has yet to be designated (in comparison to the dominance of CoO catalysts for water reduction, as demonstrated by Nocera and coworkers.[143,144])

However, recent work using catalysts with multiple, different metals (so-called heterobimetallic systems) have shown promise. The added tunability of being able to adjust effective both halves of a redox interaction separately means that the most appropriate choice, in terms of potential, can be made.[142] Of the many combinations tried, perhaps the most useful has been the cobalt-zirconium pairing. In some solid-state systems, cobalt-zirconium surface catalysts have been constructed with oxygen bridges (Figure 6.1).[28,145,146] Further study into the precise behavior of these Co-Zr systems is warranted.
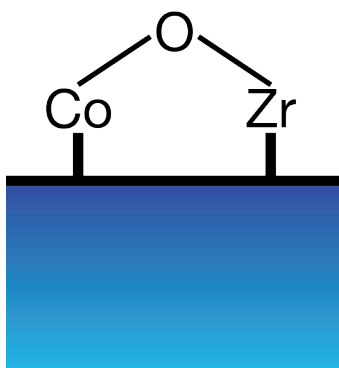
Figure 6.1 Cobalt-zirconium catalyst bridged by an oxygen atom that has shown activity in reducing CO_2.

In contrast with the surface-based systems, Christine Thomas's group at Brandeis university has developed a series of Co-Zr heterobimetallic complexes that do not require a bridging ligand to facilitate the interaction of their electrons; rather, these systems feature a direct metal-metal bond.[29-33,63,147-149] (In fact, some of the shortest metal-metal bonds ever recorded.) The complex is

easily synthesized, and the Zr-N and Co-P bonds are rigidly controlled by hard-soft acid base interactions, so the complex self-assembles with very little "synthetic oversight."

Given the similarity to surface systems, but with the much higher degree of interaction between centers, the catalytic behavior of this system promised to be fascinating—and novel. As expected, the complex can cleave CO_2 into a carbonyl and oxo-bridge ligand very effectively, without an overpotential, at room temp, in solution. The C_3 symmetry of the complex can be restored by silylation of the oxo-bridge, or by a variety of other methods (Figure 6.2).[31]
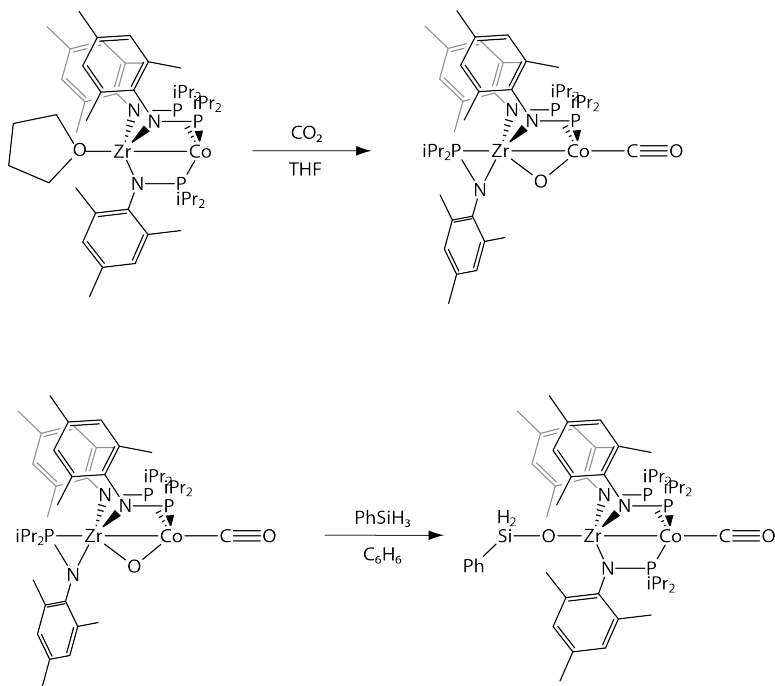
Figure 6.2 Co-Zr heterobimetallic complexes split CO_2, and appear good candidates for a model CO_2 reduction catalyst.

However, actually *completing* the catalytic cycle requires removing the CO ligand to prepare the complex to interact with another CO_2 molecule. This is where the system exhibited troubling behavior. CO ligands are typically quite labile. Under UV/visible irradiation, many metal complexes develop metal-to-ligand charge transfer (MLCT) states that facilitate the dissociation of the CO ligand. Instead, these heterobimetallic systems showed remarkable resilience to irradiation, as well as a variety of chemical approaches to removing the carbonyl ligands (Figure 6.3).[31]
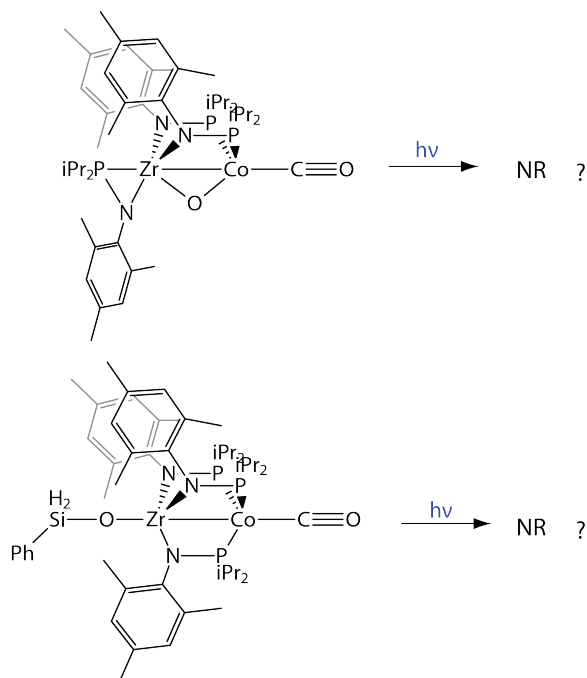
Figure 6.3 Photolysis of the carbonyl ligand does not occur, even under intense UV irradiation.

Nonetheless, the molecules are definitely absorbing the light. Ergo, some charge transfer state must be forming that protects the complex, absorbing and dissipating the excitation. Understanding the nature of this protective charge transfer state could facilitate the development of new ligands that complete the catalytic cycle.

As described in Chapter 2, the carbonyl ligand is an excellent probe of the electronic state of the system. Because previous work has shown that the CO ligand is never lost, it will remain a reliable probe of the behavior of the cobalt ion throughout the experiment; from this information, I intuit the behavior of the entire complex.

6.2 Methods

Understanding the photophysics of heterobimetallic complexes involves first synthesizing the necessary amounts of each complex (>1.6 g), followed by TR-IR spectroscopy and DFT to confirm the vibrational frequency of each molecule.

6.2.1 Synthesis

The cobalt-zirconium complexes are not commercially available, and degrade on a week timescale. Some initial studies were performed with material obtained from my collaborator Jeremy Krogman in Christine Thomas's group; further samples were synthesized by my undergraduate student, Molly Ryan.

The overall scheme of the synthesis is described in Figure 6.4, while the subsequent reduction and CO_2 activation is shown in Figure 6.5. Given the importance and simplicity of the reaction, I will also describe the complete method of synthesis undertaken by Molly Ryan. This can be subtly adapted for different desired ancillary ligands.
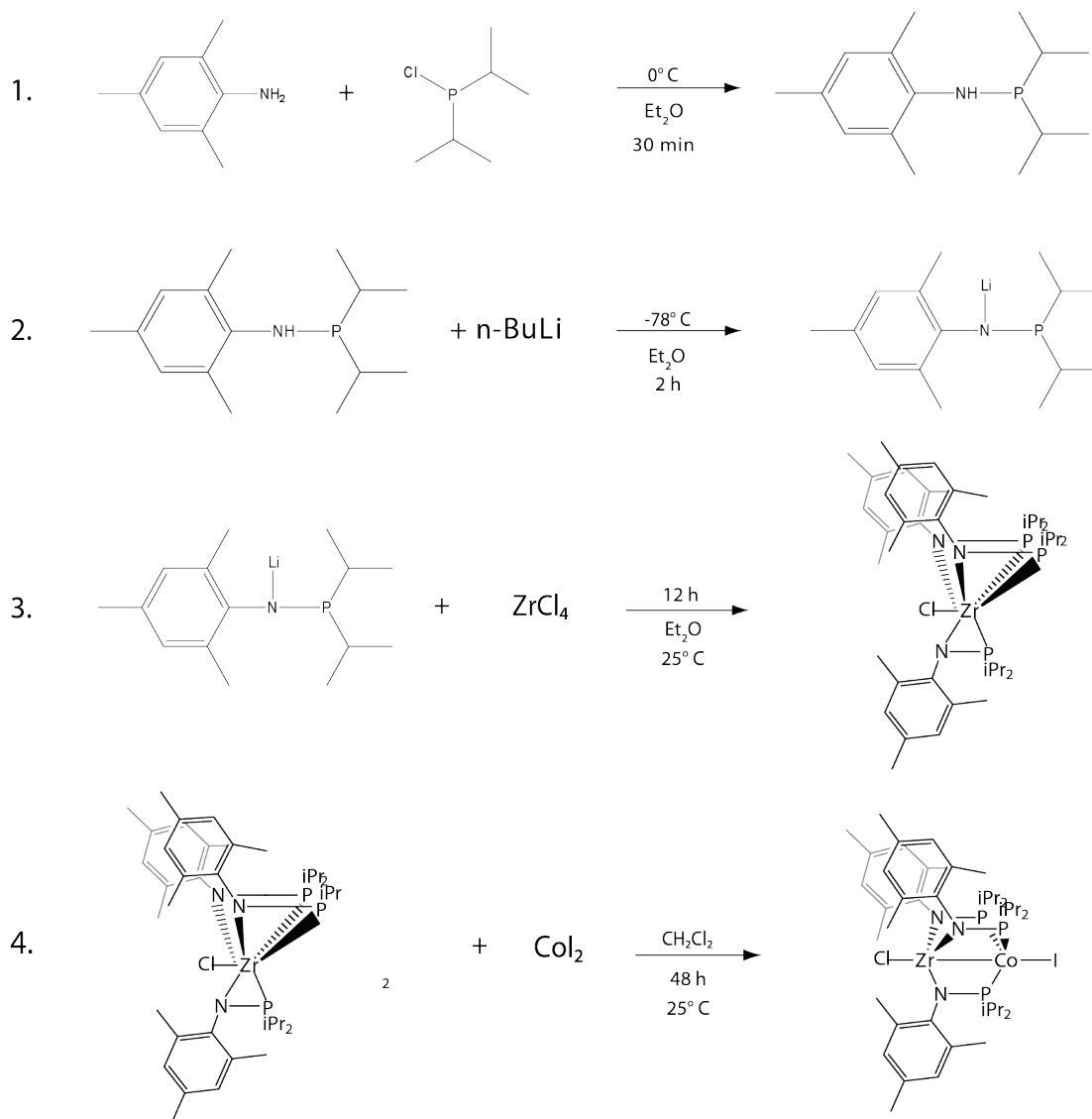
Figure 6.4 Ligand synthesis and metal complexation reactions necessary to create the initial Co-Zr heterobimetallic complex. Note that the ligands are relatively simple, and enforce geometry in the system via hard-soft acid-base interactions.
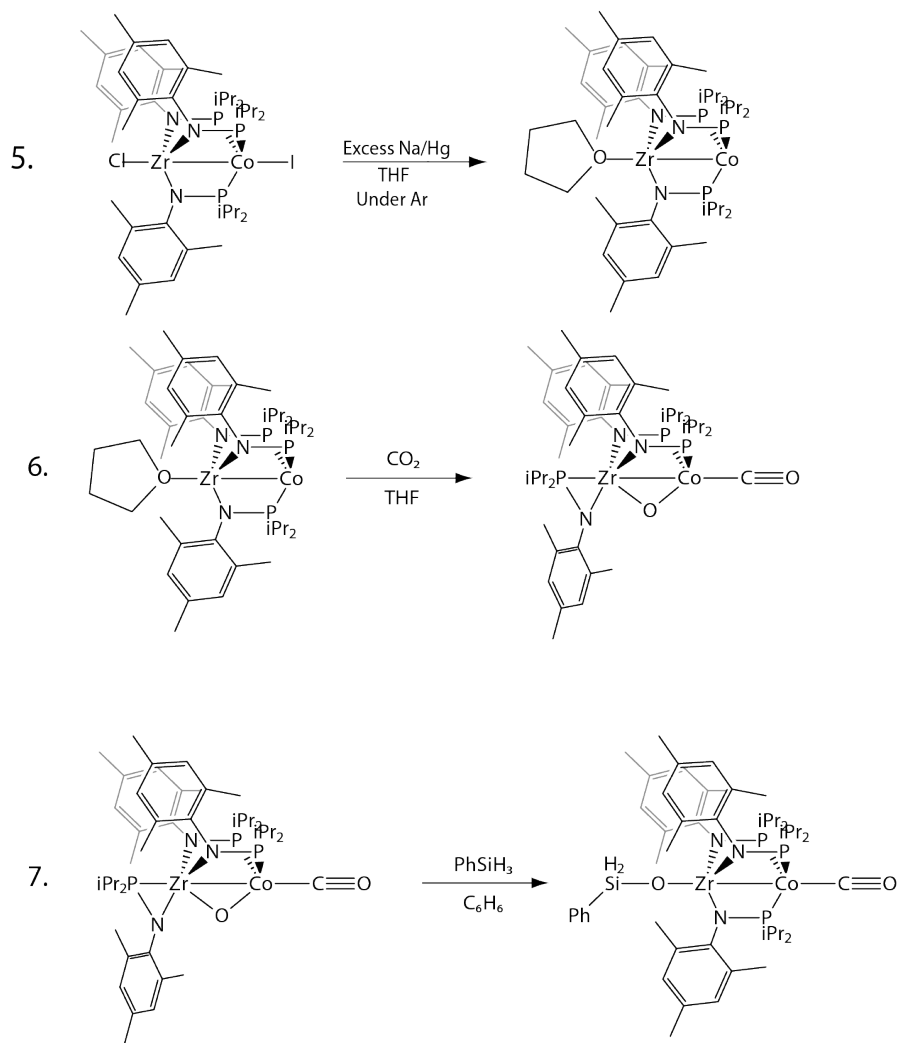
Figure 6.5 Reduction of the complex by mercury amalgam renders it ready to reduce CO_2. The structure of the complex can be restored by silylation or by trace water and irradiation.

The creation of the ligand begins with a solution of 2,4,6-trimethylaniline (5.00 g, 37.0 mmol) in Et_2O (100 mL), which was cooled to 0 °C in an ice bath. To this was added ^nBuLi (25.0 mL, 1.6 M in hexanes, 40.7 mmol) drop-wise over 20 minutes. The resulting solution was allowed to warm slowly to room temperature, resulting in the formation of a white precipitate, then refluxed for 30 minutes to ensure complete reaction.

The resulting suspension was added, drop-wise, to a stirring solution of $^iPr_2PCl$ (5.88 mL, 37.0 mmol) in Et_2O (100 mL) at −78 °C (dry ice/acetone bath). When warmed slowly to room temperature, the mixture became slightly yellow with a white LiCl precipitate. After stirring for 1 h, the reaction mixture was filtered through a pad of Celite (diatomaceous earth) (~1 cm), and solvent was removed from the filtrate *in vacuo*. The resulting oily residue was redissolved in

Et$_2$O and filtered through a plug of silica gel. Removal of the solvent *in vacuo* yielded the desired intermediate, MesNHP^{i}Pr$_2$, as a yellow oil.

This yellow oil was dissolved (1.046 g, 4.162 mmol) in Et$_2$O (50 mL) and cooled to −78 °C. To this was added ^{n}BuLi (2.6 mL, 1.6 M in hexanes, 4.2 mmol) drop-wise over 10 min. The resulting yellow/orange solution was warmed to room temperature and stirred for 2 hours. The solution was then cooled again to −78 °C, and ZrCl$_4$ (0.323 g, 1.39 mmol) was added as a solid. The reaction mixture was warmed to room temperature and stirred for 12 hours. Volatiles were removed from the solution *in vacuo*, and the resulting solids were extracted with CH$_2$Cl$_2$ (30 mL) and filtered through a pad of Celite to remove the LiCl. The volume of the filtrate was reduced to 10 mL *in vacuo*. The resulting supersaturated solution was layered with pentane and cooled to −35 °C to yield analytically pure colorless crystals of the zirconium complex.

Crystals of the zirconium complex (1.641 g, 1.87 mmol) and solid CoI$_2$ (0.585 g, 1.87 mmol) were combined in CH$_2$Cl$_2$ and stirred for 48 hours at room temperature. The resulting bright green solution was filtered through Celite, and solvent was removed from the filtrate *in vacuo*. The remaining green solids were washed with copious amounts of pentane and dried *in vacuo* to yield the pure heterobimetallic complex as a bright green solid.

A 0.5% Na/Hg amalgam was prepared in THF (10 mL) from 7.0 mg Na (0.30 mmol) and 1.4 g Hg. To this vigorously stirred amalgam was added a solution of ICo(MesNPiPr$_2$)$_3$ZrCl (0.129 g, 0.121 mmol) in THF (2 mL). The solution gradually changed color from a light green to an intense dark green. After two hours of stirring, the resulting green solution was filtered away from the amalgam and the volatiles were removed *in vacuo*. The remaining green solids were extracted into pentane (5 mL) and filtered through Celite. Removal of volatiles from the filtrate resulted in analytically pure THF-complexed molecule as a green microcrystalline solid

A solution of (THF)Zr(MesNPiPr$_2$)$_3$Co (0.1734 g, 0.1734 mmol) in THF (10 mL) was placed in a Schlenk tube equipped with a stir bar and sealed with a Teflon valve. The blue-green solids were dissolved in argon-sparged THF. The solution was frozen, then the headspace of the flask was evacuated and backfilled with 1 equivalent of CO2 using a known-volume gas bulb and partial pressure methods. The Schlenk tube was sealed and the solution was allowed to thaw. The reaction was stirred for approximately 10 minutes, until the color of the reaction mixture changed from blue-green to yellow. Solvent was removed from the resulting mixture *in vacuo*. The remaining solids were washed with pentane to give an pure yellow/green solid.

A ca. 5 mM solution of this complex was produced with THF for spectroscopic interrogation.

6.2.2 Ultrafast spectroscopy

The Harris group's ultrafast TR-IR apparatus, as described in Chapter 3, was used to determine both the time-dependence and polarization-dependence of the excited state(s) of the complex in solution. This is notably challenging, given both the relative air sensitivity of the species (theorized) and the fact that the CO absorbance is adjacent to a mid-IR peak of the THF solvent. It should be noted that acyclic solvents have the danger of either (1) not solvating the complex or (2) protonating the amine and destroying the molecule. Though the THF peak is challenging, it is ultimately less obfuscating than the equivalent modes from molecules such as benzene or toluene, and was thus tolerated.

6.2.3 Density functional theory

To confirm the identity of the chemical species associated with various excitations in the system, density functional theory calculations of both the oxo-bridged and alcohol complex were conducted using the BP86 density functional with a 6-311g** basis set for the main-group elements and the LANL2DZ effective core potential/basis set for the zirconium and cobalt ions.[75-88,126]

Though time-dependent DFT calculations (TD-DFT) to understand the charge transfer state were complicated, the large size of the molecule and the significant number of electrons made the computational cost of this approach untenable. Further computational developments within the decade should mitigate many of these concerns, but for the moment, understanding of the excited state is effectively the realm of spectroscopy.

6.3 Results and discussion

The goal of this project is to characterize the charge transfer state, be it metal-to-metal or metal-to-ligand, and understand the way the molecule's structure determines the property of that state.[55,150-156] I begin by characterizing the more basic properties of the complex, via UV/Vis and FTIR spectra.

6.3.1 Linear spectroscopies

UV/Vis and FTIR spectra were taken of the complex in solution pre- and post-ultrafast interrogation, in part to confirm the identity of the compounds in solution, and also to calibrate the frequencies of visible and mid-IR light used in the apparatus.
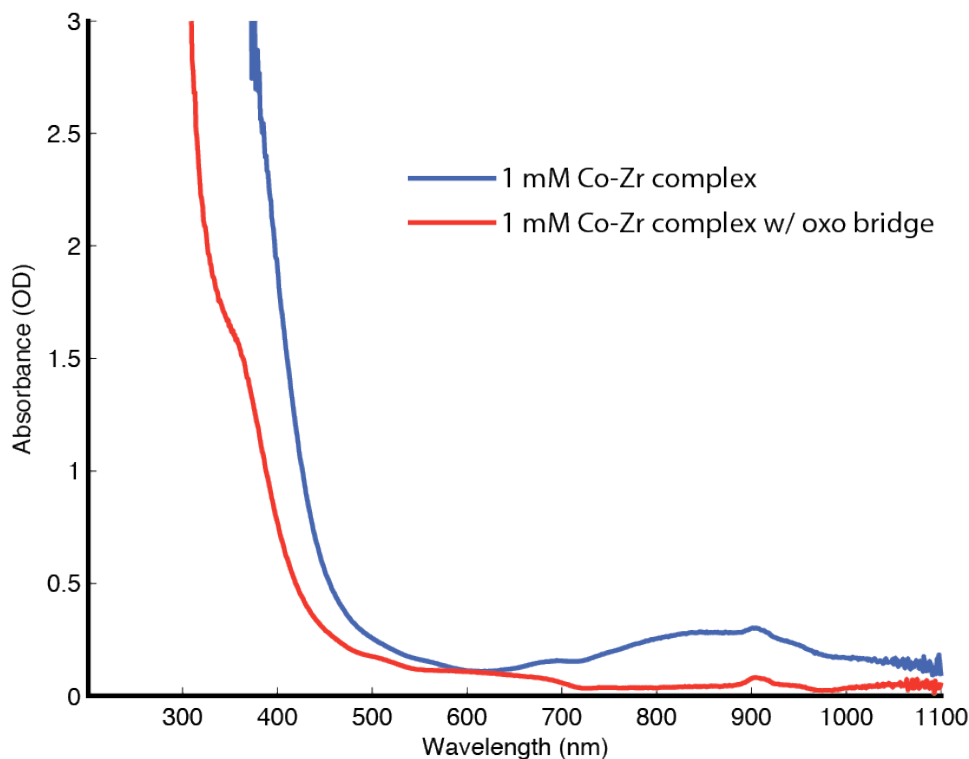
Figure 6.6 UV/Vis spectrum of Co-Zr complex at 0.1, 1, and 10 mM concentration.

The solution of the heterobimetallic complex, even at low millimolar concentrations, appears to be completely black. The UV/Vis spectra of the solution corroborate this appearance, with broad absorbance in the blue; however, the frequency of this absorbance is not specific enough to allow it to be definitively identified as either a MMCT or MLCT.[55,150,154,157-162]

Note that there is significant absorbance at both 267 and 400 nm; this is also found in later TR-IR experiments, as the system shows identical response to either UV or blue irradiation. As such, most experiments were conducted with 400 nm light. The experimental apparatus produces 400 nm light far more effectively, making it an excellent choice for improving signal:noise, all other things being equal.
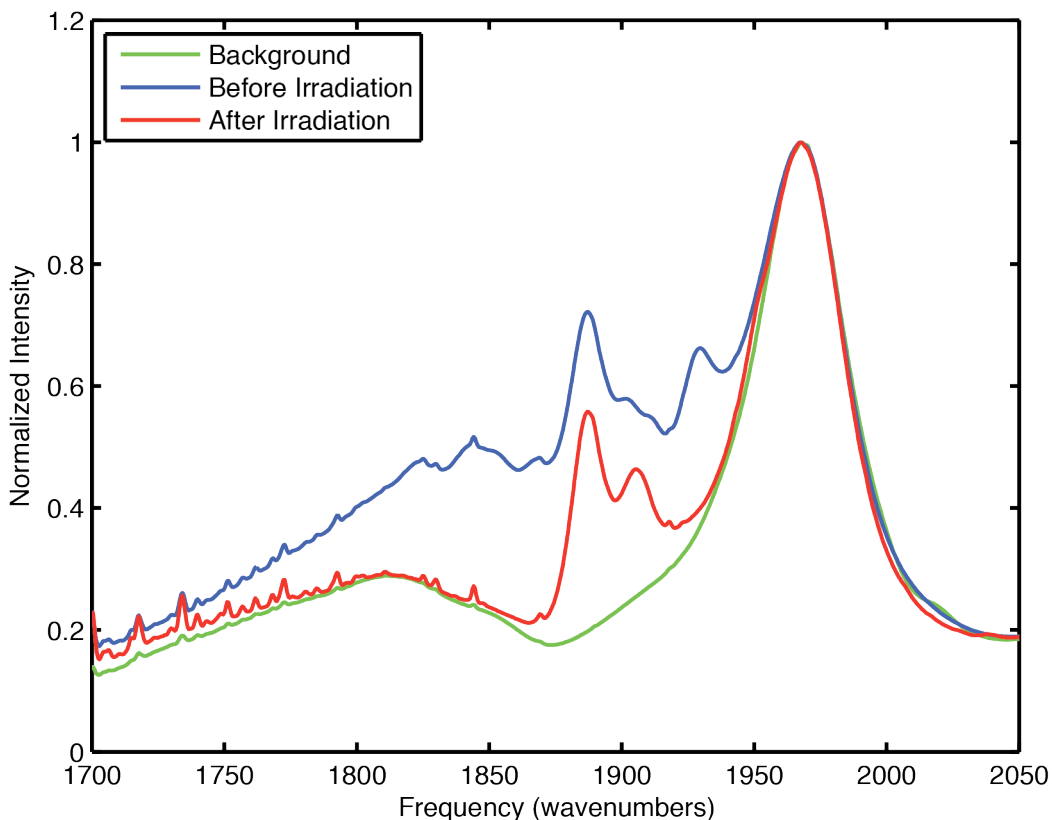
Figure 6.7 FTIR spectrum of THF, as well as the HBM-THF solution before and after irradiation. Note the loss of a variety of other species, and the dominance of just two peaks associated with the alcohol and the oxo-bridge.

FTIR spectra (Figure 6.7) show two important features of the experiment: (1) The THF peak around 1970 cm^{-1} dominates the spectrum; though this does not appear directly in TR-IR spectra, it does effectively increase the noise in this region and prevent the observation of any peaks that may be there. Unfortunately, the delicate nature of the complex means that there is little choice but to work around this peak. (2) The broad background of the complex fades after brief irradiation, leaving only two additional peaks. These are the peaks of the oxo bridging species, and the alcohol that results from protonating the oxo and reforming the C_3 symmetric system. All other compounds have apparently fallen out of solution. It's unclear what variety of compounds made up the other peaks seen earlier, but given that only two species remained after just a few minutes of irradiation, all further results can be seen as representative of the behavior of just these two peaks.

6.3.2 Density functional theory calculations

To confirm the identity of these peaks, I both consulted with my collaborator, Jeremy Krogman, and also performed density functional theory

calculations (Figures 6.7 and 6.8). The solvating moieties of the ligand cage (the isopropyl and mesityl hydrocarbon portions) add a significant number of degrees of freedom; for future work, they could likely be replaced with simpler moieties to reduce the computational effort.

Ultimately, the DFT calculations confirmed the identity of the peaks. They also corroborated crystal structures of similar complexes. Interestingly, the line from the carbonyl ligand, between the metals, to the alcohol is not actually straight; the molecule is slightly kinked, gently breaking the C_3 symmetry of the system. It's unclear of this is replicated in solution, and if it has any significant role in the behavior of the complex.
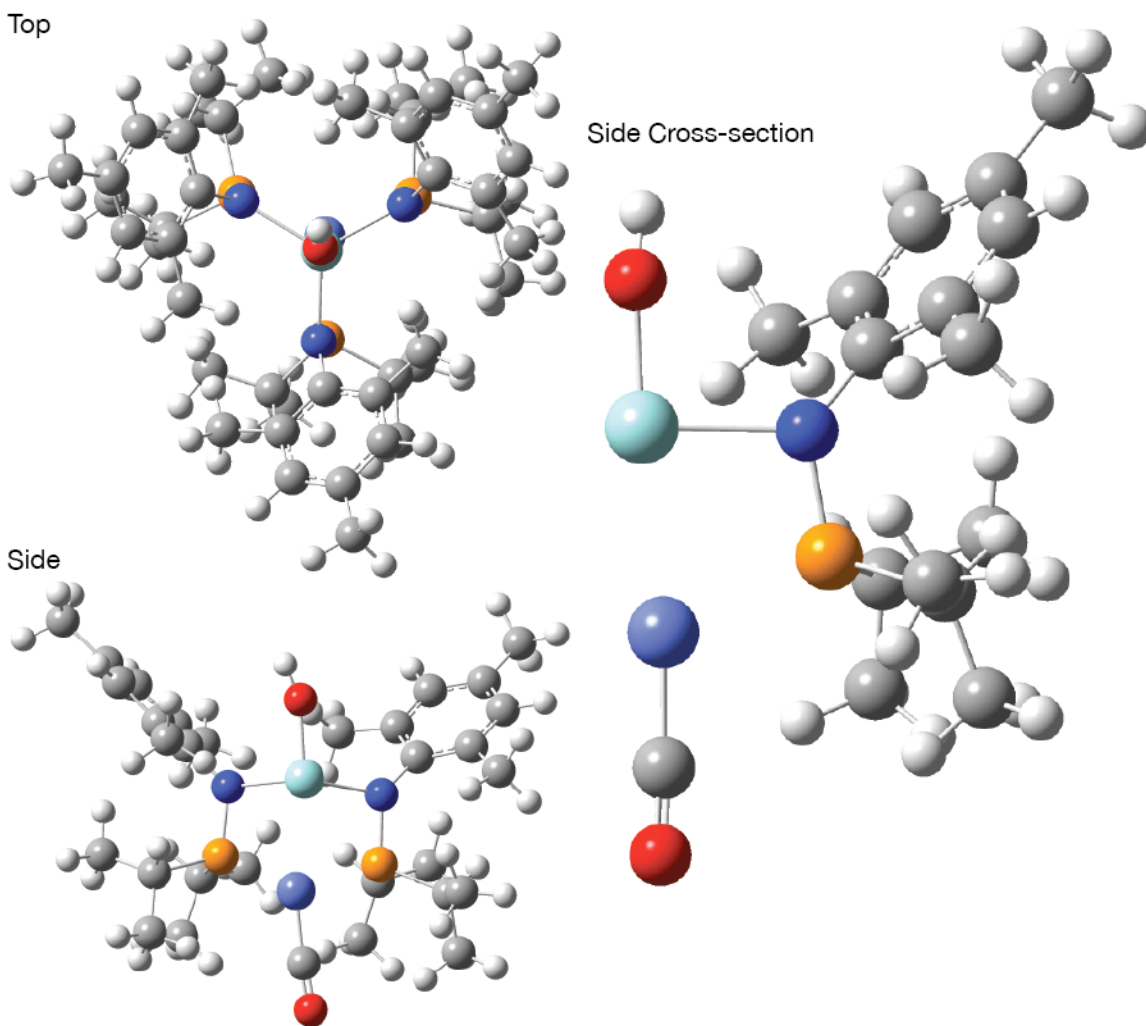
Figure 6.7 DFT structure of Co-Zr heterobimetallic complex with alcohol ancillary ligand.
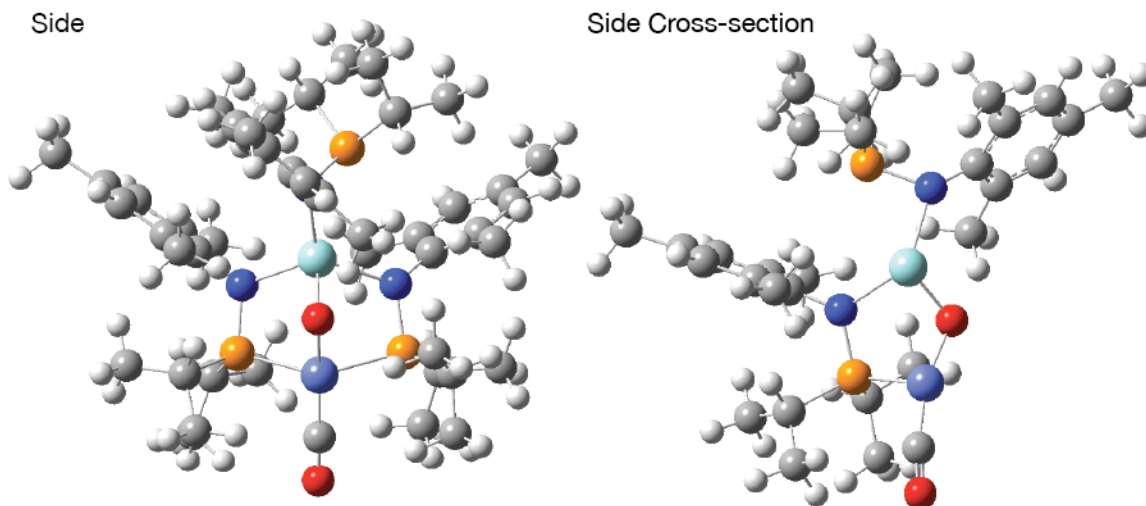
Figure 6.8 DFT structure of Co-Zr with bridging oxo ligand.

Though DFT was successful in confirming the ground state of the system, the large size and significant number of electrons made TD-DFT ultimately impractical for further characterization of excited states.

6.3.3 Ultrafast TR-IR spectroscopy

Thus far, linear spectroscopies and DFT have provided only the most minor hints as to the nature of the stubborn charge transfer state. Ultimately, little more can be expected; they are, at best, indirect observations of its behavior. In contrast, time-resolved IR spectroscopy directly observes the excited state.

The spectrum of the system following excitation by either UV or blue light has three characteristic peaks (Figure 6.9): the parent bleaches associated with the two peaks seen in FTIR, and a third, broad hot peak that is red-shifted from the parent peaks. Given that there are two parent species, it's likely that there are two product peaks existing together in this hot peak; however, given the broad and noisy character of the peak, they cannot be differentiated.[48,163] The peak decays before it cools enough to determine further information.
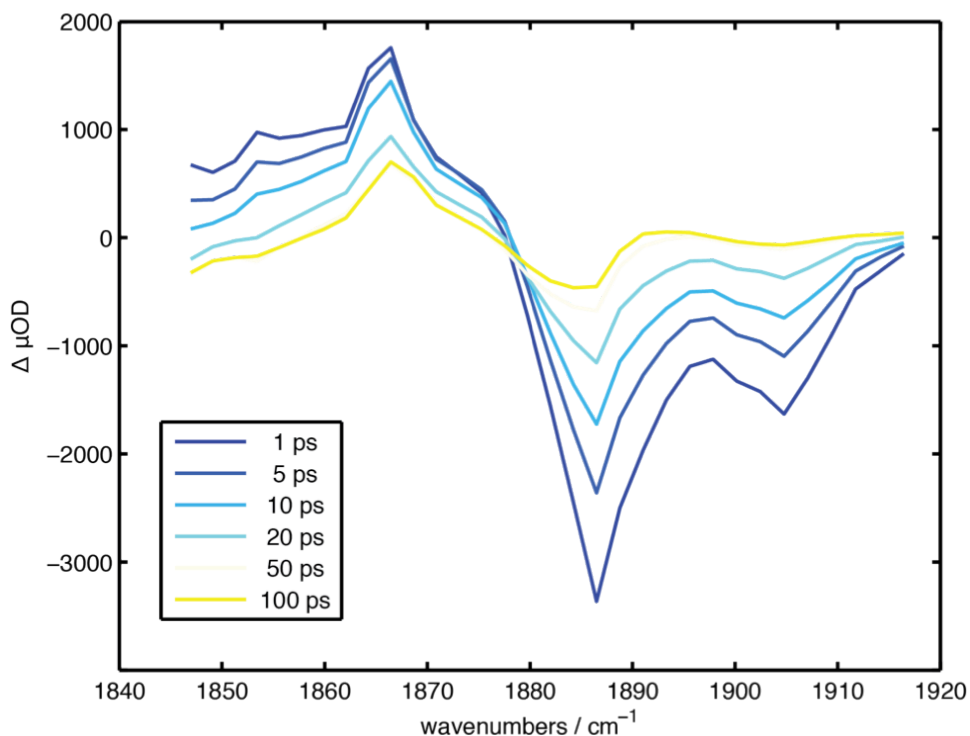
Figure 6.9 TR-IR difference spectrum of oxo/alcohol equilibrium mixture under 400 nm irradiation. Note the broad, red-shifted product peak.

Already, more information can be determined about the system by the spectrum alone. Recall that the carbonyl ligand responsible for these peaks is a pi-accepting ligand (or pi-backbonding); electron density from the cobalt center transfers into the π^* antibonding orbital of the CO, weakening the bond and reducing the pair's vibrational frequency. An increase in electron density on the metal center would result in an increase in π^* character in the CO bond, and a red-shift. As opposed to a metal-to-ligand charge transfer that might remove electron density from the cobalt atom, this is evidence for a charge transfer state that moves density *to* the cobalt.[164]

The remaining designations are either a ligand-to-metal or metal-to-metal charge transfer state. Typically, LMCTs result in visible absorbances that are lower in energy than MMCTs and MLCTs; that the broad absorbance occurs below ca. 450 nm implies that this is likely an MMCT.[156,165]

6.3.4 TR-IR: the polarization dependence

Beyond the transient spectrum (and thus the frequency domain), there are two other dimensions over which I have experimental control: the relative polarization and time delay between pulses. Recall that, within the dipole approximation, any excitation (be it vibrational or electronic) has a specific excitation dipole connecting the ground to the excited state. The pump pulse in a time resolved experiment has a particular polarization to it, and thus selectively excites molecules in solution that are aligned with that pulse. Over time, these molecules will rotationally diffuse (typically on the order of tens of picoseconds, for complexes of this size) and the "polarization label" is weakened and eventually lost. Nonetheless, for the first few picoseconds, many systems show a preferred angular dependence.[166] That is, the difference spectrum means that we should see improved absorbance of the mid-IR probe pulse when its polarization is aligned correctly relative to the electronic transition dipole (Figures 6.10 and 6.11).
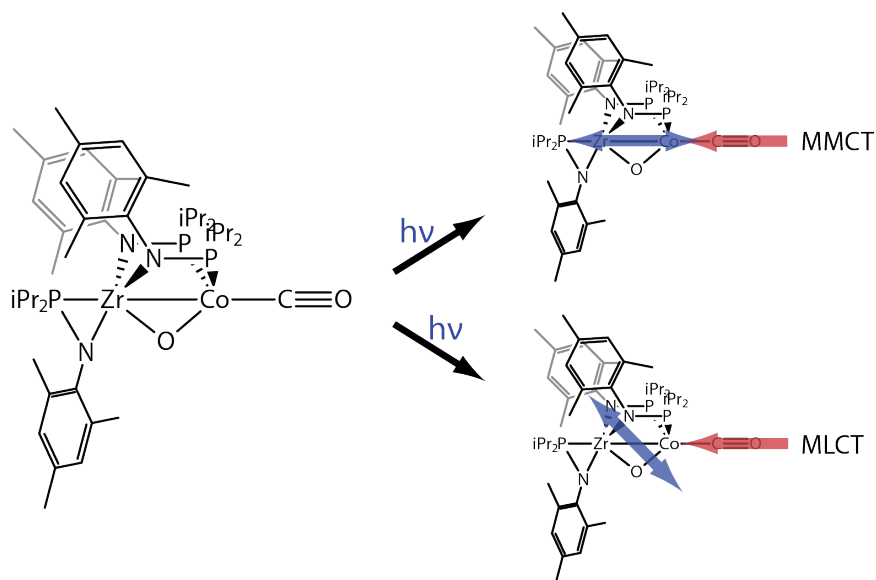
Figure 6.10 The excitation dipole for the charge transfer state can have a variety of angles, relative to the carbonyl ligand's dipole moment. Controlling the polarization of the beam can reveal this difference.

However, this polarization dependence was not observed experimentally (Figure 6.11). This is often the case in several systems, and is often the result of the truly vibronic nature of the transition (revealed in the broad hot peak.) Rather than exciting to a single state, the pump pulse actually excites the molecule to a manifold of vibronic states, each with a subtly different dipole. This is among the reasons that actually observing polarization dependence is not typically expected "in the wild." This approach cannot be used to differentiate the nature of the charge transfer state.
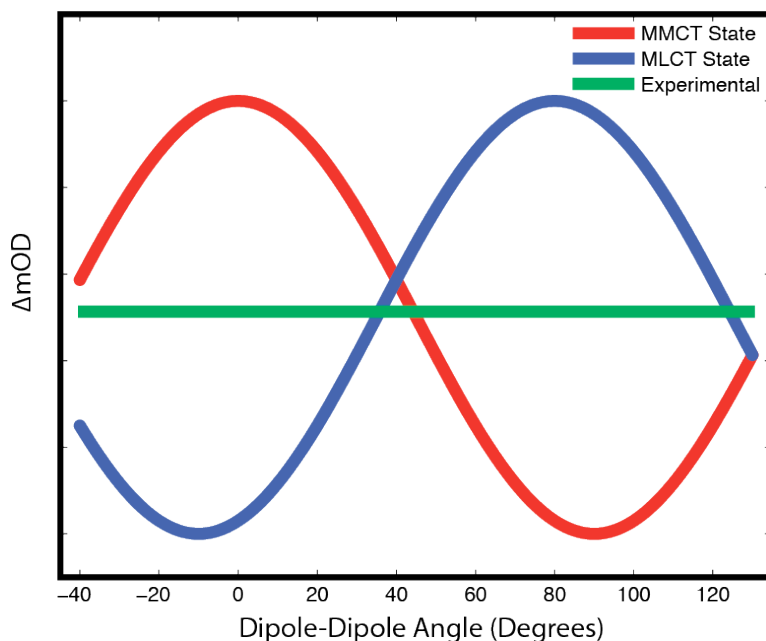
Figure 6.11 Strong polarization dependence can sometimes be indicative of excitation to a specific charge transfer state. This dependence was not observed experimentally.

Though the lack of polarization dependence is disappointing, it is ultimately not crippling to the experiment. As alluded to earlier, a third piece of information is available from TR-IR spectroscopy: the time dependence of each of the states of the system.

6.3.5 TR-IR: the time dependence

Perhaps the most important information in the experiment will be determined from the time dependence of the excited states. Though states are often fit to Voigt lineshapes in order to determine peak volume, the irregular shape of the hot peak and the general degree to which the peaks are well separated means that this approach was not chosen. Rather, the volume under a given peaks was integrated and the timescale of its behavior was fit. It's worth noting that if multiple peaks with different characteristic timescales were accidentally integrated together, bi- or multiexponential kinetics (rather than the single exponential kinetics observed) would be noticeable.

Each parent peak, as well as multiple locations in the hot product peak, were integrated and the timescales were found. For all peaks, the rise time occurred in <2 ps (i.e. instrument response time, given the length of the pump pulse) and subsequently decayed with a timescale of 19±1 ps (Figure 6.12). That all peaks in the spectrum display the same kinetics data implies that they are all

associated with the same excited state. Thus, only the behavior of this single state needs to be understood to characterize the charge transfer state in this system.
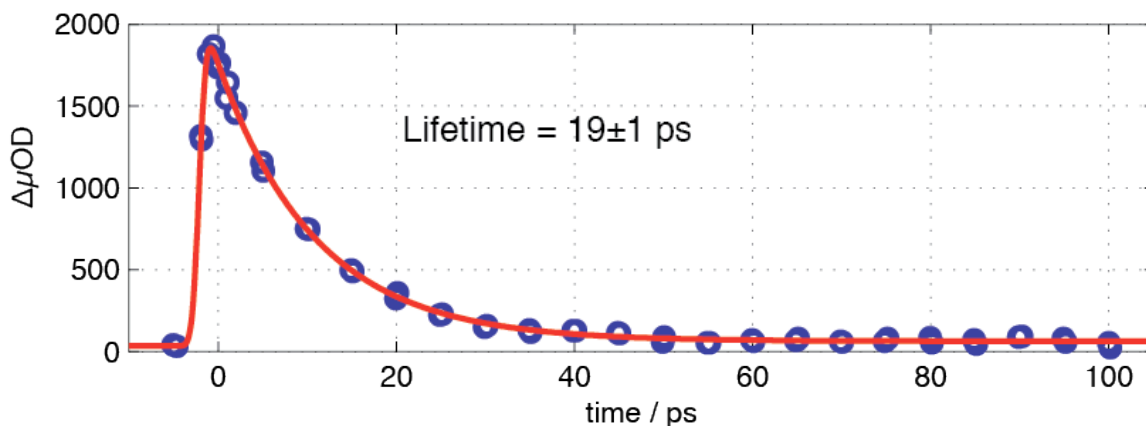
Figure 6.12 Kinetics data for the broad product peak following irradiation. Both parent peaks bleach and recover with exactly the same time constants.

In the context of the spectrum itself and our suspicions of a MMCT, this data is highly illuminating. Recall that transitions between states of different spin multiplicities are generally forbidden, and occur slowly; the <2 ps rise time implies that this state must share the singlet multiplicity of the parent molecule. That no further states appear at any later times means that these states are relaxing by coupling into heat in the bath, rather than going on to form any other states. The <20 ps decay is also consistent with a singlet state that can transition easily to lower singlet states via allowed transitions.

Thus the final assignment is that photoexcitation of this system results in the formation of a singlet metal-to-metal charge transfer state that dissipates as heat via back-electron transfer (Figure 6.13).[161] Ultimately, other work in the group suggests that a heavier metal center with a higher degree of spin-orbit coupling could likely undergo spin crossover to a triplet spin state that would be longer lived, and could ultimately result in further chemistry. In essence, this MMCT acts as a sort of "shock absorber" that dissipates the energy of the initial excitation relatively harmlessly (provided the photon flux remains low enough that massive heating of the solution does not occur.)
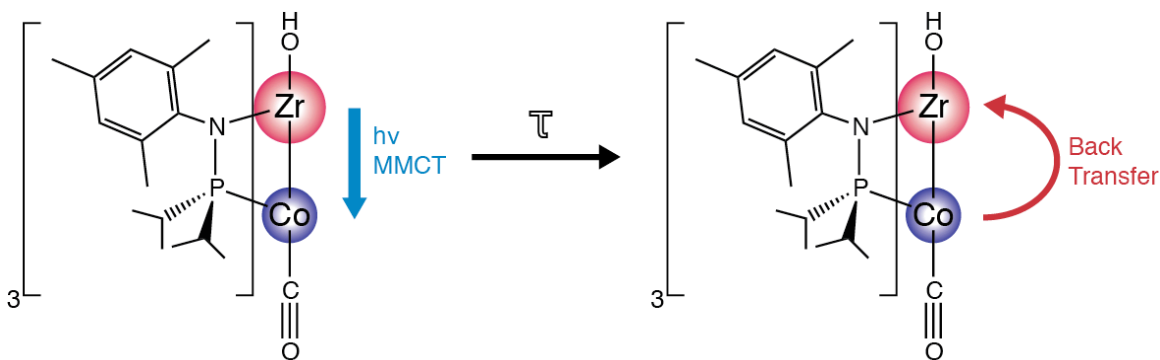
Figure 6.13 Schematic representation of the photoreaction in Co-Zr HBM complexes: light causes a singlet metal-to-metal charge transfer state which recovers in ca. 20 ps.

That this MMCT undergoes back-electron transfer to return to the ground state implies that the degree of coupling between the orbitals of the two metals is critical to determining the lifetime of the state. If the lifetime were significantly lengthened, this could leave the system with enough energy to potential undergo other processes, perhaps completing the catalytic cycle.

In light of this knowledge, and considering the synthetic requirements that place some limitations on the design of the structural N-P ligands, further work on this project should largely focus on the effect of the ancillary zirconium ligand. By permuting the identity of the ligand to alter its electronegativity, it should be possible shift the amount of electron density donated from the cobalt to the zirconium in the ground state, and perhaps alter the nature of the back-eletron transfer following excitation (Figure 6.14).
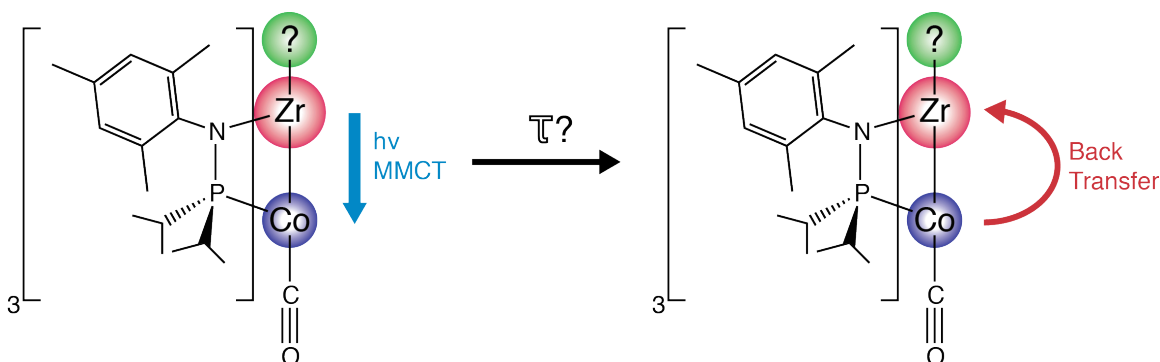
Figure 6.14 The electron donating or withdrawing character of the ancillary ligand could likely influence the lifetime of the charge transfer state. Could this lead to crossover to a dissociative triplet state?

Ultimately, however, it may be necessary to switch to heavier (and, unfortunately, rare and more expensive) metals for at least one of the centers in the heterobimetallic complex to cause the transfer to a triplet state necessary to

have effective photochemistry.[167-170] This does not, however, preclude the search for a thermal, synthetic approach to dissociating the carbonyl ligand.

6.4 Summary and conclusions

Cobalt-zirconium complexes, developed by the Christine Thomas group, show significant promise as CO_2 fixation catalysts, but their high stability to chemical and photolytic removal of the resulting CO prevents a catalytic cycle from being developed. Using UV/Vis, FTIR, and TR-IR spectroscopy, as well as density functional theory, I investigated the photophysics of these Co-Zr complexes in both an oxo-bridged and alcohol form.

The results for each complex were the same: photoexcitation results in the formation of a short-lived, singlet, metal-to-metal charge transfer state. This state moves electron density from the zirconium to the cobalt center, but thermalizes in ca. 19 ps via back-electron transfer. This state acts as a "shock absorber," stabilizing the complex and preventing any photochemistry from occurring. Future attempts to improve the properties of the system for catalysis should focus on the spin-crossover of this state to produce a long-lived triplet state that could actually undergo the desired photochemistry.

7   Conclusions

Coordination complexes represent perhaps the ultimate tool in chemistry: reusable, adaptable, and endlessly reconfigurable, with myriad experimental hooks from which to understand their behavior. Their chemistry is so wide-ranging and multifaceted that many different experimental methods can be necessary to achieve a full understanding. Though other classes of compounds offer more reactivity at higher temperatures (i.e. more "brute force"), or higher durability on solid supports, the realm of homogeneous catalysis presents an elegance and effectiveness that makes it an excellent model.

In this work, I have explored the chemistry of three important systems, demonstrating both novel experimental techniques, as well as exploring the more practical side of developing new clinical and industrial agents. As the questions in each case varied, so too did the optimal experimental techniques to conquer them. Ultimately, the development of ultrafast, nonlinear spectroscopy and its access to the fundamental field involved in chemical bonding (i.e. direct access to the electromagnetic force that governs all chemistry) makes it the crown champion of methods.

Demonstrating that potency is the temperature-dependent 2D-IR experimental method, as described here, which reveals information on the potential energy surface governing the motions of a molecule, *even* when that molecule is not crossing any barriers that were previously considered mandatory to mediate vibrational population transfer in a meaningful way. Instead, *any distortion results in breaking of the symmetry between normal modes of the molecule*—that is, even thermal fluctuations break the time reversibility of the molecule and *function as their own barriers*. Random motions within a well, if they are biased around a particular mode of motion, appear in the coupling of higher-frequency carbonyl stretching normal modes. This was demonstrated in the case of tricarbonyl(η^4-diene)iron(0) piano stool complexes, in which the "wagging" motion of the carbonyl ligands could be determined by both their coupling symmetry, and the unique signature of temperature dependence. This approach is general, and should widen the range of potential compounds to which 2D-IR can be applied. As a further test, studying the coupling in a variety of systems that show NMR timescale coalescence could reveal the full range of this technique's generality.

This understanding of the most basic, thermal motions of complexes can be applied in a more practical sense to the understanding of water exchange processes in MRI contrast agents. Much as in the wagging motions of the piano stool complexes, this is a system where the simple exchange behavior causes an important change in the energetics of the system—even in the absence of a permanent chemical change. The inner sphere coordination numbers and energies of water binding were determined for both clinical and experimental

agents, and demonstrate both the coming-of-age of DFT for broader applications, as well as the mechanism behind the high efficacy of the Raymond group's Gd-HOPO-based agents.

In the final case of a system with critically important chemistry, even in the absence of an elemental difference between reactant and product, I collaborated with the Thomas group at Brandeis, and used linear and time-resolved spectroscopies to identify the "shock absorber" singlet metal-to-metal charge transfer state in cobalt-zirconium complexes that prevents them from undergoing further photochemistry and completing a catalytic cycle. This work points future directions in identity of both the metal centers and the ancillary ligands that could facilitate the removal of the carbonyl center. More broadly, this is yet another confirmation of the subtlety of time-resolved infrared spectroscopy to solve practical problems in the world of chemical synthesis.

The parallel tools of careful chemical synthesis, time-resolved spectroscopy, and theory present a superb package for the understanding of chemical dynamics. Increasingly, the challenge is to understand not drastic nuclear motions, but rather the more subtle fluctuations of the equilibrium that can ultimately lead to big effects. Though techniques like TR-IR and 2D-IR ultimately face limitations, in the femtosecond to nanosecond timescale, they offer an understanding (and the possibility of control) that is unmatched. In facing the medical and energy challenges of the next century, the role of metals is enormous and unquestioned. Metal coordination complexes provide the flexibility and accessibility to develop the next generations of these technologies. Ultrafast spectroscopy not only offers deep mechanistic insights, but also practical knowledge for future directions in chemical exploration.

References

(1) Cotton, F. A.; Wilkinson, G.; Murillo, C. A.; Bochmann, M. *Advanced Inorganic Chemistry*; 6th Edition ed.; Wiley-Interscience: Hoboken, 1999.

(2) Housecroft, C. E.; Sharpe, A. G. *Inorganic Chemistry*; 3 Edition ed.; Prentice Hall: Upper Saddle River, 2007.

(3) Gust, D.; Moore, T. A. Mimicking Photosynthesis. *Science* **1989**, *244*, 35.

(4) Steinfeld, J. I.; Francisco, J. S.; Hase, W. L. *Chemical Kinetics and Dynamics*; 2 ed.; Prentice Hall: Upper Saddle River, 1989.

(5) Nitzan, A. *Chemical Dynamics in Condensed Phases: Relaxation, Transfer, and Reactions in Condensed Molecular Systems*; Oxford University Press: New York City, 2006.

(6) Cahoon, J. F., K.R. Sawyer, J.P. Schlegel, C.B. Harris Determining Transition-state Geometries in Liquids Using 2D-IR. *Science* **2008**, *318*, 1820.

(7) Caravan, P. Strategies for increasing the sensitivity of gadolinium based MRI contrast agents. *Chem. Soc. Rev.* **2006**, *35*, 512.

(8) Helm, L. Relaxivity in paramagnetic systems: Theory and mechanisms. *Prog. Nucl. Magn. Reson. Spectrosc.* **2006**, *49*, 45.

(9) Werner, E. J.; Avedano, S.; Botta, M.; Hay, B. P.; Moore, E. G.; Aime, S.; Raymond, K. N. Highly Soluble Tris-hydroxypyridonate Gd(III) Complexes with Increased Hydration Number, Fast Water Exchange, Slow Electronic Relaxation, and High Relaxivity1. *Journal of the American Chemical Society* **2007**, *129*, 1870.

(10) Cosentino, U.; Pitea, D.; Moro, G.; Saracino, G. A. A.; Villa, A. Conformational behaviour determines the low-relaxivity state of a conditional MRI contrast agent. *Phys. Chem. Chem. Phys.* **2009**, *11*, 3943.

(11) Solomon, I. a. N. B. Nuclear Magnetic Interactions in the HF Molecule. *J. Chem. Phys.* **1956**, *25*, 6.

(12) Bloembergen, N. Comments on "Proton Relaxation Times in Paramagnetic Solutions". *J. Chem. Phys.* **1957**, *27*, 2.

(13) Bloembergen, N. Proton Relaxation Times in Paramagnetic Solutions. *J. Chem. Phys.* **1957**, *27*, 2.

(14) Bloembergen, N., L.O. Morgan Proton Relaxation Times in Paramagnetic Solutions. Effects of Electron Spin Relaxation. *J. Chem. Phys.* **1960**, *34*, 9.

(15) Golding, R. M.; Pascual, R. O.; Ahn, S. The NMR iso-shield diagram for an f-electron system in a crystal-field environment of octahedral symmetry. *J. Magn. Reson.* **1982**, *46*, 406.

(16) Yazyev, O. V.; Helm, L. 17O nuclear quadrupole coupling constants of water bound to a metal ion: A gadolinium(III) case study. *The Journal of Chemical Physics* **2006**, *125*, 054503.

(17) Purgel, M.; Baranyai, Z.; de Blas, A.; Rodriguez-Blas, T.; Banyai, I.; Platas-Iglesias, C.; Toth, I. An NMR and DFT Investigation on the Conformational Properties of Lanthanide(III) 1,4,7,10-Tetraazacyclododecane-1,4,7,10-tetraacetate Analogues Containing Methylenephosphonate Pendant Arms. *Inorg. Chem.* **2010**, *49*, 4370.

(18) Rastrelli, F.; Bagno, A. Predicting the 1H and 13C NMR spectra of paramagnetic Ru(III) complexes by DFT. *Magn. Reson. Chem.* **2010**, *48*, S132.

(19) Yazyev, O. V.; Helm, L. Gadolinium (III) ion in liquid water: Structure, dynamics, and magnetic interactions from first principles. *The Journal of Chemical Physics* **2007**, *127*, 084506.

(20) Gust, D.; Moore, T. A.; Moore, A. L. Solar Fuels via Artificial Photosynthesis. *Acc. Chem. Res.* **2009**, *42*, 1890.

(21) Kamat, P. V.; Tvrdy, K.; Baker, D. R.; Radich, J. G. Beyond Photovoltaics: Semiconductor Nanoarchitectures for Liquid-Junction Solar Cells. *Chem. Rev.* **2010**, *110*, 6664.

(22) Nozik, A. J.; Miller, J. Introduction to Solar Photon Conversion. *Chem. Rev.* **2010**, *110*, 6443.

(23) Takeda, H.; Koike, K.; Inoue, H.; Ishitani, O. Development of an Efficient Photocatalytic System for CO2 Reduction Using Rhenium(I) Complexes Based on Mechanistic Studies. *Journal of the American Chemical Society* **2008**, *130*, 2023.

(24) Whited, M. T.; Grubbs, R. H. Oxygen-Atom Transfer from Carbon Dioxide to a Fischer Carbene at (PNP)Ir. *Journal of the American Chemical Society* **2008**, *130*, 5874.

(25) Smieja, J. M.; Kubiak, C. P. Re(bipy-tBu)(CO)3Cl-improved Catalytic Activity for Reduction of Carbon Dioxide: IR-Spectroelectrochemical and Mechanistic Studies. *Inorg. Chem.* **2010**, null.

(26) Sun, L. C.; Berglund, H.; Davydov, R.; Norrby, T.; Hammarstrom, L.; Korall, P.; Borje, A.; Philouze, C.; Berg, K.; Tran, A.; Andersson, M.; Stenhagen, G.; Martensson, J.; Almgren, M.; Styring, S.; Akermark, B. Binuclear ruthenium-manganese complexes as simple artificial models for photosystem II in green plants. *Journal of the American Chemical Society* **1997**, *119*, 6996.

(27) Jiao, F.; Frei, H. Nanostructured Cobalt Oxide Clusters in Mesoporous Silica as Efficient Oxygen-Evolving Catalysts. *Angewandte Chemie International Edition* **2009**, *48*, 1841.

(28) Sivasankar, N.; Weare, W. W.; Frei, H. Direct Observation of a Hydroperoxide Surface Intermediate upon Visible Light-Driven Water Oxidation at an Ir Oxide Nanocluster Catalyst by Rapid-Scan FT-IR Spectroscopy. *Journal of the American Chemical Society* **2011**, *133*, 12976.

(29) Greenwood, B. P.; Forman, S. I.; Rowe, G. T.; Chen, C.-H.; Foxman, B. M.; Thomas, C. M. Multielectron Redox Activity Facilitated by Metal-Metal Interactions in Early/Late Heterobimetallics: Co/Zr Complexes Supported by Phosphinoamide Ligands. *Inorg. Chem.* **2009**, *48*, 6251.

(30) Thomas, C. M.; Napoline, J. W.; Rowe, G. T.; Foxman, B. M. Oxidative addition across Zr/Co multiple bonds in early/late heterobimetallic complexes. *Chem. Commun.* **2010**, *46*, 5790.

(31) Krogman, J. P.; Foxman, B. M.; Thomas, C. M. Activation of CO2 by a Heterobimetallic Zr/Co Complex. *Journal of the American Chemical Society* **2011**, *133*, 14582.

(32) Thomas, C. M. Metal-Metal Multiple Bonds in Early/Late Heterobimetallic Complexes: Applications Toward Small Molecule Activiation and Catalysis. *Comments Inorg. Chem.* **2011**, *32*, 14.

(33) Zhou, W.; Napoline, J. W.; Thomas, C. M. A Catalytic Application of Co/Zr Heterobimetallic Complexes: Kumada Coupling of Unactivated Alkyl Halides with Alkyl Grignard Reagents. *Eur. J. Inorg. Chem.* **2011**, *2011*, 2029.

(34) Wynne, K.; Hochstrasser, R. M. The theory of ultrafast vibrational spectroscopy. *Chem. Phys.* **1995**, *193*, 211.

(35) Reid, G. D. a. K. W. Ultrafast Laser Technology and Spectroscopy. *Encyclopedia of Analytical Chemistry* **2000**, 13644.

(36) Cervetto, V.; Helbing, J.; Bredenbeck, J.; Hamm, P. Double-resonance versus pulsed Fourier transform two-dimensional infrared spectroscopy: An experimental and theoretical comparison. *The Journal of Chemical Physics* **2004**, *121*, 5935.

(37) Bredenbeck, J., Jan Helbing, Christoph Kolano, Peter Hamm, Ultrafast 2D-IR Spectroscopy of Transient Species. *ChemPhysChem.* **2007**, *8*, 1747.

(38) Boyd, R. W.; Mukamel, S. Origin of spectral holes in pump-probe studies of homogeneously broadened lines. *Phys. Rev. A* **1984**, *29*, 1973.

(39) Khalil, M.; Demirdoven, N.; Tokmakoff, A. Coherent 2D IR spectroscopy: Molecular structure and dynamics in solution. *J. Phys. Chem. A* **2003**, *107*, 5258.

(40) Bredenbeck, J.; Helbing, J.; Hamm, P. Labeling Vibrations by Light: Ultrafast Transient 2D-IR Spectroscopy Tracks Vibrational Modes during Photoinduced Charge Transfer. *Journal of the American Chemical Society* **2004**, *126*, 990.

(41) Mukamel, S. *Principles of Nonlinear Optical Spectroscopy*; Oxford University Press: New York City, 1999.

(42) Graham, M. W.; Ma, Y.-Z.; Fleming, G. R. Femtosecond Photon Echo Spectroscopy of Semiconducting Single-Walled Carbon Nanotubes. *Nano Lett.* **2008**, *8*, 3936.

(43) Bressler, C.; Chergui, M. Ultrafast X-ray Absorption Spectroscopy. *Chem. Rev.* **2004**, *104*, 1781.

(44) Bressler, C.; Milne, C.; Pham, V. T.; ElNahhas, A.; van der Veen, R. M.; Gawelda, W.; Johnson, S.; Beaud, P.; Grolimund, D.; Kaiser, M.; Borca, C. N.; Ingold, G.; Abela, R.; Chergui, M. Femtosecond XANES Study of the Light-Induced Spin Crossover Dynamics in an Iron(II) Complex. *Science* **2009**, *323*, 489.

(45) From a practical standpoint, it should be noted that RESONANT behavior from these atmospheric components is not problematic. Significant changes in humidity or temperature will change the refractive index of the air, effectively misaligning every optic in the system.

(46) Payne, C. K.; Snee, P. T.; Yang, H.; Kotz, K. T.; Schafer, L. L.; Tilley, T. D.; Harris, C. B. Intramolecular Rearrangements on Ultrafast Timescales: Femtosecond Infrared Studies of Ring Slip in (eta1-C5Cl5)Mn(CO)5. *Journal of the American Chemical Society* **2001**, *123*, 7425.

(47) Snee, P. T.; Payne, C. K.; Mebane, S. D.; Kotz, K. T.; Harris, C. B. Dynamics of Photosubstitution Reactions of Fe(CO)$_5$: An Ultrafast Infrared Study of High Spin Reactivity. *Journal of the American Chemical Society* **2001**, *123*, 6909.

(48) Asplund, M. C.; Snee, P. T.; Yeston, J. S.; Wilkens, M. J.; Payne, C. K.; Yang, H.; Kotz, K. T.; Frei, H.; Bergman, R. G.; Harris, C. B. Ultrafast UV Pump/IR Probe Studies of C-H Activation in Linear, Cyclic, and Aryl Hydrocarbons. *Journal of the American Chemical Society* **2002**, *124*, 10605.

(49) Cahoon, J. F.; Kling, M. F.; Sawyer, K. R.; Frei, H.; Harris, C. B. 19-Electron Intermediates in the Ligand Substitution of CpW(CO)$_3$. with a Lewis Base. *Journal of the American Chemical Society* **2006**, *128*, 3152.

(50) Rauscher, C.; Laenen, R. Analysis of picosecond mid-infrared pulses by two-photon absorption in germanium. *J. Appl. Phys.* **1997**, *81*, 2818.

(51) Hamm, P., M. Lim, and R.M. Hochstrasser Structure of the Amide I Band of Peptides Measured by Femtosecond Nonlinear-Infrared Spectroscopy. *J. Phys. Chem. B* **1998**, *102*, 6123.

(52) Rector, K. D.; Fayer, M. D. Vibrational echoes: a new approach to condensed-matter vibrational spectroscopy. *Int. Rev. Phys. Chem.* **1998**, *17*, 261.

(53) Asplund, M. C., M. T. Zanni, and R. M. Hochstrasser Two-dimensional infrared spectroscopy of peptides by phase-controlled femtosecond vibrational photon echoes. *Proc. Natl. Acad. Sci.* **2000**, *97*, 8219.

(54) Vlcek, A. J. Mechanistic roles of metal-to-ligand charge-transfer excited states in organometallic photochemistry. *Coord. Chem. Rev.* **1998**, *177*, 219.

(55) Farrell, I. R.; Vlcek, A. J. Mechanisms of ultrafast metal-ligand bond splitting upon MLCT excitation of carbonyl-diimine complexes. *Coord. Chem. Rev.* **2000**, *208*, 87.

(56) Snee, P. T.; Payne, C. K.; Kotz, K. T.; Yang, H.; Harris, C. B. Triplet Organometallic Reactivity under Ambient Conditions: An Ultrafast UV Pump/IR Probe Study. *Journal of the American Chemical Society* **2001**, *123*, 2255.

(57) Glascoe, E. A.; Kling, M. F.; Shanoski, J. E.; Harris, C. B. Nature and Role of Bridged Carbonyl Intermediates in the Ultrafast Photoinduced Rearrangement of Ru$_3$(CO)$_{12}$. *Organometallics*. **2005**, *25*, 775.

(58) Shanoski, J. E.; Payne, C. K.; Kling, M. F.; Glascoe, E. A.; Harris, C. B. Ultrafast Infrared Mechanistic Studies of the Interaction of 1-Hexyne with Group 6 Hexacarbonyl Complexes. *Organometallics*. **2005**, *24*, 1852.

(59) Glascoe, E. A.; Kling, M. F.; Shanoski, J. E.; DiStasio, R. A.; Payne, C. K.; Mork, B. V.; Tilley, T. D.; Harris, C. B. Photoinduced B-Hydrogen Elimination and Radical Formation with CpW(CO)$_3$(CH$_2$CH$_3$): Ultrafast IR and DFT Studies. *Organometallics*. **2007**, *26*, 1424.

(60) Cahoon, J. F.; Kling, M. F.; Sawyer, K. R.; Andersen, L. K.; Harris, C. B. DFT and time-resolved IR investigation of electron transfer between photogenerated 17- and 19-electron organometallic radicals. *J. Mol. Struct.* **2008**, *890*, 328.

(61) Sawyer, K. R.; Glascoe, E. A.; Cahoon, J. F.; Schlegel, J. P.; Harris, C. B. Mechanism for Iron-Catalyzed Alkene Isomerization in Solution. *Organometallics*. **2008**, *27*, 4370.

(62) Bomben, P. G.; Koivisto, B. D.; Berlinguette, C. P. Cyclometalated Ru Complexes of Type [Ru-II(N^N)2(C^N)]z: Physicochemical Response to Substituents Installed on the Anionic Ligand. *Inorg. Chem.* **2010**, *49*, 4960.

(63) Cooper, B. G.; Fafard, C. M.; Foxman, B. M.; Thomas, C. M. Electronic Factors Affecting Metal‚áíMetal Interactions in Early/Late Heterobimetallics: Substituent Effects in Zirconium/Platinum Bis(phosphinoamide) Complexes‚Ä†. *Organometallics.* **2010**, *29*, 5179.

(64) Vlcek, A. J.; Lees, A. J., Ed.; Springer Berlin / Heidelberg: 2010; Vol. 29, p 115.

(65) Cahoon, J. F. *Investigation of Organometallic Reaction Mechanisms with One and Two Dimentional Vibrational Spectroscopy*; University of California: Berkeley, 2008.

(66) Sawyer, K. R. *One- and two-dimensional infrared spectroscopic studies of solution-phase homogeneous catalysis and spin-forbidden reactions*; University of California: Berkeley, 2008.

(67) Zoerb, M. C. *Dynamic IR Peak Coalescence and Ultrafast Chemical Exchange Reactions Studied by Two Dimensional Infrared Spectroscopy*; University of California: Berkeley, 2012.

(68) Hamm, P.; Kaindl, R. A.; Stenger, J. Noise suppression in femtosecond mid-infrared light sources. *Opt. Lett.* **2000**, *25*, 1798.

(69) Andrews, J. R.; Hochstrasser, R. M. Transient grating effects in resonant four-wave mixing experiments. *Chem. Phys. Lett.* **1980**, *76*, 213.

(70) Kenkre, V. M.; Tsironis, G. P. Initial condition effects on the time dependence of the signal in transient grating experiments. *J. Lumin.* **1985**, *34*, 107.

(71) Delve, P. A.; Whitaker, B. J. A simple model to describe thermal grating effects in degenerate four wave mixing spectroscopy. *Phys. Chem. Chem. Phys.* **2000**, *2*, 5594.

(72) Schneider, T.; Reif, J. Influence of an ultrafast transient refractive-index grating on nonlinear optical phenomena. *Phys. Rev. A* **2002**, *65*, 023801.

(73) Glascoe, E. A.; Sawyer, K. R.; Shanoski, J. E.; Harris, C. B. The Influence of the Metal Spin State in the Iron-Catalyzed Alkene Isomerization Reaction Studied with Ultrafast Infrared Spectroscopy. *The Journal of Physical Chemistry C* **2007**, *111*, 8789.

(74) Gillespie, D. T. Exact Stochastic Simulation of Coupled Chemical Reactions. *J. Phys. Chem.* **1977**, *81*, 2340.

(75) Frisch, M. J. T., G. W.; Schlegel, H. B.; Scuseria, G. E.; Robb, M. A.; Cheeseman, J. R.; Scalmani, G.; Barone, V.; Mennucci, B.; Petersson, G. A.; Nakatsuji, H.; Caricato, M.; Li, X.; Hratchian, H. P.; Izmaylov, A. F.; Bloino, J.; Zheng, G.; Sonnenberg, J. L.; Hada, M.; Ehara, M.; Toyota, K.; Fukuda, R.; Hasegawa, J.; Ishida, M.; Nakajima, T.; Honda, Y.; Kitao, O.; Nakai, H.; Vreven, T.; Montgomery, Jr., J. A.; Peralta, J. E.; Ogliaro, F.; Bearpark, M.; Heyd, J. J.; Brothers, E.; Kudin, K. N.; Staroverov, V. N.; Kobayashi, R.; Normand, J.; Raghavachari, K.; Rendell, A.; Burant, J. C.; Iyengar, S. S.; Tomasi, J.; Cossi, M.; Rega, N.; Millam, J. M.; Klene, M.; Knox, J. E.; Cross, J. B.; Bakken, V.; Adamo, C.; Jaramillo, J.; Gomperts, R.; Stratmann, R. E.; Yazyev, O.; Austin, A. J.;

Cammi, R.; Pomelli, C.; Ochterski, J. W.; Martin, R. L.; Morokuma, K.; Zakrzewski, V. G.; Voth, G. A.; Salvador, P.; Dannenberg, J. J.; Dapprich, S.; Daniels, A. D.; Farkas, Ö.; Foresman, J. B.; Ortiz, J. V.; Cioslowski, J.; Fox, D. J., Gaussian09, Revision B.01, Gaussian, Wallingford, CT, **2009**.

(76) Ditchfield, R.; Hehre, W. J.; Pople, J. A. Self-Consistent Molecular Orbital Methods. 9. Extended Gaussian-type basis for molecular-orbital studies of organic molecules. *J. Chem. Phys.* **1971**, *54*, 724.

(77) Hehre, W. J.; Ditchfield, R.; Pople, J. A. Self-Consistent Molecular Orbital Methods. 12. Further extensions of Gaussian-type basis sets for use in molecular-orbital studies of organic-molecules. *J. Chem. Phys.* **1972**, *56*, 2257.

(78) Hariharan, P. C.; Pople, J. A. Influence of polarization functions on molecular-orbital hydrogenation energies. *Theor. Chem. Acc.* **1973**, *28*, 213.

(79) Hariharan, P. C.; Pople, J. A. Accuracy of AH equilibrium geometries by single determinant molecular-orbital theory. *Mol. Phys.* **1974**, *27*, 209.

(80) Gordon, M. S. The isomers of silacyclopropane. *Chem. Phys. Lett.* **1980**, *76*, 163.

(81) Francl, M. M.; Pietro, W. J.; Hehre, W. J.; Binkley, J. S.; DeFrees, D. J.; Pople, J. A.; Gordon, M. S. Self-Consistent Molecular Orbital Methods. 23. A polarization-type basis set for 2nd-row elements. *J. Chem. Phys.* **1982**, *77*, 3654.

(82) Binning, R. C.; Curtiss, L. A. Compact contracted basis-sets for 3rd-row atoms - GA-KR. *J, Comp. Chem.* **1990**, *11*, 1206.

(83) Bladeau, J.-P.; McGrath, M. P.; Curtiss, L. A.; Radom, L. Extension of Gaussian-2 (G2) theory to molecules containing third-row atoms K and Ca. *J. Chem. Phys.* **1997**, *107*, 5016.

(84) Rassolov, V. A.; Pople, J. A.; Ratner, M. A.; Windus, T. L. 6-31G* basis set for atoms K through Zn. *J. Chem. Phys.* **1998**, *109*, 1223.

(85) Rassolov, V. A.; Ratner, M. A.; Pople, J. A.; Redfern, P. C.; Curtiss, L. A. 6-31G* Basis Set for Third-Row Atoms. *J. Comp. Chem.* **2001**, *22*, 976.

(86) Dunning, T. H.; Hay, P. J. *Modern Theoretical Chemistry*; Plenum: New York, 1976; Vol. 3.

(87) Feller, D. The Role of Databases in Support of Computational Chemistry Calculations. *J. Comp. Chem.* **1996**, *17*, 1571.

(88) Schuchardt, K. L., Didier, B.T., Elsethagen, T., Sun, L., Gurumoorthi, V., Chase, J., Li, J., and Windus, T.L. Basis Set Exchange: A Community Database for Computational Sciences *J. Chem. Inf. Model.* **2007**, *47*, 1045.

(89) Baiz, C. R.; Kubarych, K. J.; Geva, E. Molecular Theory and Simulation of Coherence Transfer in Metal Carbonyls and Its Signature on Multidimensional Infrared Spectra. *The Journal of Physical Chemistry B* **2011**, *115*, 5322.

(90) King, J. T.; Ross, M. R.; Kubarych, K. J. Water-Assisted Vibrational Relaxation of a Metal Carbonyl Complex Studied with Ultrafast 2D-IR. *The Journal of Physical Chemistry B* **2012**, *116*, 3754.

(91) Panman, M. R.; Newton, A. C.; Vos, J.; van den Bosch, B.; Bocokic, V.; Reek, J. N. H.; Woutersen, S. Ultrafast Dynamics in Iron Tetracarbonyl Olefin Complexes Investigated with Two-Dimensional Vibrational Spectroscopy. *Phys. Chem. Chem. Phys.* **2012**.

(92) Hamm, P.; Zanni, M. T. *Concepts and Methods of 2D Infrared Spectroscopy*; Cambridge University Press: Cambridge, 2011.

(93) Tokmakoff, A. Homogeneous vibrational dynamics and inhomogeneous broadening in glass-forming liquids: Infrared photon echo experiments from room temperature to 10 K. *J. Chem. Phys.* **1995**, *103*, 2810.

(94) Sturlaugson, A. L.; Fayer, M. D. Temperature and Hydration-Dependent Rotational and Translational Dynamics of a Polyether Oligomer. *The Journal of Physical Chemistry B* **2011**, *115*, 945.

(95) Grevels, F.-W., Jürgen Jacke, Werner E. Klotzbücher, Carl Krüger, Klaus Seevogel, Yi-Hung Tsay Dynamic Processes on the IR Time Scale: Coalescence of CO Stretching Vibrational Bands in [(eta4-Diene)Fe(CO)3] Complexes. *Angewandte Chemie International Edition in English* **1987**, *26*, 885.

(96) Grevels, F. W.; Jacke, J.; Seevogel, K. Dynamics of metal carbonyls on the infrared time scale : coalescence of CO stretching vibrational bands. *J. Mol. Struct.* **1988**, *174*, 107.

(97) Strauss, H. L. Changes of the carbonyl stretching spectra with temperature. *Journal of the American Chemical Society* **1992**, *114*, 905.

(98) Turner, J. J.; Gordon, C. M.; Howdle, S. M. Infrared Spectral Features Due to Very Rapid Fluxional Motion: Changes in the Infrared Carbonyl Stretching Spectra of Tricarbonyl(.eta.4-norbornadiene)iron with Temperature. *The Journal of Physical Chemistry* **1995**, *99*, 17532.

(99) Grevels, F.-W., Klaus Kerpen, Werner E. Klotzbücher, R. E. D. McClung, Graham Russell, Manuella Viotte, and Kurt Schaffner The Very Low Barrier of CO Site Exchange in Tricarbonyl(η4-1,5-cyclooctadiene)iron: Picosecond Kinetics in Solution Investigated by Line Shape Simulation of the ν(CO) IR Bands and Complementary Evidence from the Course of 13CO Incorporation in a Low-Temperature Matrix. *Journal of the American Chemical Society* **1998**, *120*, 10423.

(100) Kruczynski, L.; Takats, J. Fluxional behavior of (diene)iron tricarbonyl type complexes. *Journal of the American Chemical Society* **1974**, *96*, 932.

(101) Davidson, G. The vibrational spectrum of (butadiene) iron tricarbonyl. *Inorg. Chim. Acta* **1969**, *3*, 596.

(102) Kruczynski, L.; Takats, J. Intramolecular rearrangement in (.eta.-diene)tricarbonyliron and -ruthenium compounds. A carbon-13 nuclear magnetic resonance study. *Inorg. Chem.* **1976**, *15*, 3140.

(103) Giordano, A. N.; Morton, S. M.; Jensen, L.; Lear, B. J. Direct Test of the Equivalency of Dynamic IR and Dynamic Raman Spectroscopies As Techniques for Observing Ultrafast Molecular Dynamics. *The Journal of Physical Chemistry A* **2013**.

(104) MacPhail, R. A.; Snyder, R. G.; Strauss, H. L. The motional collapse of the methyl C--H stretching vibration bands. *The Journal of Chemical Physics* **1982**, *77*, 1118.

(105) MacPhail, R. A.; Strauss, H. L. Can the Bloch equations describe the vibrational spectra of a reacting molecule? *The Journal of Chemical Physics* **1985**, *82*, 1156.

(106) Wood, K. A.; Strauss, H. L. Broadening and shifts of vibrational bands due to the effect of thermal chemical reactions. *The Journal of Physical Chemistry* **1990**, *94*, 5677.

(107) Perry, D. S.; Bethardy, G. A.; Wang, X. The Effect of the Torsional Barrier Height on the Acceleration of Intramolecular Vibrational Relaxation (IVR) by Molecular Flexibility. *Berichte der Bunsengesellschaft für physikalische Chemie* **1995**, *99*, 530.

(108) Lee, N. K.; Park, S.; Yoon, M.-H.; Kim, Z. H.; Kim, S. K. Effect of ring torsion on intramolecular vibrational redistribution dynamics of 1,1[prime or minute]-binaphthyl and 2,2[prime or minute]-binaphthyl. *Phys. Chem. Chem. Phys.* **2012**, *14*, 840.

(109) Koerner von Gustorf, E.; C. Hogan, J. Photochemical syntheses of 1,5- and 1,3-cyclooctadiene-iron carbonyls. *Tetrahedron Lett.* **1968**, *9*, 3191.

(110) Deeming, A. J., S. S. Ullah, A.J. P. Domingos, B.F. G. Johnson, J. Lewis Reactivity of co-ordinated ligands. Part XX. Preparation and reactions of cyclo-octadiene complexes of iron, ruthenium, and osmium. *J. Chem. Soc., Dalton Trans.* **1974**, 2093

(111) Bachler, V.; Grevels, F.-W.; Kerpen, K.; Olbrich, G.; Schaffner, K. A Novel Facet of Carbonyliron-Diene Photochemistry: The η4-s-trans Isomer of the Classical Fe(CO)3(η4-s-cis-1,3-butadiene) Discovered by Time-Resolved IR Spectroscopy and Theoretically Examined by Density Functional Methods. *Organometallics.* **2003**, *22*, 1696.

(112) Fenn, E. E.; Fayer, M. D. Extracting 2D IR frequency-frequency correlation functions from two component systems. *The Journal of Chemical Physics* **2011**, *135*, 074502.

(113) Zheng, J.; Kwak, K.; Xie, J.; Fayer, M. D. Ultrafast Carbon-Carbon Single-Bond Rotational Isomerization in Room-Temperature Solution. *Science* **2006**, *313*, 1951.

(114) Khalil, M.; Demirdoven, N.; Tokmakoff, A. Vibrational coherence transfer characterized with Fourier-transform 2D IR spectroscopy. *The Journal of Chemical Physics* **2004**, *121*, 362.

(115) Golonzka, O.; Khalil, M.; Demirdoven, N.; Tokmakoff, A. Coupling and orientation between anharmonic vibrations characterized with two-dimensional infrared vibrational echo spectroscopy. *J. Chem. Phys.* **2001**, *115*, 10814.

(116) Nesbitt, D. J.; Field, R. W. Vibrational Energy Flow in Highly Excited Molecules:‚Àâ Role of Intramolecular Vibrational Redistribution. *The Journal of Physical Chemistry* **1996**, *100*, 12735.

(117) Peak locations in both complexes shift slightly as a result of changes in temperature; frequencies listed here are necessarily approximate.

(118) Off-diagonal populations at t=0 are fit and quantified during the simulation of each system.

(119) That is, the population of this state increases to a fixed value over the duration of the pump pulse, then exhibits only decays after ca. 1 ps.

(120) As we shall show later, this is a good choice given symmetry associated with the CO wagging motion.

(121) Calculations using transition state theory (with a temperature-dependent prefactor) are qualitatively identical.

(122) Tokmakoff, A.; Sauter, B.; Fayer, M. D. Temperature-dependent vibrational relaxation in polyatomic liquids: Picosecond infrared pump--probe experiments. *The Journal of Chemical Physics* **1994**, *100*, 9035.

(123) Bakker, H. J. Effect of intermolecular interactions on vibrational-energy transfer in the liquid phase. *The Journal of Chemical Physics* **1993**, *98*, 8496.

(124) Chandler, D. *Introduction To Modern Statistical Mechanics*; Oxford University Press: New York, 1987.

(125) Winzor, D. J.; Jackson, C. M. Interpretation of the temperature dependence of equilibrium and rate constants. *J. Mol. Recognit.* **2006**, *19*, 389.

(126) Zhang, Y.; Xu, X.; Goddard, W. A. Doubly hybrid density functional for accurate descriptions of nonbond interactions, thermochemistry, and thermochemical kinetics. *Proc. Natl. Acad. Sci.* **2009**, *106*, 4963.

(127) Wales, D. J. *Energy Landscapes: Applications to Clusters, Biomolecules and Glasses*; Cambridge University Press: Cambridge, UK, 2004.

(128) Yazyev, O. V.; Helm, L.; Malkin, V. G.; Malkina, O. L. Quantum Chemical Investigation of Hyperfine Coupling Constants on First Coordination Sphere Water Molecule of Gadolinium(III) Aqua Complexes. *The Journal of Physical Chemistry A* **2005**, *109*, 10997.

(129) Li, X.; Rinkevicius, Z.; Tu, Y.; Tian, H.; Ågren, H. Nuclear Magnetic Shielding of the 113Cd(II) Ion in Aqua Solution: A Combined Molecular Dynamics/Density Functional Theory Study. *The Journal of Physical Chemistry B* **2008**, *112*, 11347.

(130) Yazyev, O. V.; Helm, L. Nuclear Spin Relaxation Parameters of MRI Contrast Agents – Insight from Quantum Mechanical Calculations. *Eur. J. Inorg. Chem.* **2008**, *2008*, 201.

(131) Rastrelli, F.; Bagno, A. Predicting the NMR Spectra of Paramagnetic Molecules by DFT: Application to Organic Free Radicals and Transition-Metal Complexes. *Chemistry – A European Journal* **2009**, *15*, 7990.

(132) Floyd, W. C.; Klemm, P. J.; Smiles, D. E.; Kohlgruber, A. C.; Pierre, V. C.; Mynar, J. L.; Fréchet, J. M. J.; Raymond, K. N. Conjugation Effects of Various Linkers on Gd(III) MRI Contrast Agents with Dendrimers: Optimizing the Hydroxypyridinonate (HOPO) Ligands with Nontoxic, Degradable Esteramide (EA) Dendrimers for High Relaxivity. *Journal of the American Chemical Society* **2011**, *133*, 2390.

(133) Andolina, C. M.; Klemm, P. J.; Floyd, W. C.; Fréchet, J. M. J.; Raymond, K. N. Analysis of Lanthanide Complex Dendrimer Conjugates for Bimodal NIR and MRI Imaging. *Macromolecules* **2012**, *45*, 8982.

(134) Duncan, A. K.; Klemm, P. J.; Raymond, K. N.; Landry, C. C. Silica Microparticles as a Solid Support for Gadolinium Phosphonate Magnetic Resonance Imaging Contrast Agents. *Journal of the American Chemical Society* **2012**, *134*, 8046.

(135) Winter, M. B.; Klemm, P. J.; Phillips-Piro, C. M.; Raymond, K. N.; Marletta, M. A. Porphyrin-Substituted H-NOX Proteins as High-Relaxivity MRI Contrast Agents. *Inorg. Chem.* **2013**, *52*, 2277.

(136) Hastings, C. J.; Pluth, M. D.; Bergman, R. G.; Raymond, K. N. Enzymelike Catalysis of the Nazarov Cyclization by Supramolecular Encapsulation. *Journal of the American Chemical Society* **2010**.

(137) Troughton, J. S.; Greenfield, M. T.; Greenwood, J. M.; Dumas, S. p.; Wiethoff, A. J.; Wang, J.; Spiller, M.; McMurry, T. J.; Caravan, P. Synthesis and Evaluation of a High Relaxivity Manganese(II)-Based MRI Contrast Agent. *Inorg. Chem.* **2004**, *43*, 6313.

(138) Jebasingh, B.; Alexander, V. Synthesis and Relaxivity Studies of a Tetranuclear Gadolinium(III) Complex of DO3A as a Contrast-Enhancing Agent for MRI. *Inorg. Chem.* **2005**, *44*, 9434.

(139) Bonnet, C. S.; Fries, P. H.; Gadelle, A.; Gambarelli, S.; Delangle, P. A Rigorous Framework To Interpret Water Relaxivity. The Case Study of a Gd(III) Complex with an Œ±-Cyclodextrin Derivative. *Journal of the American Chemical Society* **2008**, *130*, 10401.

(140) Lelyveld, V. S.; Brustad, E.; Arnold, F. H.; Jasanoff, A. Metal-Substituted Protein MRI Contrast Agents Engineered for Enhanced Relaxivity and Ligand Sensitivity. *Journal of the American Chemical Society* **2010**, *133*, 649.

(141) Tong, S.; Hou, S.; Zheng, Z.; Zhou, J.; Bao, G. Coating Optimization of Superparamagnetic Iron Oxide Nanoparticles for High T2 Relaxivity. *Nano Lett.* **2010**, *10*, 4607.

(142) Arifin, K.; Majlan, E. H.; Wan Daud, W. R.; Kassim, M. B. Bimetallic complexes in artificial photosynthesis for hydrogen production: A review. *Int. J. Hydrogen Energy* **2012**, *37*, 3066.

(143) Kanan, M. W.; Nocera, D. G. In Situ Formation of an Oxygen-Evolving Catalyst in Neutral Water Containing Phosphate and Co2+. *Science* **2008**, *321*, 1072.

(144) Faunce, T.; Styring, S.; Wasielewski, M. R.; Brudvig, G. W.; Rutherford, A. W.; Messinger, J.; Lee, A. F.; Hill, C. L.; deGroot, H.; Fontecave, M.; MacFarlane, D. R.; Hankamer, B.; Nocera, D. G.; Tiede, D. M.; Dau, H.; Hillier, W.; Wang, L.; Amal, R. Artificial photosynthesis as a frontier technology for energy sustainability. *Energy & Environmental Science* **2013**, *6*, 1074.

(145) Cuk, T.; Weare, W. W.; Frei, H. Unusually Long Lifetime of Excited Charge-Transfer State of All-Inorganic Binuclear TiOMnII Unit Anchored on Silica Nanopore Surface. *The Journal of Physical Chemistry C* **2010**, *114*, 9167.

(146) Soo, H. S.; Macnaughtan, M. L.; Weare, W. W.; Yano, J.; Frei, H. EXAFS Spectroscopic Analysis of Heterobinuclear TiOMn Charge-Transfer Chromophore in Mesoporous Silica. *The Journal of Physical Chemistry C* **2011**, *115*, 24893.

(147) Greenwood, B. P.; Rowe, G. T.; Chen, C.-H.; Foxman, B. M.; Thomas, C. M. Metal-Metal Multiple Bonds in Early/Late Heterobimetallics Support Unusual Trigonal Monopyramidal Geometries at both Zr and Co. *Journal of the American Chemical Society* **2009**, *132*, 44.

(148) Choi, J.; Wang, D. Y.; Kundu, S.; Choliy, Y.; Emge, T. J.; Krogh-Jespersen, K.; Goldman, A. S. Net Oxidative Addition of C(sp3)-F Bonds to Iridium via Initial C-H Bond Activation. *Science* **2011**, *332*, 1545.

(149) Setty, V. N.; Zhou, W.; Foxman, B. M.; Thomas, C. M. Subtle Differences Between Zr and Hf in Early/Late Heterobimetallic Complexes with Cobalt. *Inorg. Chem.* **2011**, *50*, 4647.

(150) Walker, G. C.; Barbara, P. F.; Doorn, S. K.; Dong, Y.; Hupp, J. T. Ultrafast measurements on direct photoinduced electron transfer in a mixed-valence complex. *The Journal of Physical Chemistry* **1991**, *95*, 5712.

(151) Johnson, A. E.; Levinger, N. E.; Kliner, D. A. V.; Tominaga, K.; Barbara, P. F. Ultrafast experiments on the role of vibrational modes in electron transfer. *Pure Appl. Chem.* **1992**, *64*, 1219.

(152) Kunkely, H.; Pawlowski, V.; Vogler, A. Photoredox behavior of a trinuclear Ru(III),Ru(II),Co(III) complex induced by metal-to-metal charge transfer excitations. *Inorg. Chim. Acta* **1994**, *225*, 327.

(153) Omberg, K. M.; Schoonover, J. R.; Treadway, J. A.; Leasure, R. M.; Dyer, R. B.; Meyer, T. J. Mid-Infrared Spectrum of [Ru(bpy)3]2+*. *Journal of the American Chemical Society* **1997**, *119*, 7013.

(154) Damrauer, N. H.; McCusker, J. K. Ultrafast Dynamics in the Metal-to-Ligand Charge Transfer Excited-State Evolution of [Ru(4,4'-diphenyl-2,2'-bipyridine)3]2+. *The Journal of Physical Chemistry A* **1999**, *103*, 8440.

(155) Stelling, A. L.; Ronayne, K. L.; Nappa, J. r. m.; Tonge, P. J.; Meech, S. R. Ultrafast Structural Dynamics in BLUF Domains:‚Äâ Transient Infrared Spectroscopy of AppA and Its Mutants. *Journal of the American Chemical Society* **2007**, *129*, 15556.

(156) Cho, S.; Mara, M. W.; Wang, X.; Lockard, J. V.; Rachford, A. A.; Castellano, F. N.; Chen, L. X. Coherence in Metal-Metal-to-Ligand-Charge-Transfer Excited States of a Dimetallic Complex Investigated by Ultrafast Transient Absorption Anisotropy. *The Journal of Physical Chemistry A* **2011**, *115*, 3990.

(157) Shaw, G. B.; Grant, C. D.; Shirota, H.; Castner, E. W.; Meyer, G. J.; Chen, L. X. Ultrafast Structural Rearrangements in the MLCT Excited State for Copper(I) bis-Phenanthrolines in Solution. *Journal of the American Chemical Society* **2007**, *129*, 2147.

(158) Hedley, G. J.; Ruseckas, A.; Samuel, I. D. W. Ultrafast luminescence in Ir(ppy)3. *Chem. Phys. Lett.* **2008**, *450*, 292.

(159) Rack, J. J. Electron transfer triggered sulfoxide isomerization in ruthenium and osmium complexes. *Coord. Chem. Rev.* **2009**, *253*, 78.

(160) Best, J.; Sazanovich, I. V.; Adams, H.; Bennett, R. D.; Davies, E. S.; Meijer, A. J. H. M.; Towrie, M.; Tikhomirov, S. A.; Bouganov, O. V.; Ward, M. D.; Weinstein, J. A. Structure and Ultrafast Dynamics of the Charge-Transfer Excited State and Redox Activity of the Ground State of Mono- and Binuclear Platinum(II) Diimine Catecholate and Bis-catecholate Complexes: A Transient Absorption, TRIR, DFT, and Electrochemical Study. *Inorg. Chem.* **2010**, *49*, 10041.

(161) Lynch, M. S.; Van Kuiken, B. E.; Daifuku, S. L.; Khalil, M. On the Role of High-Frequency Intramolecular Vibrations in Ultrafast Back-Electron Transfer Reactions. *The Journal of Physical Chemistry Letters* **2011**, *2*, 2252.

(162) McClure, B. A.; Rack, J. J. Ultrafast Spectroscopy of a Photochromic Ruthenium Sulfoxide Complex. *Inorg. Chem.* **2011**, *50*, 7586.

(163) Sawyer, K. R.; Cahoon, J. F.; Shanoski, J. E.; Glascoe, E. A.; Kling, M. F.; Schlegel, J. P.; Zoerb, M. C.; Hapke, M.; Hartwig, J. F.; Webster, C. E.; Harris, C. B. Time-resolved IR Studies on the Mechanism for the Functionalization of Primary C-H Bonds by Photoactivated Cp*W(CO)3(Bpin). *Journal of the American Chemical Society* **2010**, *132*, 1848.

(164) DeKock, R. L.; Gray, H. B. *Chemical Structure and Bonding*; 2 edition ed.; University Scence Books: Sausalito, 1989.

(165) Geoffroy, G. L.; Wrighton, M. S. *Organometallic Photochemistry*; Academic Press: New York, 1979.

(166) Bredenbeck, J.; Helbing, J.; Hamm, P. Transient two-dimensional infrared spectroscopy: Exploring the polarization dependence. *The Journal of Chemical Physics* **2004**, *121*, 5943.

(167) Cowan, D. O.; Drisko, R. L. E. Photochemical reactions. V. Photodimerization of acenaphthylene. Heavy-atom solvent effects. *Journal of the American Chemical Society* **1970**, *92*, 6281.

(168) Thompson, L. G.; Webber, S. E. External heavy atom effect on the phosphorescence spectra of some halonaphthalenes. *The Journal of Physical Chemistry* **1972**, *76*, 221.

(169) Cowan, D. O.; Koziar, J. C. Heavy-atom effects on the spin-forbidden processes of acenaphthylene. *Journal of the American Chemical Society* **1975**, *97*, 249.

(170) Havlas, Z.; Michl, J. Prediction of an Inverse Heavy-Atom Effect in HCCH2Br Bromine Substituent as a pi-Acceptor. *Journal of the American Chemical Society* **2002**, *124*, 5606.

Appendix A Calculated structures

DFT-calculated ground and transition state structures, as described in the appropriate methods section (3.3). All structures are listed in Cartesian coordinates

A.1 Tricarbonyl iron diene

Tricarbonyl(1,3-Butadiene)Iron(0) Ground State

Atom	X	Y	Z
Fe	0.02271900	−0.00000100	0.01615300
C	0.03846400	−0.00002300	1.77504200
O	0.06105900	−0.00004100	2.94674700
C	−1.14548400	−1.27087600	−0.33745700
O	−1.90699700	−2.13609200	−0.55395800
C	−1.14536800	1.27098800	−0.33742500
O	−1.90679800	2.13628300	−0.55390100
C	1.44937400	0.70428900	−1.30387200
C	1.60744200	1.38813700	−0.08397500
H	1.15260700	1.17004700	−2.23596600
C	1.44931600	−0.70441000	−1.30387100
H	2.28287600	0.96553300	0.63359000
H	1.36189800	2.43904600	−0.06119200
H	1.15250900	−1.17014500	−2.23596500
C	1.60732800	−1.38827000	−0.08397300
H	1.36169700	−2.43915800	−0.06118700
H	2.28280200	−0.96571900	0.63358700

Tricarbonyl(1,3-Butadiene)Iron(0) TS (Turnstile Rotation)

Atom	X	Y	Z
C	1.46107500	1.38953200	-0.84229400
C	-1.04439300	1.27083500	-0.61427400
O	-1.74629000	2.12837600	-0.99581700
C	-0.52033100	0.00000000	1.68979300
Fe	-0.00303300	0.00000000	-0.00875600
O	-0.90303000	0.00000000	2.79514700
C	-1.04439400	-1.27083400	-0.61427400
O	-1.74629000	-2.12837500	-0.99581700
C	1.92481300	-0.72024100	0.32659000
C	1.46107500	-1.38953200	-0.84229400
H	2.16238500	-1.26851300	1.24404000
C	1.92481300	0.72024000	0.32659000
H	1.66736200	-1.00457300	-1.84572600
H	1.30415300	-2.47173300	-0.78805400
H	2.16238500	1.26851200	1.24404000
H	1.30415300	2.47173300	-0.78805400
H	1.66736300	1.00457300	-1.84572600

Tricarbonyl(1,5-Cyclooctadiene)Iron(0) Ground State

Atom	X	Y	Z
Fe	−0.56101500	0.02716800	0.01708300
C	−1.76708300	−0.54572200	−1.11725000
O	−2.58930200	−0.90335500	−1.87284100
C	−1.58130600	−0.65187400	1.28227500
O	−2.27926700	−1.06649500	2.12966100
C	−1.01012600	1.74318400	−0.02552200
O	−1.35568100	2.86165300	−0.06354000
H	0.15939000	−1.48985300	−2.18422200
C	0.73097500	−1.03993100	−1.36009200
C	1.58456100	−2.05363200	−0.61617000
C	0.97146000	0.35756800	−1.47293700
C	2.07638800	−1.52728000	0.74332200
H	0.96761700	−2.95549500	−0.45041100
H	2.43561600	−2.37835800	−1.25755300
C	2.20623900	1.07449200	−0.91885000
H	0.49558700	0.84934100	−2.33065400
C	1.03538300	−0.63257500	1.41448500
H	3.02346500	−0.96794600	0.62996500
H	2.30506800	−2.37635100	1.41330900
C	2.01510000	1.60256200	0.52503600
H	2.45100900	1.92247300	−1.58397500
H	3.07663800	0.39369800	−0.97270400
C	1.02755400	0.77738500	1.33531500
H	0.55893500	−1.06745400	2.30124600
H	2.98917500	1.65114200	1.05965500
H	1.64075800	2.64096200	0.48448700
H	0.54226500	1.31197200	2.16278200

Tricarbonyl(1,5-Cyclooctadiene)Iron(0) TS (Turnstile Rotation)

Atom	X	Y	Z
Fe	0.00000000	0.00000000	0.00000000
C	0.00000000	0.00000000	1.74983085
O	0.01194137	0.00000000	2.92055231
C	−0.39540244	1.72550399	−0.08622064
O	−0.67598117	2.86390100	−0.10203795
C	−1.51986570	−0.89748172	0.04994441
O	−2.55047007	−1.45515058	0.12902410
H	2.42760251	0.54472267	1.08653307
C	2.14438270	0.12509436	0.11077611
C	2.70042522	0.91054007	−1.06620061
C	1.77534607	−1.24811497	0.09654215
C	1.93382359	0.65016002	−2.38177844
H	2.62969165	1.98505787	−0.81790205
H	3.78522267	0.69691957	−1.19524998
C	1.94668525	−2.17193137	−1.11191063
H	1.78023264	−1.76019784	1.06706825
C	0.45132565	0.35341331	−2.15832571
H	2.38832198	−0.18917635	−2.93983793
H	2.02082449	1.53289072	−3.04114264
C	0.67447816	−2.24514761	−1.97956546
H	2.20376201	−3.18662608	−0.75659314
H	2.81335797	−1.83830221	−1.71300829
C	−0.09554698	−0.93635336	−2.01678690
H	−0.24418858	1.12055726	−2.51961327
H	0.90851934	−2.56537154	−3.01986705
H	0.00067976	−3.01808939	−1.56824232
H	−1.14493394	−1.03936421	−2.32460770

A.2 MRI contrast agent complexes

Gd-DTPA Complex

Atom	X	Y	Z
C	11.20411209	3.38313736	2.22132189
N	11.55187800	1.30437300	3.58769100
O	10.15746817	2.95006865	1.89713306
C	11.52589095	2.26329703	3.03299671
N	8.94435800	0.56878500	5.23312500
O	12.05179009	4.17756836	2.21913589
C	11.91415400	0.17796600	2.69229900
N	7.11190800	3.33171300	5.86596800
O	9.59766400	0.05079000	2.01494500
C	10.68085000	−0.65228200	2.35775900
O	10.89806600	−1.62422800	1.43357500
C	11.45549600	0.94746800	5.02650500
O	6.84270100	0.92589700	3.48868700
C	10.31408700	−0.01278700	5.36400700
O	5.55327300	−0.37497500	4.80282400
C	7.94090800	−0.51392300	5.04167400
O	9.60100300	3.44844900	4.54690800
C	6.64034100	0.02373600	4.41299000
O	9.68817290	5.55506502	5.44217773
C	8.65268300	1.34231600	6.46825500
O	7.32407300	3.91153300	2.94800400
C	7.29295500	2.07129400	6.59560700
O	5.31781000	4.51669600	2.86346600
C	7.94223100	4.42537400	6.13166100
O	7.59548400	2.03131500	0.68867400
C	9.11939590	4.48986602	5.32232573
C	5.96752100	3.49540800	4.96146400
C	6.32738800	4.34922700	3.74292400
H	6.86343200	1.40143400	0.54594100
H	7.83593000	2.37469200	−0.20373300
H	12.18330995	2.30280603	2.17634571
H	11.51291595	3.04454003	3.77781071
H	12.71415000	−0.43089800	3.13604000
H	12.30324200	0.61177500	1.75864200
H	11.35747100	1.88344700	5.57874600
H	12.39803400	0.47657100	5.34640700
H	10.37158200	−0.86682500	4.68457600
H	10.47019100	−0.38884500	6.38756800

H	7.71418800	−1.03456700	5.98120100
H	8.36020400	−1.23780500	4.33665700
H	9.45787600	2.06211400	6.61687800
H	8.67392400	0.64838900	7.32475100
H	6.46176800	1.41281100	6.34359800
H	7.20111300	2.31704500	7.66304300
H	8.34596600	4.39095500	7.14686200
H	7.43803200	5.36608200	5.91726900
H	5.16036500	3.99972800	5.51463000
H	5.61880800	2.50460600	4.65320400
Na	6.42364300	4.38739600	0.73032600
Gd	8.77058600	1.92893100	2.90087600

Gd-DOTA Complex

Atom	X	Y	Z
C	6.46983700	2.65717400	13.07964000
N	6.09637800	2.08005200	11.76659600
O	3.27770100	1.00503100	10.40588700
C	6.36587600	4.17951200	13.16931100
N	5.01088700	4.73698900	12.95497600
O	3.23154800	2.53442900	13.09900200
C	5.10517500	6.18218700	12.62818500
N	4.54923500	5.87955100	10.17469900
O	2.80192400	2.76733100	15.19598200
C	5.49709900	6.43783200	11.17025500
N	5.52203300	3.23891100	9.00707200
O	2.25464700	5.27998000	11.62602100
C	5.20099900	5.75002600	8.84897400
N	3.67572200	−0.01835800	11.10701400
O	1.68698200	7.46602500	11.64293600
C	6.15456900	4.55888800	8.75901700
O	2.74467700	3.64185000	8.83502700
C	6.56857100	2.23667200	9.31596700
O	2.94315500	3.81153300	6.59053000
C	7.12066000	2.35316700	10.73696700
O	1.07689600	2.97773400	10.82031300
C	5.93924400	0.59109400	11.93483500
C	4.54710000	0.16061600	12.25286000
C	2.88935100	−1.21505900	11.04623200
C	2.82328600	−2.05805600	12.13968400
C	3.47198000	−1.76944100	13.35274900
C	3.98545400	−0.38300100	13.49869300
C	4.13231700	4.53122000	14.14552000
C	3.71013900	3.06905000	14.23602200
C	3.33617400	6.73323200	10.06982300
C	2.33508200	6.51974900	11.22388700
C	4.73896700	2.81289400	7.81665200
C	3.35796900	3.49827200	7.69701500
H	7.50408000	2.37113300	13.34332500
H	5.79911400	2.22945700	13.82972400
H	6.74007900	4.47508000	14.16392300
H	7.04037500	4.64358300	12.44419000
H	5.84427100	6.68204300	13.27565300
H	4.14224100	6.64453700	12.84293600
H	5.60316800	7.52519200	11.02491200

H	6.48371400	6.00575600	10.98008000
H	5.76969600	6.66100100	8.59910100
H	4.42021000	5.65484300	8.09397000
H	6.62419200	4.56897300	7.76159900
H	6.96584800	4.68927500	9.47937200
H	7.40523500	2.30295500	8.60034700
H	6.12379800	1.24709900	9.18243000
H	7.98290300	1.67299000	10.84175600
H	7.51295800	3.35892000	10.90093200
H	6.62946100	0.23687600	12.71283200
H	6.23855900	0.11781300	10.99346300
H	2.42378600	−1.39613900	10.08658600
H	2.27401200	−2.98816600	12.01937200
H	3.54541600	−2.50561000	14.14656800
H	3.40431400	0.31386600	14.11092700
H	3.23448500	5.14633600	13.99600300
H	4.63504800	4.86503400	15.06675600
H	2.80791700	6.44937400	9.15454300
H	3.59864400	7.79734000	10.00257900
H	4.53718200	1.74116100	7.91391400
H	5.30470000	2.96983100	6.88835700
H	1.05845100	3.16647300	9.86368200
H	0.79310700	3.80237000	11.25335300
Gd	3.55699900	3.48386700	11.02072300

Gd-HOPO Complex

Atom	X	Y	Z
C	−0.14590000	0.12620000	0.82700000
N	−0.49520000	−0.55240000	6.01750000
O	1.01140000	−0.17550000	1.29780000
C	−0.75900000	−0.66540000	−0.18550000
N	0.06210000	1.69550000	4.06980000
O	−0.11200000	−1.69980000	−0.61860000
N	−1.13550000	−2.95450000	4.06950000
O	0.08300000	3.93120000	3.59950000
C	−2.79160000	0.64000000	0.04400000
N	2.46050000	−1.49540000	5.53270000
O	0.86190000	−3.43590000	1.95230000
C	−2.19170000	1.42360000	1.04800000
O	1.38540000	−4.23390000	−0.58800000
O	−2.06150000	−4.67600000	5.24430000
C	0.03500000	2.75450000	3.23040000
O	3.31420000	−1.44270000	2.46410000
C	0.07270000	1.82990000	5.51860000
O	3.88700000	−3.67400000	1.06530000
C	−0.90710000	0.85300000	6.16940000
O	4.16110000	−1.28100000	7.04120000
C	0.44800000	−4.58120000	1.52430000
O	3.98100000	−0.39780000	0.04180000
C	0.71020000	−5.01440000	0.19370000
O	0.47430000	−3.09740000	−2.93400000
C	−0.69930000	−6.95960000	0.56390000
C	−0.95290000	−6.54710000	1.88280000
C	−1.21570000	−4.25030000	4.45020000
C	−2.04910000	−1.95060000	4.60300000
C	−1.65020000	−1.47110000	6.00770000
C	4.30390000	−2.18880000	2.81300000
C	4.60530000	−3.38350000	2.10000000
C	6.46350000	−3.79840000	3.60860000
C	6.19460000	−2.60680000	4.30380000
C	3.72800000	−1.16860000	5.88930000
C	1.49410000	−2.00740000	6.49680000
C	0.52160000	−0.93740000	7.00970000
Gd	2.13880000	−2.10010000	0.39970000
H	−1.21360000	−7.85570000	0.22870000
H	7.31110000	−4.37910000	3.96050000
H	−3.83770000	0.84000000	−0.17050000

H	−0.41590000	−2.70640000	3.39710000
H	2.18010000	−1.35060000	4.57020000
H	0.04880000	0.76100000	3.68120000
H	−0.21260000	2.85850000	5.75000000
H	1.08770000	1.67820000	5.90810000
H	−1.03800000	1.12650000	7.23100000
H	−1.88000000	0.98290000	5.68560000
H	0.05310000	−1.29830000	7.94150000
H	1.10980000	−0.05580000	7.27950000
H	2.06680000	−2.40280000	7.33830000
H	0.94310000	−2.83390000	6.03940000
H	−2.52490000	−1.00190000	6.48260000
H	−1.42190000	−2.35910000	6.60420000
H	−3.04810000	−2.39480000	4.65360000
H	−2.08510000	−1.11100000	3.90380000
H	0.70650000	−3.84120000	−2.34260000
H	3.92790000	0.30180000	−0.62360000
H	4.12590000	0.02930000	0.89970000
H	−0.06520000	−2.54680000	−2.33050000
C	5.72610000	−4.23610000	2.52910000
C	−2.12130000	−0.35050000	−0.63910000
C	0.14730000	−6.28550000	−0.29090000
N	−0.81700000	1.25270000	1.36310000
N	−0.29120000	−5.40530000	2.40440000
N	5.12610000	−1.76710000	3.89130000
C	4.62740000	−0.68300000	4.73800000
H	5.46620000	−0.14910000	5.18200000
H	4.07780000	0.00440000	4.09430000
C	−0.15110000	−5.18310000	3.84250000
H	0.84200000	−4.76410000	4.02860000
H	−0.22500000	−6.13250000	4.37090000
C	−0.00390000	2.41580000	1.73510000
H	1.02320000	2.21440000	1.41930000
H	−0.34350000	3.31350000	1.21160000
H	0.36850000	−6.61640000	−1.29760000
H	5.92940000	−5.15780000	1.99900000
H	−2.56950000	−0.93690000	−1.43140000
C	−2.96730000	2.39670000	1.87900000
H	−2.55330000	3.41180000	1.84210000
H	−4.00360000	2.44560000	1.53930000
H	−2.96570000	2.09740000	2.93660000
C	7.06520000	−2.13110000	5.42360000
H	7.58680000	−1.19870000	5.16200000

H	6.48840000	−1.92910000	6.33360000
H	7.82260000	−2.88420000	5.64900000
C	−1.89220000	−7.28650000	2.78340000
H	−1.36020000	−7.90430000	3.52150000
H	−2.53340000	−6.60360000	3.35120000
H	−2.52340000	−7.95700000	2.19630000
O	2.62670000	−1.85510000	−2.03690000
H	3.46180000	−2.19920000	−2.38180000
H	1.88940000	−2.29710000	−2.55140000

Fe-HOPO Complex

Atom	X	Y	Z
C	0.00514200	−0.00969800	0.02811800
C	0.02855400	0.03798600	4.41293800
C	4.06060500	0.03187000	2.17780700
N	−0.49188400	0.54843800	−1.11588900
N	−0.86952000	0.56742000	5.29213500
N	5.27946200	0.59617900	2.41285200
O	1.05490600	0.47905000	0.59774100
O	0.22594100	0.58692300	3.25928800
O	2.98067800	0.59599200	2.60553400
C	−0.62741500	−1.16049200	0.60311400
C	0.80122100	−1.11776500	4.76213900
C	3.95617600	−1.20305300	1.45721600
N	−0.14352500	3.28990900	0.14872600
N	0.24646000	3.29463200	4.48311000
N	3.93815000	3.33925100	1.93630000
O	−0.03374900	−1.65853500	1.67970800
O	1.66457700	−1.51994300	3.84568500
O	2.72949200	−1.68524500	1.34221100
C	−1.76966300	−1.65256900	−0.00231200
C	0.61560000	−1.66789900	6.02010400
C	5.11688700	−1.75999100	0.95016500
N	1.36639300	5.07460100	2.21544200
O	−0.87030700	3.82424900	−1.95337300
O	−1.35373200	3.84792800	6.02355000
O	6.12447400	3.87995300	2.34511400
C	−2.26487900	−1.02663300	−1.16571700
C	−0.31481200	−1.08184200	6.90347800
C	6.35416200	−1.11532900	1.17356600
C	−1.64090700	0.06113700	−1.73065800
C	−1.05456500	0.02713100	6.56033700
C	6.45330000	0.04715800	1.89938200
C	0.24355500	1.70441300	−1.67015200
C	−1.61897500	1.75981200	4.84205900
C	5.30059300	1.80630400	3.26108600
C	−0.31051700	3.05160600	−1.17301300
C	−0.89476400	3.07850100	5.17711100
C	5.16379300	3.11607900	2.46333900
C	−0.60492200	4.52405900	0.77477000
C	1.03382800	4.51247200	4.63434000
C	3.61121900	4.56801100	1.22369000

C	0.53880100	5.49941500	1.07380900
C	0.78609700	5.51128000	3.49784400
C	2.76109300	5.52453700	2.06892600
Fe	1.43369900	-0.56871400	2.22999800
H	-3.16182000	-1.40688400	-1.64016800
H	0.16879700	1.69075600	-2.75364100
H	1.28813500	1.59098100	-1.37930000
H	0.39028300	2.62520200	0.69780100
H	-1.14814400	4.27468700	1.69208100
H	-1.30758100	4.98673800	0.07949200
H	0.12237400	6.50853000	1.23510400
H	1.16739000	5.56156700	0.18076700
H	-0.45804500	-1.50629600	7.89019700
H	7.26278000	-1.54533400	0.76849500
H	-2.58952400	1.77729000	5.32829200
H	-1.75758300	1.66568600	3.76456300
H	6.24198500	1.84410300	3.80092900
H	0.50793800	2.62163900	3.77014000
H	4.48075000	1.71171700	3.97411300
H	2.09378200	4.24346500	4.68721400
H	3.20672500	2.66047900	2.12109000
H	0.74930300	4.96407900	5.58676000
H	3.09599900	4.31449400	0.29141200
H	1.17007800	6.50205200	3.79373300
H	4.55708000	5.04868900	0.96748700
H	2.81049900	6.53695700	1.63221600
H	-0.29613300	5.62040500	3.38184500
H	3.21873500	5.58985500	3.06044100
C	7.75971400	0.73781800	2.17097000
H	7.72094900	1.80368200	1.92803000
H	8.05958800	0.64896100	3.22260800
H	8.53993400	0.27245500	1.56655800
C	-2.13725400	0.72763600	-2.98237000
H	-2.23705800	1.81021600	-2.86375700
H	-1.46593000	0.54901800	-3.83135300
H	-3.11337100	0.31487800	-3.24136900
C	-2.04837300	0.66722200	7.48746600
H	-1.87665200	1.74229500	7.59520800
H	-3.07966600	0.52935500	7.14015900
H	-1.96674800	0.20354200	8.47163500
H	1.19535200	-2.53392900	6.32278700
H	5.07123400	-2.68322700	0.38146400
H	-2.27625900	-2.51469600	0.41951300

H	0.60592400	-3.49091500	1.48334100
O	1.32569600	-4.11863000	1.29899600
H	2.06400200	-3.48712100	1.23963900

A.3 Heterobimetallic zirconium-cobalt complexes

Co-Zr Heterobimetallic Complex, O Ligand

Atom	X	Y	Z
P	4.83696300	2.42007600	7.65512800
P	4.69853000	5.51721900	4.72573100
P	0.89778000	0.95344800	4.27705200
C	4.39098300	2.93134900	9.43483600
N	3.31626700	1.97536500	6.94395700
O	7.20440100	5.62458600	7.68466100
C	5.20483300	4.11743500	9.97710300
N	3.21965700	4.78240400	4.20616100
O	5.03459400	2.61077000	4.76794300
C	4.36066300	1.77933100	10.45619200
N	2.24945400	1.40142700	3.29308900
C	6.04304200	0.98033800	7.89554400
C	7.33632300	1.53618200	8.52317900
C	6.38032300	0.28311800	6.57226900
C	2.24463100	1.45722600	7.74521100
C	2.16272600	0.08713600	8.10083700
C	1.11134700	−0.35689200	8.91353100
C	0.11011800	0.49555200	9.38137500
C	0.16785700	1.83013200	8.97446800
C	1.19965300	2.31872300	8.16696200
C	3.14828900	−0.93666500	7.59257200
C	−0.98567200	−0.00288000	10.29337300
C	1.14381800	3.75625700	7.71471100
C	4.24962500	7.17829200	5.50652100
C	5.43745100	8.13843900	5.70228000
C	3.56197100	6.96516400	6.86588500
C	5.79404400	5.92018400	3.23635700
C	5.38021100	7.09291500	2.33044400
C	7.27219500	6.02293600	3.66181800
C	2.40524200	5.34696900	3.15717800
C	1.28771300	6.17287400	3.45663200
C	0.52535400	6.72162000	2.41932900
C	0.80553400	6.48082600	1.07392100
C	1.86745200	5.62277100	0.79131200
C	2.66033100	5.04383400	1.79079800
C	0.84765500	6.47052800	4.87003600
C	−0.00647800	7.12077200	−0.02702600
C	3.75796400	4.11158300	1.32427300

C	−0.75028000	1.60636300	3.60754200
C	−0.74492900	3.14033400	3.63650500
C	−1.91261400	1.08251000	4.47129800
C	0.76965700	−0.93328300	4.13439500
C	0.12910900	−1.58711300	5.37181800
C	0.12863500	−1.45376800	2.83671400
C	2.68736400	0.75470100	2.08814400
C	2.08236900	0.99749600	0.82997600
C	2.56285800	0.33727400	−0.30864400
C	3.62772000	−0.56126900	−0.26457400
C	4.22955100	−0.77377000	0.97702300
C	3.79119800	−0.13864800	2.14305500
C	0.93284600	1.95805700	0.64188100
C	4.10222100	−1.28558400	−1.50205400
C	4.54352400	−0.40641300	3.42324600
C	6.43276700	4.97242100	7.10584500
Co	5.50819100	3.92081700	6.10062400
Zr	3.17193900	2.64407200	4.81515100
H	3.35989300	3.27796500	9.31963200
H	5.08901000	5.00760000	9.35704000
H	6.27420500	3.90042500	10.05006700
H	4.85222900	4.36630600	10.98539200
H	3.94581900	2.14866500	11.40158000
H	3.73364700	0.94819000	10.12723000
H	5.36139000	1.39379000	10.67358000
H	5.60444700	0.25631600	8.58965400
H	8.07053100	0.72822200	8.62225800
H	7.18470500	1.96364100	9.51708900
H	7.77873900	2.30980800	7.88620500
H	6.78455900	0.99662100	5.84952400
H	5.50785300	−0.18259800	6.11504900
H	7.12821600	−0.49988400	6.74871100
H	1.07195400	−1.41290300	9.17519100
H	−0.61438000	2.51686700	9.29221300
H	4.03991200	−1.01231100	8.22352600
H	2.68992300	−1.92962400	7.56936700
H	3.48776100	−0.68768400	6.58595200
H	−0.70352300	0.09727800	11.34943500
H	−1.91279400	0.56151500	10.15236400
H	−1.20391500	−1.06074000	10.11664900
H	0.85705900	3.81758800	6.65599000
H	0.39196500	4.31679200	8.27763200
H	2.10336000	4.26887700	7.81473600

H	3.53849400	7.64274200	4.81144000
H	5.89708600	8.45496000	4.76552700
H	6.21403900	7.69517800	6.33198600
H	5.08457600	9.04245600	6.21314200
H	3.10311400	7.90109400	7.20693100
H	4.29378400	6.66065400	7.61912000
H	2.78535600	6.20211900	6.82833500
H	5.71109200	4.99479100	2.66212400
H	4.34271400	7.02177800	1.99945400
H	6.01596400	7.10641800	1.43625200
H	5.50844300	8.05981800	2.82469400
H	7.47715800	6.90842900	4.26944200
H	7.90436100	6.08610600	2.76792500
H	7.58073800	5.14276000	4.23320900
H	−0.32374400	7.35090900	2.67994000
H	2.09084000	5.37994500	−0.24620400
H	1.11208100	5.66251700	5.55045400
H	−0.23643500	6.61486100	4.90687900
H	1.30583700	7.38508300	5.26190700
H	−0.03336400	6.49232800	−0.92261400
H	−1.03811600	7.30332200	0.28972400
H	0.41716100	8.08899200	−0.32331800
H	3.36767000	3.39460300	0.59827300
H	4.21146000	3.54391300	2.13594400
H	4.55659900	4.66826100	0.82045500
H	−0.89568400	1.26404500	2.57941200
H	−1.66082400	3.53269500	3.17889600
H	−0.71318000	3.50629600	4.66986800
H	0.10108000	3.57631100	3.10248800
H	−2.09614400	0.01526000	4.33117400
H	−1.73114700	1.25826900	5.53821600
H	−2.83604400	1.60998700	4.20435500
H	1.82662500	−1.22240400	4.12149300
H	0.28932700	−2.67171000	5.33788200
H	−0.95139900	−1.42354300	5.40820700
H	0.55125500	−1.20704000	6.30397600
H	0.20082100	−2.54801500	2.80541600
H	0.62397800	−1.06361000	1.94531500
H	−0.93503600	−1.20082800	2.77924200
H	2.08442000	0.54589200	−1.26404500
H	5.07522100	−1.45502700	1.04694100
H	0.94086100	2.75402000	1.38430100
H	0.98141600	2.42016400	−0.34901300

H	−0.03595200	1.44843400	0.70216600
H	3.65756200	−2.28645800	−1.57571100
H	5.18918800	−1.41631500	−1.49834900
H	3.83079800	−0.74225500	−2.41232000
H	5.22881500	−1.24922000	3.29510100
H	5.13348900	0.46187800	3.73449200
H	3.87401100	−0.64742200	4.25521700

Co-Zr Heterobimetallic Complex, OH Ligand

Atom	X	Y	Z
P	5.09730600	2.91703300	7.76698200
P	4.70910900	5.73796300	5.06970500
P	7.07988000	2.46423200	4.35853600
C	4.23704000	4.07584100	9.00481600
N	3.83037100	2.03879500	6.97286700
O	8.50771500	5.20835200	7.54288200
C	5.13424300	5.21411800	9.52794700
N	3.43915600	4.79444100	4.39347200
C	3.48137700	3.39535400	10.16137600
N	5.65383800	1.75875100	3.69938700
C	6.01515100	1.75292000	8.96754100
C	6.85994800	2.48261800	10.03185900
C	6.94263400	0.75010600	8.27749500
C	2.71428800	1.33328800	7.56892100
C	2.80871800	0.03706400	8.13860000
C	1.67290100	−0.56730100	8.70161200
C	0.42045600	0.03330300	8.71645200
C	0.32174200	1.28682700	8.10790100
C	1.42072600	1.93010000	7.53827000
C	4.06275900	−0.79991100	8.16539100
C	−0.77672000	−0.62846600	9.35496700
C	1.17898000	3.25666400	6.87541400
C	3.96294400	7.23220400	6.00371200
C	5.01764900	8.29109300	6.37920500
C	3.16911600	6.90490000	7.27358400
C	5.53165600	6.65909400	3.61847200
C	4.68564500	7.75218600	2.93833800
C	6.94556400	7.18542800	3.93503600
C	2.46401400	5.19644000	3.40314000
C	1.23832500	5.84118900	3.73148600
C	0.33074700	6.18888200	2.72287900
C	0.55316100	5.92085500	1.37426600
C	1.73519700	5.25506200	1.06064000
C	2.67719900	4.89304600	2.03008400
C	0.81552600	6.18069600	5.13720500
C	−0.43299500	6.33626800	0.30918900
C	3.90464600	4.18624300	1.52045700
C	8.14272700	1.01990800	5.00718000
C	9.28523400	1.44086800	5.95386600
C	8.66820600	0.04088900	3.94048800

118

C	8.21390200	3.09127400	2.95363500
C	7.68975100	4.31618900	2.19918500
C	9.64662900	3.41676400	3.42087700
C	5.51454700	0.59178000	2.85566400
C	5.06287100	−0.63025700	3.43475100
C	4.89637300	−1.77354600	2.65262200
C	5.14825600	−1.78541500	1.27881500
C	5.56222900	−0.58610300	0.71293600
C	5.74374900	0.59230900	1.45546900
C	4.74390900	−0.74556200	4.89928100
C	4.97971900	−3.04147400	0.45825500
C	6.17339500	1.79596700	0.65375300
C	7.63529700	4.80618700	6.88455800
Co	6.27723300	4.10280600	5.94191400
Zr	4.09100600	2.74101000	4.91588600
H	3.48713200	4.53867300	8.36092400
H	5.68276000	5.70653000	8.72226800
H	5.86359400	4.87291300	10.26256200
H	4.51089000	5.96502100	10.02825100
H	2.91131100	4.15308800	10.71353500
H	2.77530400	2.64119400	9.81137500
H	4.15630700	2.92034100	10.87925300
H	5.21116600	1.21280600	9.47789100
H	7.47902700	1.74355200	10.55457600
H	6.26343600	2.98979700	10.78923900
H	7.53990300	3.21108500	9.57899300
H	7.88833900	1.23064600	8.03245200
H	6.53239900	0.33482900	7.36015400
H	7.15995300	−0.08582300	8.95265700
H	1.78875100	−1.56003200	9.13324800
H	−0.64473800	1.78548400	8.06984100
H	4.50780000	−0.84225500	9.16653200
H	3.83013100	−1.83131800	7.88067900
H	4.81078300	−0.42413500	7.48085200
H	−1.03753200	−0.14969400	10.30727400
H	−1.66121000	−0.56428000	8.71188900
H	−0.58603800	−1.68575400	9.56081400
H	1.23725600	3.17609600	5.78479400
H	0.18394600	3.63707200	7.12144700
H	1.91172500	4.00123400	7.18696600
H	3.27772800	7.66850200	5.26775200
H	5.39046000	8.85238800	5.52347300
H	5.87396000	7.84137100	6.89358600

H	4.56823300	9.01699700	7.06707000
H	2.49562600	7.73764200	7.50900800
H	3.84129900	6.78536800	8.12107600
H	2.55957500	6.00918300	7.18892300
H	5.64222300	5.84645000	2.89910500
H	3.69062500	7.39980500	2.66180600
H	5.19009700	8.07700300	2.01963700
H	4.57070100	8.63988300	3.56711600
H	6.92561000	8.09745200	4.53335400
H	7.46431300	7.42907900	3.00012900
H	7.54560900	6.45330000	4.48075500
H	−0.59552100	6.67832800	3.01859800
H	1.94332500	5.00025200	0.02266700
H	1.26485700	5.51055200	5.85899300
H	−0.27215600	6.10793700	5.23302600
H	1.09102400	7.20464500	5.41399500
H	−0.39924600	5.66276500	−0.55288200
H	−1.45796400	6.34313600	0.69311400
H	−0.21946300	7.34728600	−0.06109900
H	3.63049600	3.40730100	0.80256700
H	4.47791300	3.71382400	2.31440600
H	4.57154400	4.88123800	0.99424700
H	7.40898700	0.47835300	5.60728200
H	9.54788800	0.60057200	6.60638000
H	10.19076800	1.70862300	5.40790000
H	9.01579800	2.29229900	6.58255400
H	7.87840500	−0.34285000	3.29393800
H	9.43727900	0.49619500	3.30948200
H	9.13497500	−0.81672900	4.44112600
H	8.26237100	2.24569700	2.26059400
H	8.18492900	4.38951400	1.22351400
H	7.92417700	5.22498300	2.75149200
H	6.61766500	4.29499300	2.02161200
H	10.16337300	3.96617300	2.62513600
H	10.24191600	2.52961900	3.63288200
H	9.64989300	4.05408900	4.31171600
H	4.55713900	−2.68610800	3.13888300
H	5.75050000	−0.54442500	−0.35854500
H	5.53911700	−0.33076200	5.51851500
H	3.81937700	−0.22143200	5.16202500
H	4.61072600	−1.79289500	5.18313100
H	5.73188800	−3.79551700	0.72134000
H	5.07948000	−2.83557500	−0.61137500

H	3.99780800	-3.49981200	0.62182600
H	5.62098200	1.83655100	-0.29087800
H	5.99876500	2.72235300	1.18347100
H	7.23787700	1.75132100	0.39216200
O	2.60978400	1.89654600	3.94885300
H	2.06172100	1.65890300	3.19522500

Appendix B   Data processing code

This code, written for MATLAB R2010a and back-compatible, takes the various outputs of the ultrafast laser apparatus's Labview operating system and converts it into a format suitable for further analysis and presentation.

The scripts are significantly long; scripts that have not changed over the course of my tenure are not included, and can instead be found in the theses of Matthew Zoerb, Karma Sawyer, and James Cahoon. Only scripts altered significantly by me are included.

B.1   avgt2d_v02

This code is designed to process, extract, average, and perform statistical tests on the output of the laser when running in T2D-IR mode; as such, it takes as input *seven* rather than *three* columns of data, and requires the added degree of sophistication in processing and producing difference spectra that this implies.

```
%_____
%_____
% "avgt2d" program written by Adam Hill, based upon code originally
% finalized by James Cahoon and Karma Sawyer.
% This version is currently functional with minor sections that could be
% expanded for further funcionality as of April 11, 2009.
%
% This program is designed to average T2D-IR data
%  collected at one or multiple polarization angles, one or multiple UVpump-IRprobe
%  and IRpump-IRprobe delay times, and one or multiple IRpump frequencies. The
% data is written as a binary Matlab file (.mat), which contains several variables:
% 1) sorteddata: contains the actual experimental data organized as cell
%    arrays of cell arrays. Each cell array row and column organizes the
%    data, as follows:
%    first cell array:
%      row 1, column 1:  absorbance data
%      row 1, column 2:  standard deviation data
%    fourth array (not a cell array, contains the actual data)
%      column 1:  wavenumbers
%      column 2:  absorbance data or standard deviation data
% 2) IRtimes: contains the IR-pump-IRprobe delay times
```

```
% 3) UVtimes: contains the UV-pump-IRprobe delay times
% 4) datafilename: string with the data filename, not including .mat
%    extension
% 5) polarizations: each row contains the different polarization conditions
%    with which data was collected. For T2D-IR data, the first column is the
%    UVpump-IRprobe relative polarization and the second column is IRpump-
%    IRprobe relative polarization
% 6) waves: contains the wavenumbers collected

% This program assumes that the data filenames are contained in the file
% "datinfo.txt" and goes through all files specified by it

% This program does NOT plot the data, calculate kinetics, or calculate
% anisotropy data. These functions are performed by a separate matlab
% program "analyze2d" which relies on all the variables created by this
% program and written in the binary matlab file "datafilename.mat"
%_____
_____

%START BY RESETING ALL VARIABLES, ETC.
clear;
echo off;

%Initialize cell arrays that are used later in the program to store data;
%by doing so at this point, there is no possiblity of bugs being induced
%due to these arrays being instantiated inside a loop and then called later
%after the loop has ended.
alldata = {};
alldatat1d = {};
alldata2d = {};
alldatat2d = {};

%Attempt to fix error on line 883 found on 4/16/2009 (due to this value
previously being instantiated in a loop):
nmbrcolumns=6;

% -------------------------------------------------------------------------
% Parameters used by program which you may want to adjust as needed:

% determines number of standard deviations outside of which data must be
% to be determined as an outlier and deleted
stddevthresh = 3;

% determines the number of standard deviations for oscillations in the
% data less than 2 cm-1 apart in order for data set to be removed
stddevthreshoscillations = 1;
```

```matlab
%  determines the number of data points needed before noise analysis will
%  throw away outliers (e.g. at least three for some statistics)
dataptsthresh = 3;

%  determines how to round the IR time delays, for
%  10 fs set to 100
%  5 fs set to 200
%  1 fs set to 1000
timerounding = 100;

%  determines the name of the input file
inputfile='datinfo.txt';
%  ------------------------------------------------------------------------

%THIS SECTION IMPORTS AND PREPARES THE APPROPRIATE FILE TO BE
PROCESSED
fin = fopen(inputfile,'r');
if fin < 0
  error(['Could not open ',inputfile,' for input']);
end

%How do you want the output to come out? This is a carryover from the
%original avg2d program by Cahoon and Sawyer.
outputfileboolean = input('Write output binary file (.mat)? ','s');
if length(outputfileboolean)==0
  outputfileboolean='y';
end

%Statistical stuff--this is a carryover from avg2d program.
oscillationanalysis = input('Perform error analysis on oscillations? ','s');
if oscillationanalysis == 'y'
  minimization = input('Scale individual data sets to mean? (requires chi.m,
simps.m, scaleddata.m) ','s');
  if length(minimization) == 0
    minimization = 'y';
  end
else
  oscillationanalysis = 'n';
  minimization = 'n';
end
%Gets the file, figures out how many data files need to be processed.
filebody = fgetl(fin);
specinfo = fscanf(fin,'%f');
nmbrfiles = length(specinfo);
```

```
%_____
_____
% This for loop goes through all the files as specified by the datinfo
% file, picking out the details of the data. Note that all data files
% should be of the same format, so it's not technically necessary to check
% much of this information twice (in terms of computational time) but it
% does provide a good self-check to ensure that all files are consistent.
for filenmbr=1:nmbrfiles

    %
    
    _____
    _____
    % This section determines the properties of this particular file, e.g.
    % are there multiple IRpump frequencies, how many lines are there
    % between specification of polarization / pump freqs, etc
    filename = strcat(filebody,num2str(specinfo(filenmbr,1)));
    fin = fopen(filename,'r');
    %This loop skips through data we don't need.
    %Skips through: compound name, solvent, pump wavelength, probe center,
    %and IR frequency numbers. It just wants to know if they're there in
    %the original data, and we now know that they definitely are.
    for i=1:5
        header = fgetl(fin);
    end
    %Initializes these variables so that they can be accessed between loops
    %later.
    counterpolar=0;
    counterUVpolar=0;
    counterIRpolar=0;
    counter=0;  %initialize counter for the number of lines between polarizations
here
    polarizationcounter=0;
    %The only case we need from avg2d: if IR Frequency is present.
    counterfreq=0;
    IRfreqindex=1;
    yesIRfreqs='y'; %IRfreqs are definitely listed for T2D--*****this is an old
variable that is no longer necessary.*****
    polarizationdone = 'n'; %There will definitely be polarizations listed too.

    %Now, a while loop to determine the number of polarization sections,
    %and the number of lines of data that make up each section.
    done = 'n';
    line = fgetl(fin);
    nmbrpolarizationsections = 0;
```

```matlab
    while done == 'n'   %when this loop starts, we should be in case 2
        if length(line) <3  %case 0
            done = 'y';
            %loop is done if it hits a blank line
        elseif line(1:20)=='IR Pump Polarization';  %case 1
            nmbrpolarizationsections = nmbrpolarizationsections;
            %don't do anything if we hit an IR pump polarization
        elseif line(1:20)=='UV Pump Polarization';  %case 2
            nmbrpolarizationsections = nmbrpolarizationsections+1;
            %the variable is modified when we hit UV pump
            %polarization--this always occurs in a pair with IR pol
            %information, thus we only need to make the incrementation
            %once. this is modifying the already-instantiated variable.
        elseif line(1:12)=='IR Frequency';  %case 3
            done='y';
            %if we hit a new IR frequency, then we've finished a given
            %section of the data file and the loop completes.
        else    %case 4
            counter=counter+1;
            %if we're on a line with regular data, the counter tracking the
            %total number of data lines in a section is incremented
        end %end of if-else structure
        line = fgetl(fin);  %go to the next line in preparation for a new pass through
the loop
    end %while loop
    polarizationcounter = counter/nmbrpolarizationsections;
    %'counter' now contains the number of lines between different IR
    %frequency sections; 'nmbrpolarizationsections' contains the number of
    %polarizations in that section of length counter; 'polarizationcounter'
    %contains the number of lines of data in a given polarization section.

    %Now we're approaching the data again; reset to the start of the file
    %here and jump through the code again.
    fclose(fin);
    fin = fopen(filename,'r');
    for i=1:4
        header = fgetl(fin);
    end

    %Here we set up the data structure that we'll be putting our actually
    %data into later. It's not necessary to do this for later files,
    %because at that point it's already been done.
    if filenmbr==1
        IRfreqs(1,1:2)=[10000 10000];
        tempfreq(1,1:2)=[20000 20000];
        UVpolarizations(1,1)=500;
```

```
        IRpolarizations(1,1)=500;
    end


%_____
_____
    % This section reads the data out of the file while simultaneously
    % organizing it by polarization and IRpump frequency.

    %Variables are instantiated outside of the loop:
    counterpolarizationsections = 0;
    UVtemppolarization(1,1) = double(0.00);
    IRtemppolarization(1,1) = double(0.00);
    done = 'n';
    %_-_-_-_-_-_-_-_-_-_-_-_-_-_-_-_-_-_-_-_-_-_-_-_-_-_-_-_-_-_-_-
_-_-_
    while done=='n'              %WHILE LOOP BEGINS HERE
        clear line;
        line = fgetl(fin);
        if length(line)<5   %ending condition for the while loop
            break;
        end


%_____
_____
        %Now we get the initial information about center IR frequency and
        %polarizations which we'll later use to organize the information we
        %get from the file. Note that the original document splits this into
        %two different cases for one polarization or several.
        if nmbrpolarizationsections > 1 %this is for the multipolarization case
            if counterpolarizationsections==0
                clear index;
                tempfreq(1,1) = str2num(line(15:20));   %get the IR center frequency
                index  =  find(tempfreq(1,1)-1  <=  IRfreqs(:,1)+1  &  IRfreqs(:,1)-1  <=
tempfreq(1,1)+1); %does the tempfreq match an existing IRfreq within one cm-1?
                if length(index)==0 %case where they don't match
                    newIRfreq='y';
                    counterfreq=counterfreq+1;
                    IRfreqindex=counterfreq;
                    tempfreq(1,2) = 0;
                    IRfreqs(IRfreqindex,1) = tempfreq(1,1);
                elseif length(index)==1; %case where they do match
                    IRfreqindex=index(1,1);
                end
                %Now that we have the IRfreq data, we go to the next two lines
                %and get the appropriate UV and IR polarization values.
```

127

```
        clear line;
        line = fgetl(fin);
        UVtemppolarization(1,1) = str2num(line(23:26));
        clear line;
        line = fgetl(fin);
        IRtemppolarization(1,1) = str2num(line(23:26));
    else    %If we're just switching polarizations, not IR freqs, all we need to do
is pull out the new polarization.
        UVtemppolarization(1,1) = str2num(line(23:26));
        clear line;
        line = fgetl(fin);
        IRtemppolarization(1,1) = str2num(line(23:26));
    end
  elseif nmbrpolarizationsections < 2 %This is the single polarization case.
Doesn't have code for getting just polarizations w/o IR freqs.
    clear index;
    tempfreq(1,1) = str2num(line(15:20));
    index = find(tempfreq(1,1)-1 <= IRfreqs(:,1)+1 & IRfreqs(:,1)-1 <=
tempfreq(1,1)+1);
      if length(index)==0 %i3
        newIRfreq='y';
        counterfreq=counterfreq+1;
        IRfreqindex=counterfreq;
        tempfreq(1,2) = 0;
        IRfreqs(IRfreqindex,1) = tempfreq(1,1);
      elseif length(index)==1;
        IRfreqindex=index(1,1);
        %This is not okay. This means that if the IR freq matches ANY previous
frequency,
        %it will be appended onto position 1. This needs to be fixed.
        %The only possible exception is if tempfreq keeps track of
        %past frequencies as well as the current one. Check the use
        %of these variables in particular; concatenation to old
        %data if this matches may be messed up.
      end
      %Now that we have the IRfreq data, we go to the next two lines
      %and get the appropriate UV and IR polarization values.
      clear line;
      line = fgetl(fin);
      UVtemppolarization(1,1) = str2num(line(23:26));
      clear line;
      line = fgetl(fin);
      IRtemppolarization(1,1) = str2num(line(23:26));
    end %done with getting IR frequencies and polarizations.

    %- - - - - - - - - - - - - - - - - - - - - - - - - - - - - -
```

%Now we get the actual data points from the file. Note that fscaf()
%takes advantage of a filestream data structure, so if called
%repeatedly, it will return sequential sections of the input file.
%"data" should now be the the entirety of a matrix of data between
%lines of text in the input file. %g specifies that the new
%imported data will be formatted as floats or exponentials,
%whichever is more compact; the [] matrix descibes the size of the
%data to be input--i.e. where to stop. Since this is the t2d case
%only, the input file should ALWAYS have 7 columns.
data = fscanf(fin,'%g %g %g %g %g %g %g',[7 polarizationcounter]);

%fscanf() essentially removes the data from the file stream.
%Because of this, it is necessary to jump over that gap left by the
%method. Thus fgetl is called just once to go through that null
%space.
clear line;
line = fgetl(fin);

data = data'; %transposes the data

%The time delay values are now rounded to the nearest time step
%according to the variable "timerounding," as defined above. (see
%comments earlier)
data(:,2) = round(timerounding*data(:,2))/timerounding; %IR delay time
data(:,1) = round(timerounding*data(:,1))/timerounding; %UV delay time

%_____

%Further code now sets up the data structure into which the data
%will be placed. Though in the original, multipurpose program, this
%had various if/else clauses to handle different numbers of input
%columns, this has been dispensed with due to the more singular
%nature of this piece of code.

%Just as is was decided previously if the IR center frequency
%matches one that had been seen before, this code decides whether
%the polarizations are ones we've seen before--i.e., are one or
%both of them the same.
IRpolarizationindex = find(IRtemppolarization(1,1)-1 <= IRpolarizations(:,1)
& IRpolarizations(:,1) <= IRtemppolarization(1,1)+1);
    UVpolarizationindex   =   find(UVtemppolarization(1,1)-1   <=
UVpolarizations(:,1) & UVpolarizations(:,1) <= UVtemppolarization(1,1)+1);
    polarizationindex = find(UVtemppolarization(1,1)-1 <= UVpolarizations(:,1)
& UVpolarizations(:,1) <= UVtemppolarization(1,1)+1 & IRtemppolarization(1,1)-
1   <=   IRpolarizations(:,1)   &   IRpolarizations(:,1)   <=

IRtemppolarization(1,1)+1);%If IR and UV polarizations are BOTH the same as ones seen before, returns 1. Otherwise, returns null.

```
    newpolarization='n';    %by default, the newly-input polarization is one that's already been seen
    %- - - - - - - - - - - - - - - - - - - - - - - - - - - - - - - -
    %Each of these three cases deals with implementing a new
    %polarization index. The first "if" statement deals with the case
    %of either being new; the subsequent two create the data structures
    %for only their respective polarization being new.
    if length(polarizationindex)==0 %Either one is new.
        newpolarization='y';
        counterpolar=counterpolar+1;
        polarizationindex=counterpolar; %This allows the polarization index to later be used as an actual index, without getting null pointer errors.
        UVpolarizations(polarizationindex,1)=UVtemppolarization;
        IRpolarizations(polarizationindex,1)=IRtemppolarization;
        %polarizations(polarizationindex,1:2)=[UVtemppolarization IRtemppolarization];
        polarizations(polarizationindex,1)=UVtemppolarization;
        polarizations(polarizationindex,2)=IRtemppolarization;
    else
    end %Either
    if length(IRpolarizationindex)==0 %IR is new.
        newpolarization='y';
        counterIRpolar=counterIRpolar+1;
        IRpolarizationindex=counterIRpolar;
        onlyIRpolarizations(IRpolarizationindex,1)=IRtemppolarization;
        nmbrIRpolarizations=length(onlyIRpolarizations);
    else
    end %IR
    if length(UVpolarizationindex)==0 %UV is new.
        newpolarization='y';
        counterUVpolar=counterUVpolar+1;
        UVpolarizationindex=counterUVpolar;
        onlyUVpolarizations(UVpolarizationindex,1)=UVtemppolarization;
        nmbrUVpolarizations=length(onlyUVpolarizations);
    else
    end %UV

    %If we stopped, we must have in one way or another finished a polarization section.
    counterpolarizationsections=counterpolarizationsections+1;
```

%_____

_____

```matlab
    %Now the data that had been collected into a matrix(data) from the
    %input file is placed in the data structure designed based upon the
    %information about IR center frequencies and polarizations gathered
    %earlier.
    if   counterpolarizationsections==nmbrpolarizationsections   %Case   where
we're at the end of a section under one IR center freq.
        counterpolarizationsections=0;
        clear line;
        line = fgetl(fin);   %skips over the final line that repeats the IR center
frequency.
        tempfreq(1,2) = str2num(line(15:20));
        IRfreqs(IRfreqindex,2) = tempfreq(1,2);
        %The following commented-out block of code is only necessary if
        %you can have repeats of the exact same IR pump frequency and
        %polarization settings together. Labview code has been altered
        %as of 2009.04.11 to make this impossible, i.e. limit of 1
        %kinetic scan. However, this portion of the code is being left
        %in case it should become necessar to implement it. Note that
        %it requires some polishing before it can be used, notably to
        %correct errors in indexing with IRfreqindex.
        %if newpolarization=='n'   %If it's a polarization we've seen before, we
concatenate it on to what we already have at that polarization.
            %tempdata = alldata{polarizationindex(1),IRfreqindex};
            %tempdata = tempdata';
            %tempdata = [tempdata data'];    %concatenates the new data on
            %tempdata = tempdata';
            %tempdata = sortrows(tempdata,1);
            %alldata{polarizationindex(1),IRfreqindex} = tempdata;
            %clear tempdata;
        %else   %Otherwise, it goes in as a new polarization.
            data = sortrows(data,1);
            alldata{polarizationindex(1),IRfreqindex}=data;
        %end %f2
    else   %Otherwise, case where we're in the middle of an IR section, switching
between polarizations.
        if newpolarization=='y' | newIRfreq=='y' %If it's a new polarization at a
new IR center frequency.
            newpolarization = 'n';
            newIRfreq = 'n';
            data = sortrows(data,1);
            alldata{polarizationindex(1),IRfreqindex}=data;
        else   %Otherwise, it's a polarization we've already seen in the middle of an
IR center section that's already been set up.
            tempdata = alldata{polarizationindex(1),IRfreqindex};
            tempdata = tempdata';
```

```
            tempdata = [tempdata data'];    %concatenates the new data onto the
old.
            tempdata = tempdata';
            tempdata = sortrows(tempdata,1);
            alldata{polarizationindex(1),IRfreqindex} = tempdata;
            clear tempdata;
        end %f2
    end %f1
    nmbrpolarizations=nmbrUVpolarizations*nmbrIRpolarizations;
  end %f0 THIS IS THE END OF THE WHILE LOOP FROM ABOVE
  %_-_-_-_-_-_-_-_-_-_-_-_-_-_-_-_-_-_-_-_-_-_-_-_-_-_-_-_-_-_-_-_-_-
_-_-


%_____
_____
  %In this for loop, the data that has been compiled above is now sorted
  %by polarization. In addition, computations that had originally been
  %done in Labview have been trasfered to this section. Data is switched
  %from the "current" format to the "original" format. Columns in the
  %data are as follows:
  %Line        Original      Current
  %1           tUV          same
  %2           tIR          same
  %3           IRfreq        same
  %4         T1D intensity    A00 absorbance (neither)
  %5          2D intensity    A-IR absorbance
  %6         T2D intensity    A-UV asorbance
  %7           null        A11 absorbance (both)

%_____
_____
  for i=1:length(IRfreqs(:,1))
    if nmbrpolarizations==4
      data00=alldata{1,i};
      data090=alldata{2,i};
      data900=alldata{3,i};
      data9090=alldata{4,i};
      %Here, data originally in the alldata array is converted to the
      %correct format for further analysis and computation, i.e.
      %essentially rawr labview data is processed as it would have been
      %originally before changes were made.
      tempdata00=data00; %Creates a temporar array with which to manipulate
the data.
      tempdata00(:,4)=(data00(:,4)-data00(:,5)); %T1D Data
      tempdata00(:,5)=(data00(:,4)-data00(:,6)); %2D Data
```

tempdata00(:,6)=((data00(:,4)+data00(:,7))-(data00(:,5)+data00(:,6)));
%T2D Data
    data00=tempdata00(:,1:6); %Puts the modified data back into the array.
    tempdata090=data090; %Creates a temporar array with which to
manipulate the data.
    tempdata090(:,4)=(data090(:,4)-data090(:,5)); %T1D Data
    tempdata090(:,5)=(data090(:,4)-data090(:,6)); %2D Data
    tempdata090(:,6)=((data090(:,4)+data090(:,7))-
(data090(:,5)+data090(:,6))); %T2D Data
    data090=tempdata090(:,1:6); %Puts the modified data back into the
array.
    tempdata900=data900; %Creates a temporar array with which to
manipulate the data.
    tempdata900(:,4)=(data900(:,4)-data900(:,5)); %T1D Data
    tempdata900(:,5)=(data900(:,4)-data900(:,6)); %2D Data
    tempdata900(:,6)=((data900(:,4)+data900(:,7))-
(data900(:,5)+data900(:,6))); %T2D Data
    data900=tempdata900(:,1:6); %Puts the modified data back into the
array.
    tempdata9090=data9090; %Creates a temporar array with which to
manipulate the data.
    tempdata9090(:,4)=(data9090(:,4)-data9090(:,5)); %T1D Data
    tempdata9090(:,5)=(data9090(:,4)-data9090(:,6)); %2D Data
    tempdata9090(:,6)=((data9090(:,4)+data9090(:,7))-
(data9090(:,5)+data9090(:,6))); %T2D Data
    data9090=tempdata9090(:,1:6); %Puts the modified data back into the
array.
    %data00, data090, data900, and data9090 should now look like it would
    %have had changes to labview not been made.
    %T2D data sorted by polarization
    alldatat2d{1,i}=[data00(:,1) data00(:,2) data00(:,3) data00(:,6)];
    alldatat2d{1,i}=sortrows(alldatat2d{1,i},2);
    alldatat2d{1,i}=sortrows(alldatat2d{1,i},1);
    alldatat2d{2,i}=[data090(:,1) data090(:,2) data090(:,3) data090(:,6)];
    alldatat2d{2,i}=sortrows(alldatat2d{1,i},2);
    alldatat2d{2,i}=sortrows(alldatat2d{1,i},1);
    alldatat2d{3,i}=[data900(:,1) data900(:,2) data900(:,3) data900(:,6)];
    alldatat2d{3,i}=sortrows(alldatat2d{1,i},2);
    alldatat2d{3,i}=sortrows(alldatat2d{1,i},1);
    alldatat2d{4,i}=[data9090(:,1)   data9090(:,2)   data9090(:,3)
data9090(:,6)];
    alldatat2d{4,i}=sortrows(alldatat2d{1,i},2);
    alldatat2d{4,i}=sortrows(alldatat2d{1,i},1);
    %T1D data sorted by polarization
    alldatat1d{1,i}(1:length(data00),:)=[data00(:,1) data00(:,3) data00(:,4)];

```
        alldatat1d{1,i}(length(data00)+1:2*length(data00),:)=[data090(:,1)
data090(:,3) data090(:,4)];
        alldatat1d{1,i}=sortrows(alldatat1d{1,i},1);
        alldatat1d{2,i}(1:length(data900),:)=[data900(:,1)          data900(:,3)
data900(:,4)];
        alldatat1d{2,i}(length(data900)+1:2*length(data900),:)=[data9090(:,1)
data9090(:,3) data9090(:,4)];
        alldatat1d{2,i}=sortrows(alldatat1d{2,i},1);
        %2D data sorted by polarization
        alldata2d{1,i}(1:length(data00),:)=[data00(:,2) data00(:,3) data00(:,5)];
        alldata2d{1,i}(length(data00)+1:2*length(data00),:)=[data900(:,2)
data900(:,3) data900(:,5)];
        alldata2d{1,i}=sortrows(alldata2d{1,i},1);
        alldata2d{2,i}(1:length(data900),:)=[data090(:,2)          data090(:,3)
data090(:,5)];
        alldata2d{2,i}(length(data900)+1:2*length(data900),:)=[data9090(:,2)
data9090(:,3) data9090(:,5)];
        alldata2d{2,i}=sortrows(alldata2d{2,i},1);
    elseif nmbrpolarizations==1
      if polarizations(1)==0
        data00=alldata{1,i};
        %Here, data originally in the alldata array is converted to the
        %correct format for further analysis and computation, i.e.
        %essentially rawr labview data is processed as it would have been
        %originally before changes were made.
        tempdata00=data00;  %Creates  a  temporar  array  with  which  to
manipulate the data.
        tempdata00(:,4)=(data00(:,4)-data00(:,5)); %T1D Data
        tempdata00(:,5)=(data00(:,4)-data00(:,6)); %2D Data
        tempdata00(:,6)=((data00(:,4)+data00(:,7))-
(data00(:,5)+data00(:,6))); %T2D Data
        data00=tempdata00(:,1:6); %Puts the modified data back into the array.
        %data00 should now look like it would have had changes to labview
        %not been made.
        alldatat2d{1,i}=[data00(:,1) data00(:,2) data00(:,3) data00(:,6)];
        alldatat2d{1,i}=sortrows(alldatat2d{1,i},2);
        alldatat2d{1,i}=sortrows(alldatat2d{1,i},1);
        alldatat1d{1,i}=[data00(:,1) data00(:,3) data00(:,4)];
        alldatat1d{1,i}=sortrows(alldatat1d{1,i},1);
        alldata2d{1,i}=[data00(:,2) data00(:,3) data00(:,5)];
        alldata2d{1,i}=sortrows(alldata2d{1,i},1);
      elseif polarizations(1)==90
        data9090=alldata{1,i};
        %Here, data originally in the alldata array is converted to the
        %correct format for further analysis and computation, i.e.
        %essentially rawr labview data is processed as it would have been
```

```
        %originally before changes were made.
        tempdata9090=data9090; %Creates a temporar array with which to
manipulate the data.
        tempdata9090(:,4)=(data9090(:,4)-data9090(:,5)); %T1D Data
        tempdata9090(:,5)=(data9090(:,4)-data9090(:,6)); %2D Data
        tempdata9090(:,6)=((data9090(:,4)+data9090(:,7))-
(data9090(:,5)+data9090(:,6))); %T2D Data
        data9090=tempdata9090(:,1:6); %Puts the modified data back into the
array.
        %data00 should now look like it would have had changes to labview
        %not been made.
        alldatat2d{1,i}=[data9090(:,1)        data9090(:,2)        data9090(:,3)
data9090(:,6)];
        alldatat2d{1,i}=sortrows(alldatat2d{1,i},2);
        alldatat2d{1,i}=sortrows(alldatat2d{1,i},1);
        alldatat1d{1,i}=[data9090(:,1) data9090(:,3) data9090(:,4)];
        alldatat1d{1,i}=sortrows(alldatat1d{1,i},1);
        alldata2d{1,i}=[data9090(:,2) data9090(:,3) data9090(:,5)];
        alldata2d{1,i}=sortrows(alldata2d{1,i},1);
    else %Magic angle case, basically. If only one polarization, and it's some
value we don't know/care. This portion added 2009-04-17.
        datamagic=alldata{1,i};
        %Here, data originally in the alldata array is converted to the
        %correct format for further analysis and computation, i.e.
        %essentially rawr labview data is processed as it would have been
        %originally before changes were made.
        tempdatamagic=datamagic; %Creates a temporar array with which to
manipulate the data.
        tempdatamagic(:,4)=(datamagic(:,4)-datamagic(:,5)); %T1D Data
        tempdatamagic(:,5)=(datamagic(:,4)-datamagic(:,6)); %2D Data
        tempdatamagic(:,6)=((datamagic(:,4)+datamagic(:,7))-
(datamagic(:,5)+datamagic(:,6))); %T2D Data
        datamagic=tempdatamagic(:,1:6); %Puts the modified data back into the
array.
        %data00 should now look like it would have had changes to labview
        %not been made.
        alldatat2d{1,i}=[datamagic(:,1)        datamagic(:,2)        datamagic(:,3)
datamagic(:,6)];
        alldatat2d{1,i}=sortrows(alldatat2d{1,i},2);
        alldatat2d{1,i}=sortrows(alldatat2d{1,i},1);
        alldatat1d{1,i}=[datamagic(:,1) datamagic(:,3) datamagic(:,4)];
        alldatat1d{1,i}=sortrows(alldatat1d{1,i},1);
        alldata2d{1,i}=[datamagic(:,2) datamagic(:,3) datamagic(:,5)];
        alldata2d{1,i}=sortrows(alldata2d{1,i},1);
    end
end
```

end %End of data sorting 'for' loop for all IR frequencies.

%_____
_____
%_____
_____
%_____
_____
    %At this point, we're now reverting to the original version of the
    %averaging code. The problem presented by the input and sorting of the
    %new labview output should be corrected by this point, i.e. the current
    %alldata array should contain data as though the labview file had never
    %been changed.

    %In the original program, the number of columns in the data field was
    %used to differentiate between T1D or 2D and T2D. Because this program
    %functions only with T2D data, this variable has now been necessary
    %before now. However, with the reversion back to the original code, the
    %possible cases for other data input types return (until I have time to
    %remove them), so for now this should make sure that they correct case
    %is used.
    nmbrcolumns=6;

%---
%---
    %BEGIN ORIGINAL PROGRAM VERSION:

    % ---

    % ---
    % Rounds IRpump frequencies to the nearest 0.1 cm-1
    if yesIRfreqs=='y'
       IRfreqs=round(IRfreqs*10)/10;
    end
    % ---

    % ---
    % This section organizes data by time delays into the new variable
    % alldatatimesorted where each row is a new IR time delay
if nmbrcolumns==3
    done='n';
    timecounter=0;
while done=='n'
    %sorts 2D-IR and T1D-IR data by time delay
       tempdata=alldata{1,1};
       if length(tempdata)==0;

```
            break;
        end
        timecounter=timecounter+1;
        times(timecounter)=tempdata(1,1);
        clear tempdata;
        for i=1:length(IRfreqs(:,1))
            for j=1:nmbrpolarizations
                tempdata=alldata{j,i};
                clear index;
                index = find(tempdata(:,1)==times(timecounter));
                if length(index)==0
                    tempcell{j,i} = 0;
                else
                    tempcell{j,i} = tempdata(index(1):index(end),:);
                    alldata{j,i} = tempdata(index(end)+1:end,:);
                    clear tempdata;
                end
            end
        end
    alldatatimesorted{timecounter,1}=tempcell;
    clear tempcell;
  end
    nmbrtimes=length(times);
  end
%sorts T1D-IR, 2D-IR and T2D-IR data measured during T2D-IR data collection
%by the relevant time delays
% sorts 2D-IR data by IR time delay
if nmbrcolumns ==6;
done='n';
timecounter2d=0;
while done=='n';
    tempdata2d=alldata2d{1,1};
     if length(tempdata2d)==0
         break;
     end
     timecounter2d=timecounter2d+1;
     IRtimes(timecounter2d)=tempdata2d(1,1);
     clear tempdata2d;
     for i=1:length(IRfreqs(:,1))
       for j=1:nmbrIRpolarizations
         tempdata2d=alldata2d{j,i};
         clear IRindex;
         IRindex = find(tempdata2d(:,1)==IRtimes(timecounter2d));
         if length(IRindex)==0
            tempcell2d{j,i} = 0;
         else
```

```
            tempcell2d{j,i} = tempdata2d(IRindex(1):IRindex(end),:);
            alldata2d{j,i} = tempdata2d(IRindex(end)+1:end,:);
          end
        end
      end
     alldata2dtimesorted{timecounter2d,1}=tempcell2d;
      clear tempcell2d;
    end
      nmbrIRtimes=length(IRtimes);
    % sorts T1D-IR data by UV time delay
done = 'n';
timecountert1d=0;
while done=='n';
     tempdatat1d=alldatat1d{1,1};
      if length(tempdatat1d)==0;
         break;
       end
       timecountert1d=timecountert1d+1;
       UVtimes(timecountert1d)=tempdatat1d(1,1);
      clear tempdatat1d;
      for i=1:length(IRfreqs(:,1))
        for j=1:nmbrUVpolarizations
           tempdatat1d=alldatat1d{j,i};
           clear UVindex;
           UVindex = find(tempdatat1d(:,1)==UVtimes(timecountert1d));
           if length(UVindex)==0
             tempcellt1d{j,i} = 0;
           else
             tempcellt1d{j,i} = tempdatat1d(UVindex(1):UVindex(end),:);
              alldatat1d{j,i} = tempdatat1d(UVindex(end)+1:end,:);
              clear tempdatat1d;
           end
         end
       end
     alldatat1dtimesorted{timecountert1d,1}=tempcellt1d;
      clear tempcellt1d;
    end
      nmbrUVtimes=length(UVtimes);
      %sorts T2D-IR data by both time delays
done = 'n';
timecountert2d=0;
while done=='n';
   tempdatat2d=alldatat2d{1,1};
     if length(tempdatat2d)==0;
        break;
      end
```

```
    timecountert2d=timecountert2d+1;
    t2dUVtimes(timecountert2d) = tempdatat2d(1,1);
     t2dIRtimes(timecountert2d) = tempdatat2d(1,2);
     clear tempdatat2d;
     for i=1:length(IRfreqs(:,1))
        for j=1:nmbrpolarizations
            tempdatat2d=alldatat2d{j,i};
            clear index;
            index   =   find(tempdatat2d(:,1)==t2dUVtimes(timecountert2d)   &
tempdatat2d(:,2)==t2dIRtimes(timecountert2d));
            if length(index)==0
               tempcell{j,i} = 0;
            else
              tempcell{j,i} = tempdatat2d(index(1):index(end),:);
              alldatat2d{j,i} = tempdatat2d(index(end)+1:end,:);
             clear tempdatat2d;
           end
         end
       end
     tempalldatat2dtimesorted{timecountert2d,1}=tempcell;
     clear tempcell;
   end

alldatat2dtimesorted=reshape(tempalldatat2dtimesorted,nmbrIRtimes,nmbrUV
times);
end
  % ------------------------------------------------------------------------

  % ------------------------------------------------------------------------
  %  This section organizes the data by wavenumbers and accrues data from
different
  % files in the variable 'alldatafiles'.
  if nmbrcolumns==3
  for m=1:nmbrtimes
    clear tempdata;
    tempdata=alldatatimesorted{m,1};
    for k=1:nmbrpolarizations;
      for i=1:length(IRfreqs(:,1))
        clear secondtempdata;
        secondtempdata = tempdata{k,i};
        secondtempdata = sortrows(secondtempdata,2);
        wavecounter=0;
        nmbrwaveavgs=0;
        done='n';
        while done=='n';
           wavecounter=wavecounter+1;
```

```matlab
                    if length(secondtempdata(:,3))==0;
                      clear secondtempdata;
                      break
                    elseif filenmbr > 1
                      if wavecounter == nmbrwaves+1
                        break
                      end
                    end
                    if filenmbr==1
                      waves(wavecounter)=secondtempdata(1,2);
                      nmbrwaves = length(waves);
                    else
                      nmbrwaves = length(waves);
                    end
                    clear index;
                    index = find(secondtempdata(:,2) >= (waves(wavecounter)-0.2) &
secondtempdata(:,2) <= (waves(wavecounter)+0.2));
                    if filenmbr==1
                      alldatafiles{m,1}{k,i}(wavecounter,1)=waves(wavecounter);
                      nmbrdatapts{m,1}{k,i}(wavecounter,1)=0;
                    end
                    if wavecounter == 1
                      clear nmbraddedpts;
                      nmbraddedpts = length(secondtempdata(index(1):index(end),3));

alldatafiles{m,1}{k,i}(wavecounter,1:length(alldatafiles{m,1}{k,i}(wavecounter,:))
+nmbraddedpts)=[alldatafiles{m,1}{k,i}(wavecounter,:)
secondtempdata(index(1):index(end),3)'];

nmbrdatapts{m,1}{k,i}(wavecounter,1)=length(alldatafiles{m,1}{k,i}(wavecounte
r,:))-1;
                      secondtempdata = secondtempdata(index(end)+1:end,:);
                    else

alldatafiles{m,1}{k,i}(wavecounter,1:length(alldatafiles{m,1}{k,i}(wavecounter,:))
)=[alldatafiles{m,1}{k,i}(wavecounter,1:length(alldatafiles{m,1}{k,i}(wavecounte
r,:))-nmbraddedpts) secondtempdata(index(1):index(end),3)'];
                      secondtempdata = secondtempdata(index(end)+1:end,:);
                      nmbrdatapts{m,1}{k,i}(wavecounter,1)=nmbrdatapts{m,1}{k,i}(1,1);
                    end
                  end
                end
              end
                clear tempdata;
              end
          elseif nmbrcolumns==6
```

```matlab
% for T1DIR data measured using T2DIR
 for m=1:nmbrUVtimes
   clear tempdata;
   tempdata=alldatat1dtimesorted{m,1};
   for k=1:nmbrUVpolarizations;
      for i=1:length(IRfreqs(:,1))
         clear secondtempdata;
         secondtempdata = tempdata{k,i};
         secondtempdata = sortrows(secondtempdata,2);
         wavecounter=0;
         nmbrwaveavgs=0;
         done='n';
         while done=='n';
            wavecounter=wavecounter+1;
            if length(secondtempdata(:,3))==0;
               clear secondtempdata;
               break
            elseif filenmbr > 1
               if wavecounter == nmbrwaves+1
                  break
               end
            end
            if filenmbr==1
               waves(wavecounter)=secondtempdata(1,2);
               nmbrwaves = length(waves);
            else
               nmbrwaves = length(waves);
            end
            clear index;
            index = find(secondtempdata(:,2) >= (waves(wavecounter)-0.2) &
secondtempdata(:,2) <= (waves(wavecounter)+0.2));
            if filenmbr==1
               alldatat1dfiles{m,1}{k,i}(wavecounter,1)=waves(wavecounter);
               nmbrdatapts{m,1}{k,i}(wavecounter,1)=0;
            end
            if wavecounter == 1
               clear nmbraddedpts;
               nmbraddedpts = length(secondtempdata(index(1):index(end),3));

alldatat1dfiles{m,1}{k,i}(wavecounter,1:length(alldatat1dfiles{m,1}{k,i}(wavecou
nter,:))+nmbraddedpts)=[alldatat1dfiles{m,1}{k,i}(wavecounter,:)
secondtempdata(index(1):index(end),3)'];

nmbrdatapts{m,1}{k,i}(wavecounter,1)=length(alldatat1dfiles{m,1}{k,i}(wavecou
nter,:))-1;
               secondtempdata = secondtempdata(index(end)+1:end,:);
```

```
        else

alldatat1dfiles{m,1}{k,i}(wavecounter,1:length(alldatat1dfiles{m,1}{k,i}(wavecou
nter,:)))=[alldatat1dfiles{m,1}{k,i}(wavecounter,1:length(alldatat1dfiles{m,1}{k,i}
(wavecounter,:))-nmbraddedpts) secondtempdata(index(1):index(end),3)'];
            secondtempdata = secondtempdata(index(end)+1:end,:);
            nmbrdatapts{m,1}{k,i}(wavecounter,1)=nmbrdatapts{m,1}{k,i}(1,1);
          end
        end
      end
    end
    clear tempdata;
  end
  % for 2DIR data measured using T2DIR
    for m=1:nmbrIRtimes
    clear tempdata;
    tempdata=alldata2dtimesorted{m,1};
    for k=1:nmbrIRpolarizations;
      for i=1:length(IRfreqs(:,1))
        clear secondtempdata;
        secondtempdata = tempdata{k,i};
        secondtempdata = sortrows(secondtempdata,2);
        wavecounter=0;
        nmbrwaveavgs=0;
        done='n';
        while done=='n';
          wavecounter=wavecounter+1;
          if length(secondtempdata(:,3))==0;
            clear secondtempdata;
            break
          elseif filenmbr > 1
            if wavecounter == nmbrwaves+1
              break
            end
          end
          if filenmbr==1
            waves(wavecounter)=secondtempdata(1,2);
            nmbrwaves = length(waves);
          else
            nmbrwaves = length(waves);
          end
          clear index;
          index = find(secondtempdata(:,2) >= (waves(wavecounter)-0.2) &
secondtempdata(:,2) <= (waves(wavecounter)+0.2));
          if filenmbr==1
            alldata2dfiles{m,1}{k,i}(wavecounter,1)=waves(wavecounter);
```

142

```
                nmbrdatapts{m,1}{k,i}(wavecounter,1)=0;
              end
              if wavecounter == 1
                clear nmbraddedpts;
                nmbraddedpts = length(secondtempdata(index(1):index(end),3));

alldata2dfiles{m,1}{k,i}(wavecounter,1:length(alldata2dfiles{m,1}{k,i}(wavecount
er,:))+nmbraddedpts)=[alldata2dfiles{m,1}{k,i}(wavecounter,:)
secondtempdata(index(1):index(end),3)'];

nmbrdatapts{m,1}{k,i}(wavecounter,1)=length(alldata2dfiles{m,1}{k,i}(wavecou
nter,:))-1;
                secondtempdata = secondtempdata(index(end)+1:end,:);
              else

alldata2dfiles{m,1}{k,i}(wavecounter,1:length(alldata2dfiles{m,1}{k,i}(wavecount
er,:)))=[alldata2dfiles{m,1}{k,i}(wavecounter,1:length(alldata2dfiles{m,1}{k,i}(w
avecounter,:))-nmbraddedpts) secondtempdata(index(1):index(end),3)'];
                secondtempdata = secondtempdata(index(end)+1:end,:);
                nmbrdatapts{m,1}{k,i}(wavecounter,1)=nmbrdatapts{m,1}{k,i}(1,1);
              end
            end
          end
        end
        clear tempdata;
      end
%  for T2DIR data measured using T2DIR
     for m=1:nmbrIRtimes
        for h=1:nmbrUVtimes
          clear tempdata;
          tempdata=alldatat2dtimesorted{m,h};
        for k=1:nmbrpolarizations;
          for i=1:length(IRfreqs(:,1))
            clear secondtempdata;
            secondtempdata = tempdata{k,i};
            secondtempdata = sortrows(secondtempdata,3);
            wavecounter=0;
            nmbrwaveavgs=0;
            done='n';
            while done=='n';
              wavecounter=wavecounter+1;
              if length(secondtempdata(:,4))==0;
                 clear secondtempdata;
                 break;
              elseif filenmbr > 1
                if wavecounter == nmbrwaves+1
```

```
                    break;
                  end
                end
              if filenmbr==1
                 waves(wavecounter)=secondtempdata(1,3);
                 nmbrwaves = length(waves);
              else
                 nmbrwaves = length(waves);
              end
              clear index;
              index = find(secondtempdata(:,3) >= (waves(wavecounter)-0.2) &
secondtempdata(:,3) <= (waves(wavecounter)+0.2));
              if filenmbr==1
                 alldatat2dfiles{m,h}{k,i}(wavecounter,1)=waves(wavecounter);
                 nmbrdatapts{m,h}{k,i}(wavecounter,1)=0;
              end
              if wavecounter == 1
                 clear nmbraddedpts;
                 nmbraddedpts = length(secondtempdata(index(1):index(end),4));

alldatat2dfiles{m,h}{k,i}(wavecounter,1:length(alldatat2dfiles{m,h}{k,i}(waveco
unter,:))+nmbraddedpts)=[alldatat2dfiles{m,h}{k,i}(wavecounter,:)
secondtempdata(index(1):index(end),4)'];

nmbrdatapts{m,h}{k,i}(wavecounter,1)=length(alldatat2dfiles{m,h}{k,i}(waveco
unter,:))-1;
                 secondtempdata = secondtempdata(index(end)+1:end,:);
              else

alldatat2dfiles{m,h}{k,i}(wavecounter,1:length(alldatat2dfiles{m,h}{k,i}(waveco
unter,:)))=[alldatat2dfiles{m,h}{k,i}(wavecounter,1:length(alldatat2dfiles{m,h}{
k,i}(wavecounter,:))-nmbraddedpts) secondtempdata(index(1):index(end),4)'];
                 secondtempdata = secondtempdata(index(end)+1:end,:);
                 nmbrdatapts{m,h}{k,i}(wavecounter,1)=nmbrdatapts{m,h}{k,i}(1,1);
              end
            end
          end
        end
      end
    clear tempdata;
  end

    % -----------------------------------------------------------------

    % now goes back to the top and begins with the next file
end
```

```
end

if nmbrcolumns==3
  tempalldatafiles=alldatafiles;
elseif nmbrcolumns==6
  tempalldata2dfiles=alldata2dfiles;
  tempalldatat1dfiles=alldatat1dfiles;
  tempalldatat2dfiles=alldatat2dfiles;
end


% ---------------------------------------------------------------------


% ---------------------------------------------------------------------
% This section performs an error analysis on the data, throwing away data
% deemed outside the acceptable standard deviations. It averages the
% remaining data and calculates standard deviations. It also checks if there
% are readings of 100.00 in the data and removes them.  If there is no
% good data at all for a particular wavenumber, it places a 200.00 in the
% data file.  This 200.00 is then removed by the program "analyze2d" when
% plotting the data

% for 2DIR and T1DIR data
if nmbrcolumns==3
nmbrarraypositions=length(waves)/32;
averagedalldatafiles=alldatafiles;
for m=1:nmbrtimes
  for k=1:nmbrpolarizations;
    for i=1:length(IRfreqs(:,1))

      % ---------------------------------------------------------------
      % this section identifies data points well outside the standard
      % deviation of data
      clear allstddata allmeandata;
      allstddata=zeros(nmbrwaves,2);
      allmeandata=zeros(nmbrwaves,2);
      allstddata(:,1)=alldatafiles{m,1}{k,i}(:,1);
      allmeandata(:,1)=alldatafiles{m,1}{k,i}(:,1);
      for j=1:nmbrwaves
        nmbrpts = length(alldatafiles{m,1}{k,i}(j,2:end));
        clear tempdata stddev;
        tempdata = alldatafiles{m,1}{k,i}(j,2:nmbrpts);
        clear delindex;
        delindex = find(tempdata==100 | tempdata==-100);
        tempdata(delindex)=[];
        nmbrpts = length(tempdata);
        if nmbrpts==0
```

```matlab
        tempdata = 200
      elseif nmbrpts >= dataptsthresh
        stddata=std(tempdata);
        meandata=mean(tempdata);
        delindex   =   find(tempdata   <   meandata-stddevthresh*stddata   |
tempdata > meandata+stddevthresh*stddata);
        tempdata(delindex) = [];
        allstddata(j,2)=std(tempdata);
        allmeandata(j,2)=mean(tempdata);
      else
        allstddata(j,2)=std(tempdata);
        allmeandata(j,2)=mean(tempdata);
      end
    end
    averagedalldatafiles{m,1}{k,i}=[];
    averagedalldatafiles{m,1}{k,i}{1,1}=allmeandata;
    averagedalldatafiles{m,1}{k,i}{1,2}=allstddata;
    % -------------------------------------------------------------

    % -------------------------------------------------------------
    % this section identifies data sets with large oscillations
    % between adjacent wavenumbers (< 2 cm-1) and removes them
    if oscillationanalysis == 'y'
      clear allstddata allmeandata;
      allstddata=zeros(nmbrwaves,2);
      allmeandata=zeros(nmbrwaves,2);
      allstddata(:,1)=alldatat1dfiles{m,1}{k,i}(:,1);
      allmeandata(:,1)=alldatat1dfiles{m,1}{k,i}(:,1);
      if nmbrarraypositions>1
        clear arrayoscillations;
        index=0;
        baddataindex=[];
        for j=1:nmbrdatapts{m,1}{k,i}(1,1)
          clear arrayoscillations
          arrayoscillations = [];
          clear tempdata;
          tempdata = alldatafiles{m,1}{k,i}(:,1+j);
          clear delindex;
          baddata = 'n';
          delindex = find(tempdata==100 | tempdata==-100);
          if length(delindex) > 0
            baddata = 'y';
            baddataindex=[baddataindex j];
          end
          if baddata == 'n'
            index=index+1;
```

```
        for q=2:nmbrarraypositions
            for p=1:nmbrarraypositions-1
                if  abs(waves(32*q)-waves(32*q-p))<1.8  &  abs(waves(32*q)-
waves(32*q-p))>0.1
                    arrayoscillations            =            [arrayoscillations
abs((tempdata([32*q:-1*(p+1):32*q-31*(p+1)])-tempdata([32*q-p:-1*(p+1):32*q-
31*(p+1)-p])))'];
                end
            end
        end
        avgarrayoscillations(index) = mean(arrayoscillations);
    end
end
if length(avgarrayoscillations)>0
    stdoscillations=stddevthreshoscillations*std(avgarrayoscillations);
    meanoscillations=mean(avgarrayoscillations);
    baddataindex=[baddataindex        find(avgarrayoscillations        >
meanoscillations+stdoscillations)];
    if nmbrdatapts{m,1}{k,i}(1,1)-length(baddataindex) < dataptsthresh
    else
        alldatafiles{m,1}{k,i}(:,1+baddataindex)=[];
        if minimization == 'y'
            for j=1:length(alldatafiles{m,1}{k,i}(1,2:end));
                % variable contains scaling factors and
                % offset for each data set
                scalefactors{m,1}{k,i}(1:2,j)=[1 0.0001]';
                avgdata = averagedalldatafiles{m,1}{k,i}{1,1}(:,2);
                data = alldatafiles{m,1}{k,i}(:,j+1);
                low = [0.5 -0.2];
                high = [2 0.2];
                options = foptions;
                deltachi = 2000;
                oldchi = 1000;
                searchparam = [1 0.001]';
                nmbrparam = 1:2;
                while deltachi > 0.01*oldchi

searchparam=simps('chi',searchparam,nmbrparam,options,low,high,avgdata,dat
a);
                    scaleddataset = scaleddata(data,searchparam);
                    newchi=sum((scaleddataset-avgdata).^2);
                    deltachi = oldchi-newchi;
                    oldchi = newchi;
                end
                scalefactors{m,1}{k,i}(1:2,j)=searchparam;
                alldatafiles{m,1}{k,i}(:,1+j) = scaleddataset;
```

147

```
                    clear scaleddataset searchaparam;
                 end
              end
              allstddata(:,2)=std(alldatafiles{m,1}{k,i}(:,2:end)')';
              allmeandata(:,2)=mean(alldatafiles{m,1}{k,i}(:,2:end)')';
              averagedalldatafiles{m,1}{k,i}{1,1}=allmeandata;
              averagedalldatafiles{m,1}{k,i}{1,2}=allstddata;
           end
        end
      end
   end
   % ------------------------------------------------------------
 end
  end
end
elseif nmbrcolumns==6
nmbrarraypositions=length(waves)/32;
% T1DIR data collected with T2DIR
averagedalldatat1dfiles=alldatat1dfiles;
for m=1:nmbrUVtimes
   for k=1:nmbrUVpolarizations;
      for i=1:length(IRfreqs(:,1))

        % ------------------------------------------------------------
        % this section identifies data points well outside the standard
        % deviation of data
        clear allstddata allmeandata;
        allstddata=zeros(nmbrwaves,2);
        allmeandata=zeros(nmbrwaves,2);
        allstddata(:,1)=alldatat1dfiles{m,1}{k,i}(:,1);
        allmeandata(:,1)=alldatat1dfiles{m,1}{k,i}(:,1);
        for j=1:nmbrwaves
           nmbrpts = length(alldatat1dfiles{m,1}{k,i}(j,2:end));
           clear tempdata stddev;
           tempdata = alldatat1dfiles{m,1}{k,i}(j,2:nmbrpts);
           clear delindex;
           delindex = find(tempdata==100 | tempdata==-100);
           tempdata(delindex)=[];
           nmbrpts = length(tempdata);
           if nmbrpts==0
             tempdata = 200
          elseif nmbrpts >= dataptsthresh
             stddata=std(tempdata);
             meandata=mean(tempdata);
             delindex  =  find(tempdata  <  meandata-stddevthresh*stddata  |
tempdata > meandata+stddevthresh*stddata);
```

```matlab
        tempdata(delindex) = [];
        allstddata(j,2)=std(tempdata);
        allmeandata(j,2)=mean(tempdata);
      else
        allstddata(j,2)=std(tempdata);
        allmeandata(j,2)=mean(tempdata);
      end
  end
  averagedalldatat1dfiles{m,1}{k,i}=[];
  averagedalldatat1dfiles{m,1}{k,i}{1,1}=allmeandata;
  averagedalldatat1dfiles{m,1}{k,i}{1,2}=allstddata;
  % --------------------------------------------------------------

  % --------------------------------------------------------------
  % this section identifies data sets with large oscillations
  % between adjacent wavenumbers (< 2 cm-1) and removes them
  if oscillationanalysis == 'y'
     clear allstddata allmeandata;
     allstddata=zeros(nmbrwaves,2);
     allmeandata=zeros(nmbrwaves,2);
     allstddata(:,1)=alldata2dfiles{m,1}{k,i}(:,1);
     allmeandata(:,1)=alldata2dfiles{m,1}{k,i}(:,1);
     if nmbrarraypositions>1
        clear arrayoscillations;
        index=0;
        baddataindex=[];
        for j=1:nmbrdatapts{m,1}{k,i}(1,1)
           clear arrayoscillations
           arrayoscillations = [];
           clear tempdata;
           tempdata = alldatat1dfiles{m,1}{k,i}(:,1+j);
           clear delindex;
           baddata = 'n';
           delindex = find(tempdata==100 | tempdata==-100);
           if length(delindex) > 0
              baddata = 'y';
              baddataindex=[baddataindex j];
           end
           if baddata == 'n'
              index=index+1;
              for q=2:nmbrarraypositions
                 for p=1:nmbrarraypositions-1
                    if  abs(waves(32*q)-waves(32*q-p))<1.8  &  abs(waves(32*q)-
waves(32*q-p))>0.1
```

149

```matlab
                    arrayoscillations                =              [arrayoscillations
abs((tempdata([32*q:-1*(p+1):32*q-31*(p+1)])-tempdata([32*q-p:-1*(p+1):32*q-
31*(p+1)-p])))'];
                    end
                end
            end
            avgarrayoscillations(index) = mean(arrayoscillations);
        end
    end
    if length(avgarrayoscillations)>0
        stdoscillations=stddevthreshoscillations*std(avgarrayoscillations);
        meanoscillations=mean(avgarrayoscillations);
        baddataindex=[baddataindex        find(avgarrayoscillations        >
meanoscillations+stdoscillations)];
        if nmbrdatapts{m,1}{k,i}(1,1)-length(baddataindex) < dataptsthresh
        else
            alldatat1dfiles{m,1}{k,i}(:,1+baddataindex)=[];
            if minimization == 'y'
                for j=1:length(alldatafiles{m,1}{k,i}(1,2:end));
                    % variable contains scaling factors and
                    % offset for each data set
                    scalefactors{m,1}{k,i}(1:2,j)=[1 0.0001]';
                    avgdata = averagedalldatat1dfiles{m,1}{k,i}{1,1}(:,2);
                    data = alldatat1dfiles{m,1}{k,i}(:,j+1);
                    low = [0.5 -0.2];
                    high = [2 0.2];
                    options = foptions;
                    deltachi = 2000;
                    oldchi = 1000;
                    searchparam = [1 0.001]';
                    nmbrparam = 1:2;
                    while deltachi > 0.01*oldchi

searchparam=simps('chi',searchparam,nmbrparam,options,low,high,avgdata,dat
a);
                        scaleddataset = scaleddata(data,searchparam);
                        newchi=sum((scaleddataset-avgdata).^2);
                        deltachi = oldchi-newchi;
                        oldchi = newchi;
                    end
                    scalefactors{m,1}{k,i}(1:2,j)=searchparam;
                    alldatat1dfiles{m,1}{k,i}(:,1+j) = scaleddataset;
                    clear scaleddataset searchaparam;
                end
            end
            allstddata(:,2)=std(alldatat1dfiles{m,1}{k,i}(:,2:end)')';
```

```matlab
            allmeandata(:,2)=mean(alldatat1dfiles{m,1}{k,i}(:,2:end)')';
            averagedalldatat1dfiles{m,1}{k,i}{1,1}=allmeandata;
            averagedalldatat1dfiles{m,1}{k,i}{1,2}=allstddata;
          end
        end
      end
    end
    % ----------------------------------------------------------

  end
 end
end
% 2DIR data collected with T2DIR
averagedalldata2dfiles=alldata2dfiles;
for m=1:nmbrIRtimes
  for k=1:nmbrIRpolarizations;
    for i=1:length(IRfreqs(:,1))

      % ----------------------------------------------------------
      % this section identifies data points well outside the standard
      % deviation of data
      clear allstddata allmeandata;
      allstddata=zeros(nmbrwaves,2);
      allmeandata=zeros(nmbrwaves,2);
      allstddata(:,1)=alldata2dfiles{m,1}{k,i}(:,1);
      allmeandata(:,1)=alldata2dfiles{m,1}{k,i}(:,1);
      for j=1:nmbrwaves
        nmbrpts = length(alldata2dfiles{m,1}{k,i}(j,2:end));
        clear tempdata stddev;
       tempdata = alldata2dfiles{m,1}{k,i}(j,2:nmbrpts);
        clear delindex;
        delindex = find(tempdata==100 | tempdata==-100);
       tempdata(delindex)=[];
      nmbrpts = length(tempdata);
       if nmbrpts==0
         tempdata = 200
      elseif nmbrpts >= dataptsthresh
         stddata=std(tempdata);
         meandata=mean(tempdata);
         delindex  =  find(tempdata  <  meandata-stddevthresh*stddata  |
tempdata > meandata+stddevthresh*stddata);
         tempdata(delindex) = [];
         allstddata(j,2)=std(tempdata);
         allmeandata(j,2)=mean(tempdata);
       else
         allstddata(j,2)=std(tempdata);
```

```
        allmeandata(j,2)=mean(tempdata);
      end
    end
    averagedalldata2dfiles{m,1}{k,i}=[];
    averagedalldata2dfiles{m,1}{k,i}{1,1}=allmeandata;
    averagedalldata2dfiles{m,1}{k,i}{1,2}=allstddata;
    % --------------------------------------------------------------

    % --------------------------------------------------------------
    % this section identifies data sets with large oscillations
    % between adjacent wavenumbers (< 2 cm-1) and removes them
    if oscillationanalysis == 'y'
      clear allstddata allmeandata;
      allstddata=zeros(nmbrwaves,2);
      allmeandata=zeros(nmbrwaves,2);
      allstddata(:,1)=alldata2dfiles{m,1}{k,i}(:,1);
      allmeandata(:,1)=alldata2dfiles{m,1}{k,i}(:,1);
      if nmbrarraypositions>1
        clear arrayoscillations;
        index=0;
        baddataindex=[];
        for j=1:nmbrdatapts{m,1}{k,i}(1,1)
          clear arrayoscillations
          arrayoscillations = [];
          clear tempdata;
          tempdata = alldata2dfiles{m,1}{k,i}(:,1+j);
          clear delindex;
          baddata = 'n';
          delindex = find(tempdata==100 | tempdata==-100);
          if length(delindex) > 0
            baddata = 'y';
            baddataindex=[baddataindex j];
          end
          if baddata == 'n'
            index=index+1;
            for q=2:nmbrarraypositions
              for p=1:nmbrarraypositions-1
                if  abs(waves(32*q)-waves(32*q-p))<1.8  &  abs(waves(32*q)-
waves(32*q-p))>0.1
                  arrayoscillations           =           [arrayoscillations
abs((tempdata([32*q:-1*(p+1):32*q-31*(p+1)])-tempdata([32*q-p:-1*(p+1):32*q-
31*(p+1)-p])))'];
                end
              end
            end
            avgarrayoscillations(index) = mean(arrayoscillations);
```

```
                    end
                end
            if length(avgarrayoscillations)>0
                stdoscillations=stddevthreshoscillations*std(avgarrayoscillations);
                meanoscillations=mean(avgarrayoscillations);
                baddataindex=[baddataindex        find(avgarrayoscillations      >
meanoscillations+stdoscillations)];
                if nmbrdatapts{m,1}{k,i}(1,1)-length(baddataindex) < dataptsthresh
                else
                    alldata2dfiles{m,1}{k,i}(:,1+baddataindex)=[];
                    if minimization == 'y'
                        for j=1:length(alldatafiles{m,1}{k,i}(1,2:end));
                            % variable contains scaling factors and
                            % offset for each data set
                            scalefactors{m,1}{k,i}(1:2,j)=[1 0.0001]';
                            avgdata = averagedalldata2dfiles{m,1}{k,i}{1,1}(:,2);
                            data = alldata2dfiles{m,1}{k,i}(:,j+1);
                            low = [0.5 -0.2];
                            high = [2 0.2];
                            options = foptions;
                            deltachi = 2000;
                            oldchi = 1000;
                            searchparam = [1 0.001]';
                            nmbrparam = 1:2;
                            while deltachi > 0.01*oldchi

searchparam=simps('chi',searchparam,nmbrparam,options,low,high,avgdata,dat
a);
                                scaleddataset = scaleddata(data,searchparam);
                                newchi=sum((scaleddataset-avgdata).^2);
                                deltachi = oldchi-newchi;
                                oldchi = newchi;
                            end
                            scalefactors{m,1}{k,i}(1:2,j)=searchparam;
                            alldata2dfiles{m,1}{k,i}(:,1+j) = scaleddataset;
                            clear scaleddataset searchaparam;
                        end
                    end
                    allstddata(:,2)=std(alldata2dfiles{m,1}{k,i}(:,2:end)')';
                    allmeandata(:,2)=mean(alldata2dfiles{m,1}{k,i}(:,2:end)')';
                    averagedalldata2dfiles{m,1}{k,i}{1,1}=allmeandata;
                    averagedalldata2dfiles{m,1}{k,i}{1,2}=allstddata;
                end
            end
        end
    end
```

```
      % -----------------------------------------------------------

    end
  end
end
% T2DIR data collected with T2DIR
averagedalldatat2dfiles=alldatat2dfiles;
for h=1:nmbrUVtimes
for m=1:nmbrIRtimes
   for k=1:nmbrpolarizations;
      for i=1:length(IRfreqs(:,1))

         % -----------------------------------------------------------
         % this section identifies data points well outside the standard
         % deviation of data
         clear allstddata allmeandata;
         allstddata=zeros(nmbrwaves,2);
         allmeandata=zeros(nmbrwaves,2);
         allstddata(:,1)=alldatat2dfiles{m,h}{k,i}(:,1);
         allmeandata(:,1)=alldatat2dfiles{m,h}{k,i}(:,1);
         for j=1:nmbrwaves
            nmbrpts = length(alldatat2dfiles{m,h}{k,i}(j,2:end));
            clear tempdata stddev;
            tempdata = alldatat2dfiles{m,h}{k,i}(j,2:nmbrpts);
            clear delindex;
            delindex = find(tempdata==100 | tempdata==-100);
            tempdata(delindex)=[];
            nmbrpts = length(tempdata);
           if nmbrpts==0
              tempdata = 200
           elseif nmbrpts >= dataptsthresh
              stddata=std(tempdata);
              meandata=mean(tempdata);
              delindex   =   find(tempdata   <   meandata-stddevthresh*stddata   |
tempdata > meandata+stddevthresh*stddata);
              tempdata(delindex) = [];
              allstddata(j,2)=std(tempdata);
              allmeandata(j,2)=mean(tempdata);
           else
              allstddata(j,2)=std(tempdata);
              allmeandata(j,2)=mean(tempdata);
           end
        end
         averagedalldatat2dfiles{m,h}{k,i}=[];
         averagedalldatat2dfiles{m,h}{k,i}{1,1}=allmeandata;
         averagedalldatat2dfiles{m,h}{k,i}{1,2}=allstddata;
```

```
%       % ------------------------------------------------------------
%
%       % ------------------------------------------------------------
%       % this section identifies data sets with large oscillations
%       % between adjacent wavenumbers (< 2 cm-1) and removes them
        if oscillationanalysis == 'y'
          clear allstddata allmeandata;
          allstddata=zeros(nmbrwaves,2);
          allmeandata=zeros(nmbrwaves,2);
          allstddata(:,1)=alldatat2dfiles{m,h}{k,i}(:,1);
          allmeandata(:,1)=alldatat2dfiles{m,h}{k,i}(:,1);
          if nmbrarraypositions>1
            clear arrayoscillations;
            index=0;
            baddataindex=[];
            for j=1:nmbrdatapts{m,h}{k,i}(1,1)
              clear arrayoscillations
              arrayoscillations = [];
              clear tempdata;
              tempdata = alldatat2dfiles{m,h}{k,i}(:,1+j);
              clear delindex;
              baddata = 'n';
              delindex = find(tempdata==100 | tempdata==-100);
              if length(delindex) > 0
                baddata = 'y';
                baddataindex=[baddataindex j];
              end
              if baddata == 'n'
                index=index+1;
                for q=2:nmbrarraypositions
                  for p=1:nmbrarraypositions-1
                    if abs(waves(32*q)-waves(32*q-p))<1.8 & abs(waves(32*q)-
waves(32*q-p))>0.1
                      arrayoscillations            =            [arrayoscillations
abs((tempdata([32*q:-1*(p+1):32*q-31*(p+1)])-tempdata([32*q-p:-1*(p+1):32*q-
31*(p+1)-p])))'];
                    end
                  end
                end
                avgarrayoscillations(index) = mean(arrayoscillations);
              end
            end
            if length(avgarrayoscillations)>0
              stdoscillations=stddevthreshoscillations*std(avgarrayoscillations);
              meanoscillations=mean(avgarrayoscillations);
```

```matlab
            baddataindex=[baddataindex        find(avgarrayoscillations        >
meanoscillations+stdoscillations)];
            if nmbrdatapts{m,h}{k,i}(1,1)-length(baddataindex) < dataptsthresh
            else
                alldatat2dfiles{m,h}{k,i}(:,1+baddataindex)=[];
                if minimization == 'y'
                    for j=1:length(alldatat2dfiles{m,h}{k,i}(1,2:end));
                        % variable contains scaling factors and
                        % offset for each data set
                        scalefactors{m,h}{k,i}(1:2,j)=[1 0.0001]';
                        avgdata = averagedalldatat2dfiles{m,h}{k,i}{1,1}(:,2);
                        data = alldatat2dfiles{m,h}{k,i}(:,j+1);
                        low = [0.5 -0.2];
                        high = [2 0.2];
                        options = foptions;
                        deltachi = 2000;
                        oldchi = 1000;
                        searchparam = [1 0.001]';
                        nmbrparam = 1:2;
                        while deltachi > 0.01*oldchi

searchparam=simps('chi',searchparam,nmbrparam,options,low,high,avgdata,dat
a);
                            scaleddataset = scaleddata(data,searchparam);
                            newchi=sum((scaleddataset-avgdata).^2);
                            deltachi = oldchi-newchi;
                            oldchi = newchi;
                        end
                        scalefactors{m,h}{k,i}(1:2,j)=searchparam;
                        alldatat2dfiles{m,h}{k,i}(:,1+j) = scaleddataset;
                        clear scaleddataset searchaparam;
                    end
                end
                allstddata(:,2)=std(alldatat2dfiles{m,h}{k,i}(:,2:end)')';
                allmeandata(:,2)=mean(alldatat2dfiles{m,h}{k,i}(:,2:end)')';
                averagedalldatat2dfiles{m,h}{k,i}{1,1}=allmeandata;
                averagedalldatat2dfiles{m,h}{k,i}{1,2}=allstddata;
            end
        end
    end
end
    % ------------------------------------------------------------

    end
  end
end
```

```
end
end

% ----------------------------------------------------------------------

% -------------------------------------------------------------------------
%  This section puts all the data into the proper format, clears variables
%  which are not to be saved, and saves the .mat data file
if nmbrcolumns==3
sorteddata=averagedalldatafiles;
if yesIRfreqs=='n'
  clear IRfreqs;
  IRfreqs='NA';
end

times=times';
waves=waves';
sorteddata=sorteddata;

clear newtempdata index i plotthedata fin line nmbrfiles nmbrwaveavgs;
clear k timecounter ans counter whichtime done counterfreq;
clear wavecounter inputfile tempfreq header filename;
clear nmbrcolors data minimum maximum limit;
clear counterpolar j newpolarization nmbrpolarizations;
clear nmbrIRtimes polarizationcounter polarizationdone polarizationindex
polarizationline;
clear temppolarization yesIRfreqs m;
clear averagedata averagestd databyfiles filenmbr tempdata tempstd
counterpolarizationsections newIRfreq;
clear IRfreqindex allmeandata allstddata arrayoscillations avgarrayoscillations
baddata;
clear baddataindex dataptsthresh delindex meandata meanoscillations
nmbrarraypositions nmbrpts nmbrwaves;
clear p q secondtempdata stddata stddevthresh stddevthreshoscillations
stdoscillations timerounding;
clear averagedalldatafiles avgdata deltachi high low newchi nmbraddedpts
nmbrdatapts nmbrparam;
clear oldchi options oscillationanalysis scalefactors searchparam
tempalldatafiles;
clear minimization;

if length(specinfo) == 1
  datafilename = strcat(filebody,num2str(specinfo(1)));
else
  datafilename                =                strcat(filebody,num2str(specinfo(1)),'-
',num2str(specinfo(end)));
```

```
end
datafilename=strcat('data_',datafilename);
clear filebody specinfo;

if outputfileboolean=='y'
  clear outputfileboolean;
  save(datafilename);
else
  clear outputfileboolean;
end

elseif nmbrcolumns==6
sorteddatat1d=averagedalldatat1dfiles;
sorteddata2d=averagedalldata2dfiles;
sorteddatat2d=averagedalldatat2dfiles;
if yesIRfreqs=='n'
  clear IRfreqs;
  IRfreqs='NA';
end
UVtimes=UVtimes';
IRtimes=IRtimes';
waves=waves';
sorteddatat1d=sorteddatat1d;
sorteddata2d=sorteddata2d;
sorteddatat2d=sorteddatat2d;



clear newtempdata index i plotthedata fin line nmbrfiles nmbrwaveavgs;
clear k timecounter ans counter whichtime done counterfreq;
clear inputfile tempfreq header filename;
clear nmbrcolors data minimum maximum limit tempdata;
clear counterpolar j newpolarization nmbrpolarizations;
clear nmbrIRtimes polarizationcounter polarizationdone polarizationindex
polarizationline;
clear temppolarization yesIRfreqs m;
clear averagedata averagestd databyfiles filenmbr tempdata tempstd
counterpolarizationsections newIRfreq;
clear IRfreqindex allmeandata allstddata arrayoscillations avgarrayoscillations
baddata;
clear baddataindex dataptsthresh delindex meandata meanoscillations
nmbrarraypositions nmbrpts nmbrwaves;
clear p q secondtempdata stddata stddevthresh stddevthreshoscillations
stdoscillations timerounding;
clear averagedalldatafiles avgdata deltachi high low newchi nmbraddedpts
nmbrdatapts nmbrparam;
```

```matlab
clear   oldchi   options   oscillationanalysis   scalefactors   searchparam
tempalldatafiles;
clear minimization;

if length(specinfo) == 1
  datafilename = strcat(filebody,num2str(specinfo(1)));
else
  datafilename                =                strcat(filebody,num2str(specinfo(1)),'-
',num2str(specinfo(end)));
end
datafilename=strcat('data_',datafilename);
clear filebody specinfo;

if outputfileboolean=='y'
  clear outputfileboolean;
  save(datafilename);
else
 clear outputfileboolean;
end
end
%-----------------------------------------------------------------------
```

B.2 SpectralFitIntPeaks1955

This script takes output from the analyze.m (see James Cahoon's thesis) script and individually integrates the peaks of each spectra, producing more accurate kinetics plots. It iteratively adjusts the input parameters using the simps.m algorithm (developed by Zeljko Bajzer (bajzer@mayo.edu) and Ivo Penzar (penzar@mayo.edu), Mayo Clinic and Foundation, Rochester, Minnesota, USA June, 1998/February, 1999).

%SpectraFitIntPeaks should be used following analyze.m to integrate peaks
%in 2D-IR kinetics files. It functions in place of intpeaks.m and functions
%by fitting voigt functions to the peaks in the spectrum. It functions
%particularly well in cases where there is significant overlap between 0-1
%and 1-2 peaks.

%Side note: because this algorithm iteratively uses previous peak center
%positions, there is a risk that selecting dramatically-different time
%positions will result in poor fits. However, given that 2D-IR peaks should
%not be moving in any significant way over the course of an experiment,
%this system should still work reasonably well.

%_____
_____
%Don't want to "clear all" at the start, or that would eliminate the
%"Output" and "StdDev" variables created by analyze.m that this program
%uses. Still, I'll have to be careful about initialization of variables.
disp('_____
_____');
disp('Now fitting spectra from analyze.m.')
disp('If this script is run before running "analyze.m", errors may occur.');
disp(' ');

%Clearing just the variables that will be used later:
clear FitData;
clear when;
clear osize;

%Times we'll be fitting.
when = input('What times would you like to fit? (Default: ALL) ');

%Size of the output matrix we'll be using. This information could also come
%from the "times" and "waves" vectors.
osize = size(Output);

```
%Get data from Output and jam it into a working array. Do the same with
%StDev data.
%Case for if we don't give it any initial set of times:
if(isempty(when))
    FitData = zeros(osize(1)-1,osize(2)-1);
    FitStdDev = zeros(osize(1)-1,osize(2)-1);
    when=times;
    for i=2:osize(1)
        for j=2:osize(2)
            FitData(i-1,j-1)=Output(i,j);
            FitStdDev(i-1,j-1)=StdDev(i,j);
        end
    end
%Case for selecting only some times:
else
    FitData = zeros(osize(1)-1,length(when));
    FitStdDev = zeros(osize(1)-1,length(when));
    %Assumes each time position appears only once in "times"
    %For each given time,
    for i=1:length(when)
        %Find that time in the list of possible times
        for j=1:length(times)
            if when(i)==times(j)
                %Put the spectra associated with those times into FitData
                FitData(:,i)=Output(2:osize(1),j);
                %Put the standard deviation for each point into FitStDev
                FitStdDev(:,i)=StdDev(2:osize(1),j);
            end
        end
    end
end

%In order to avoid fitting errors around the switch from negative to
%positive times, I'll want to start fitting at the first number>=0.
zindex = 1; %Default value says start at the start of "when" if there are no positive
values.
foundzero = 0;
for i=1:length(when)
    if foundzero==0&&when(i)>=0
        zindex=i;
        foundzero=1;
    end
end
```

%Adjust for reversed chopper phase, s.t. fitting parameters make a little
%more sense.
cphase = input('Is chopper phase reversed? (Default: no; else, "y") ','s');
if cphase=='y'
    FitData = -FitData;
end

%Now the data is in memory. Let's actually do some fitting with it.

%FITTING PARAMETERS--
fitP = zeros(length(when)+1,16); %Pre-assign fitP for speed.
f = zeros(length(when),1);
%Starting Values:
%par= [amp1   pos1   tau1   tau1   amp2   pos2   tau2   tau2 amp3   pos3
tau3   tau3   amp4   pos4   tau4   tau4]
fitP(1,:)=[2000   1937   1.5   7.0   2000   1945   1.5   10.0 -1500 1955   1.5
10.0 -1500 1965   1.5   10.0];
high=   [100000   1945   3.0   15.0   10000   1950   2.0   15.0 0   1957   2.0
30.0 0   1967   2.0   30.0];
low=   [0   1935   1.0   0.0   0   1945   1.0   0.0 -10000 1953   1.0   0.0
-100000 1963   1.0   0.0];
%--
%Note: the first tau is the lorentzian peak width, the second is the
%gaussian width.

%This loop runs over all times specified and deposits all of the necessary
%information into a big honkin' matrix for later plotting.
exampleplotted = 0;
tic;
for i=2:(length(when)+1)
   if (i-1)==zindex %If at zero, re-initialize the fit parameters to starting.
      fitP(i, :) = fitP(1, :);
   else
      fitP(i, :) = fitP(i-1, :); %Otherwise, use the previous fit as the starting point
for this one.
   end
   [fitP(i,:), G] = simps('fit4v', fitP(i,:), (1:16), [], low, high, FitData(:,i-1), waves,
FitStdDev(:,i-1));

   %Now do that fit again, but such that it can be displayed in a figure.
   [f(i-1) g fit out]=fit4v(fitP(i,:), FitData(:,i-1), waves, FitStdDev(:,i-1));

   %If you have a kinetics run, plot a representative slice of the resulting
   %fits for an representative time slice, to make sure things are working properly.
   if length(when)>10

162

```
    if exampleplotted==0
       if when(i-1)>=0.01&&when(i-1)<=5
          figure(1);clf; plot(out{1}, out{2}, out{1}, out{3}, out{1}, out{4}, out{1},
out{5}, out{1}, out{6}, out{1}, out{7});title(when(i-1));
          exampleplotted=1;
       end
    end
  %Otherwise, plot them all.
  else
     figure(i-1);clf; plot(out{1}, out{2}, out{1}, out{3}, out{1}, out{4}, out{1},
out{5}, out{1}, out{6}, out{1}, out{7});title(when(i-1));
  end
end
%END FITTING---------------------------------------------------------------

%Now, plot up the volumes of the peaks as a function of time.
peak1937dyn = fitP(2:(length(when)+1),1);
peak1945dyn = fitP(2:(length(when)+1),5);
peak1955dyn = fitP(2:(length(when)+1),9);
peak1965dyn = fitP(2:(length(when)+1),13);
%If you're dealing with a kinetics run, plot the kinetics.
if length(when)>10
  figure(2);plot(when,peak1937dyn,'o');
  figure(3);plot(when,peak1965dyn,'o');
  %peakdiff=zeros(length(when),1);
  %for i=1:length(peak1dyn)
  %   peakdiff(i,1)=peak4dyn(i,1)/peak1dyn(i,1);
  %end
  %figure(4);plot(when,peakdiff,'o');ylim([-2 0]);xlim([-12 31])
end
toc


%This outputs the integrated volume of each peak so that it can be analyzed
%using                    the                 Fitte.m                 script.
```

B.3   fit4v

This function describes the form of the function to which a spectrum is fit, and is used by the spectral fitting program as the basis of its fitting.

```
function [f,G,fit,out] = fit4v(p,y,x,sigma)
%FIT4V Fits to 4 voigts for slices of 2D spectra,
%returns chi2 and G (vector of constraints for simps.m)
%
% usage [f,G,output] = fit2v1g1b([a1,pos1,tau1l,tau1g,a2,pos2,tau2l, ...
%                 tau2g,a3,pos3,tau3g,offset],data,abcissa,std);
%
% f   chi2
% G   used by simps
% fit  fit to data
% out  output for plotting

 a1    = p(1);
 pos1  = p(2);
 tau1l  = p(3); % lorentzian width of peak1 (fwhm)
 tau1g  = p(4); % gaussian width of peak1 (fwhm)
 a2    = p(5);
 pos2  = p(6);
 tau2l  = p(7); % lorentzian width of peak2 (fwhm)
 tau2g  = p(8); % gaussian width of peak2 (fwhm)
 a3    = p(9);
 pos3  = p(10);
 tau3l  = p(11); % lorentzian width of peak3 (fwhm)
 tau3g  = p(12); % gaussian width of peak3 (fwhm)
 a4    = p(13);
 pos4  = p(14);
 tau4l  = p(15); % lorentzian width of peak4 (fwhm)
 tau4g  = p(16); % gaussian width of peak4 (fwhm)

 voight1 = a1*voightvol(x-pos1,[tau1l,tau1g]);
 voight2 = a2*voightvol(x-pos2,[tau2l,tau2g]);
 voight3 = a3*voightvol(x-pos3,[tau3l,tau3g]);
 voight4 = a4*voightvol(x-pos4,[tau4l,tau4g]);
 fit =  voight1 + voight2 + voight3 + voight4;
 %f is a measure of how good the fit is.
 f = sum(((y - fit)./sigma).^2);
 G=[];

 out = {x,y,fit,voight1,voight2,voight3,voight4};
```

Appendix C   Simulation code

These scripts use Gillespie's stochastic algorithm to simulate a classical master equation for the purposes of comparing these kinetic traces with results from 2D-IR experiments.

C.1   master3x3

This script uses Gillespie's algorithm to probabilistically propagate an ensemble of states from a set of initial population values, over a period of time, based on a rate and probability matrix defined at run time. Given the three-state nature of my 2D-IR experiment, this simple algorithm has been specifically configured to work for a three-level experiment.

```
function [f,G,out] = master3x3(p,y,x,sigma)
%MASTER3X3 Fits the probability matrix and reaction rate necessary to
%propagate a three-mode system through time, returns chi2 (quality of fit),
%G (vector of contraints for simps.m), and out (all resulting points, etc.)
%
%   usage [f,G,output] = master3x3(parameters,[9xn-kinetcs for each peak],...
%                    abscissa,stddevs);
%   p     rate constant, probability, and intensity parameters (to be determined)
%   y     [9 x N] matrix with dynamics of each peak, for each time
%   x     N-length vector containing times when data was taken
%   sigma   [9 x N] matrix with the quality of the fit of each peak
%
%   f     chi2
%   G     contraints used by simps (none inherent for this system)
%   out   output of all relevant values for plotting

%Extract the master equation parameters from the input vector.
rate = p(1); %Unimolecular rate constant, in inverse femtoseconds.
Paa  = p(2);
Pab  = p(3);
Pac  = p(4);
Pba  = p(5);
Pbb  = p(6);
Pbc  = p(7);
Pca  = p(8);
Pcb  = p(9);
Pcc  = p(10);
```

%Also extract further values from parameter input vector to fit the initial
%intensity.
Iaa = p(11);
Iab = p(12);
Iac = p(13);
Iba = p(14);
Ibb = p(15);
Ibc = p(16);
Ica = p(17);
Icb = p(18);
Icc = p(19);
%Correct values for the difference in dipole strength between different
%vibrations: (These are obtained from FTIR spectra, and thus not free
parameters.)
uA = 1;
uB = p(20);
uC = p(21);
%Concentration/Response adjustments to account for different concentrations
%and overlaps on the various days on which the data was taken. Since each
%pump position pair is simulated independently, I need only introduce one
%correction factor for each pair.
CorA = p(22);
CorB = p(23);
CorC = p(24);

%Show the parameters that were input, so that the status of the fit can be
%followed during iterations.
disp('---NEXT RUN:');
data = ['Rate const: ' num2str(rate)];
disp(data);
moredata1 = [num2str(Paa) ' ' num2str(Pab) ' ' num2str(Pac)];
moredata2 = [num2str(Pba) ' ' num2str(Pbb) ' ' num2str(Pbc)];
moredata3 = [num2str(Pca) ' ' num2str(Pcb) ' ' num2str(Pcc)];
disp(moredata1);
disp(moredata2);
disp(moredata3);
moreint1 = [num2str(Iaa) ' ' num2str(Iab) ' ' num2str(Iac)];
moreint2 = [num2str(Iba) ' ' num2str(Ibb) ' ' num2str(Ibc)];
moreint3 = [num2str(Ica) ' ' num2str(Icb) ' ' num2str(Icc)];
disp(moreint1);
disp(moreint2);
disp(moreint3);
disp('Correction values: (A, B, C)');
dipoles = ['A: ' num2str(CorA) ' B: ' num2str(CorB) ' C: ' num2str(CorC)];
disp(dipoles);

%Apply the correction factors and dipoles uniformly to intensities from the spectra:
%(Weaker dipole->need to enhance initial value. These are third-order responses,
%thus we need to *SQUARE* the response as appropriate!)
Iaa = Iaa/(uA^2);
Iab = Iab/(uA*uB);
Iac = CorA*(Iac/(uA*uC));
Iba = Iba/(uB*uA);
Ibb = Ibb/(uB^2);
Ibc = CorB*(Ibc/(uB*uC));
Ica = Ica/(uC*uA);
Icb = Icb/(uC*uB);
Icc = CorC*(Icc/(uC^2));

%Apply the same corrections to the experimental data, s.t. it now contains
%information about populations, rather than absorbance.
%y(:,1) = y(:,1)./(uA^2); This makes no change; here for your reference, but commented out so as to not waste processor time.
y(:,2) = y(:,2)./(uA*uB);
y(:,3) = CorA.*(y(:,3)./(uA*uC));
y(:,4) = y(:,4)./(uB*uA);
y(:,5) = y(:,5)./(uB^2);
y(:,6) = CorB.*(y(:,6)/(uB*uC));
y(:,7) = y(:,7)./(uC*uA);
y(:,8) = y(:,8)./(uC*uB);
y(:,9) = CorC.*(y(:,9)./(uC^2));

%Number of parallel systems to simulate:
N = 10000; %Increase for higher precision.

%Time (in femtoseconds) over which to simulate:
time=50000;
%Time (in fs) of step:
tstep=100;
nslices=time/tstep;

%_____

%Initialize the state of the system based upon the initial intensities.
%(May be error here based upon differing spectrograph positions. Each
%system is three-state.
system1 = zeros(N,3);
system2 = zeros(N,3);
system3 = zeros(N,3);
%Initialize based upon initial intensity values.

```
%PUMP-A---------------------------------------
OccAA=N*(Iaa/(Iaa+Iab+Iac));
OccAB=N*((Iaa+Iab)/(Iaa+Iab+Iac));
for i=1:N
    if i<OccAA
        system1(i,1)=1;
    elseif i>=OccAA&&i<OccAB
        system1(i,2)=1;
    else
        system1(i,3)=1;
    end
end
%PUMP-B---------------------------------------
OccBA=N*(Iba/(Iba+Ibb+Ibc));
OccBB=N*((Iba+Ibb)/(Iba+Ibb+Ibc));
for i=1:N
    if i<OccBA
        system2(i,1)=1;
    elseif i>=OccBA&&i<OccBB
        system2(i,2)=1;
    else
        system2(i,3)=1;
    end
end
%PUMP-C---------------------------------------
OccCA=N*(Ica/(Ica+Icb+Icc));
OccCB=N*((Ica+Icb)/(Ica+Icb+Icc));
for i=1:N
    if i<OccCA
        system3(i,1)=1;
    elseif i>=OccCA&&i<OccCB
        system3(i,2)=1;
    else
        system3(i,3)=1;
    end
end

%Initialize "state" vector that tracks the dynamics of the system at each
%slice.
record1=zeros(nslices,4);
record2=zeros(nslices,4);
record3=zeros(nslices,4);

%_____
_____
%Loop uses Gillespie's stochastic algorithm to time-propagate the system
```

```
%based on the probability of it crosses the barrier, and the probability of
%a coupling between modes (as taken from p(1:10).)
i=0;
while i<=time
   if mod(i,tstep)==0 %If we're at a timestep to update the system
      for j=1:N     %Loop over all systems in the simulation
         r=rand;
         deltat=(1/rate)*log(1/r);   %How long until the system reacts again?
         if deltat<=tstep        %If it's going to react during this time step,
            r2=rand;             %Use a new rand to be sure we uncouple the crossing
and the coupling.
            %PUMP-A----------------------------------------------------
            if system1(j,1)==1     %Modify the system based upon its current state.
            %Treat probability of going from one state to another based upon the
value of r2 between 0 and 1.
               if       r2>(Paa/(Paa+Pab+Pac))&&r2<((Paa+Pab)/(Paa+Pab+Pac))
%Between aa and ac is ab.
                  system1(j,1)=0;
                  system1(j,2)=1;
               elseif r2>=((Paa+Pab)/(Paa+Pab+Pac))
                  system1(j,1)=0;
                  system1(j,3)=1;
               else
                  %If we aren't in Pab or Pac, we must be in Paa-do nothing.
               end
            elseif system1(j,2)==1
               if r2>(Pbb/(Pba+Pbb+Pbc))&&r2<((Pbb+Pba)/(Pba+Pbb+Pbc)) %Go
to A
                  system1(j,2)=0;
                  system1(j,1)=1;
               elseif r2>=((Pba+Pbb)/(Pba+Pbb+Pbc)) %Go to C
                  system1(j,2)=0;
                  system1(j,3)=1;
               else
                  %If we aren't in Pba or Pbc, we must be in Pbb-do nothing.
               end
            else
               if r2>(Pcc/(Pca+Pcb+Pcc))&&r2<((Pcc+Pca)/(Pca+Pcb+Pcc)) %Go to
A
                  system1(j,3)=0;
                  system1(j,1)=1;
               elseif r2>=((Pca+Pcc)/(Pca+Pcb+Pcc)) %Go to B
                  system1(j,3)=0;
                  system1(j,2)=1;
               else
                  %If we aren't in Pca or Pcb, we must be in Pcc-do nothing.
```

```
        end
    end

    %PUMP-B----------------------------------------------------
    if system2(j,1)==1      %Modify the system based upon its current state.
        %Treat probability of going from one state to another based upon the
value of r2 between 0 and 1.
        if      r2>(Paa/(Paa+Pab+Pac))&&r2<((Paa+Pab)/(Paa+Pab+Pac))
%Between aa and ac is ab.
            system2(j,1)=0;
            system2(j,2)=1;
        elseif r2>=((Paa+Pab)/(Paa+Pab+Pac))
            system2(j,1)=0;
            system2(j,3)=1;
        else
            %If we aren't in Pab or Pac, we must be in Paa-do nothing.
        end
    elseif system2(j,2)==1
        if r2>(Pbb/(Pba+Pbb+Pbc))&&r2<((Pbb+Pba)/(Pba+Pbb+Pbc))
            system2(j,2)=0;
            system2(j,1)=1;
        elseif r2>=((Pba+Pbb)/(Pba+Pbb+Pbc))
            system2(j,2)=0;
            system2(j,3)=1;
        else
            %If we aren't in Pba or Pbc, we must be in Pbb-do nothing.
        end
    else
        if r2>(Pcc/(Pca+Pcb+Pcc))&&r2<((Pcc+Pca)/(Pca+Pcb+Pcc))
            system2(j,3)=0;
            system2(j,1)=1;
        elseif r2>=((Pca+Pcc)/(Pca+Pcb+Pcc))
            system2(j,3)=0;
            system2(j,2)=1;
        else
            %If we aren't in Pca or Pcb, we must be in Pcc-do nothing.
        end
    end

    %PUMP-C----------------------------------------------------
    if system3(j,1)==1      %Modify the system based upon its current state.
        %Treat probability of going from one state to another based upon the
value of r2 between 0 and 1.
        if      r2>(Paa/(Paa+Pab+Pac))&&r2<((Paa+Pab)/(Paa+Pab+Pac))
%Between aa and ac is ab.
            system3(j,1)=0;
```

```matlab
            system3(j,2)=1;
        elseif r2>=((Paa+Pab)/(Paa+Pab+Pac))
            system3(j,1)=0;
            system3(j,3)=1;
        else
            %If we aren't in Pab or Pac, we must be in Paa-do nothing.
        end
    elseif system3(j,2)==1
        if r2>(Pbb/(Pba+Pbb+Pbc))&&r2<((Pbb+Pba)/(Pba+Pbb+Pbc))
            system3(j,2)=0;
            system3(j,1)=1;
        elseif r2>=((Pba+Pbb)/(Pba+Pbb+Pbc))
            system3(j,2)=0;
            system3(j,3)=1;
        else
            %If we aren't in Pba or Pbc, we must be in Pbb-do nothing.
        end
    else
        if r2>(Pcc/(Pca+Pcb+Pcc))&&r2<((Pcc+Pca)/(Pca+Pcb+Pcc))
            system3(j,3)=0;
            system3(j,1)=1;
        elseif r2>=((Pca+Pcc)/(Pca+Pcb+Pcc))
            system3(j,3)=0;
            system3(j,2)=1;
        else
            %If we aren't in Pca or Pcb, we must be in Pcc-do nothing.
        end
    end
  end
end

%Record the results to plot or do calculations with later.
tpos=(i/tstep)+1;
record1(tpos,1)=i;
record1(tpos,2)=sum(system1(:,1))/N;
record1(tpos,3)=sum(system1(:,2))/N;
record1(tpos,4)=sum(system1(:,3))/N;
record2(tpos,1)=i;
record2(tpos,2)=sum(system2(:,1))/N;
record2(tpos,3)=sum(system2(:,2))/N;
record2(tpos,4)=sum(system2(:,3))/N;
record3(tpos,1)=i;
record3(tpos,2)=sum(system3(:,1))/N;
record3(tpos,3)=sum(system3(:,2))/N;
record3(tpos,4)=sum(system3(:,3))/N;
```

```
    i=i+1;        %Increment time

  else          %Otherwise, just increment time.
    i=i+1;
  end
end
```

%Multiply the simulation values (always {0<y<1}) by the original
%intensities to compare them with spectroscopic values accurately.
%Ia = Iaa+Iab+Iac;
%Ib = Iba+Ibb+Icc;
%Ic = Ica+Icb+Icc;
%These f values will contain the OLS for each curve, i.e. the goodness of
%the fit. Might be dangerous to instantiate them to 0, as this is
%equivalent to instantiating them to the "best" value. But I need them at 0
%to add to them with confidence.
faa = 0;
fab = 0;
fac = 0;
fba = 0;
fbb = 0;
fbc = 0;
fca = 0;
fcb = 0;
fcc = 0;
%Because we'll need it a lot, pick out the length of x.
lengthx = length(x);
%We'll store the relevant parts of the record files in a new, small matrix
%(basically, the "simulated" version of the y matrix.) Call it z.
z=zeros(lengthx,9);
for i=1:lengthx
   for j=i:(length(record1)-1) %For this technique to work, your simulation time
resolution must be higher than your experimental, anyway. Cut down search
space.
     if x(i)==record1(j,1)
        %Put good simulated values into z[]:
        z(i,1)=record1(j,2);
        z(i,2)=record1(j,3);
        z(i,3)=record1(j,4);
        z(i,4)=record2(j,2);
        z(i,5)=record2(j,3);
        z(i,6)=record2(j,4);
        z(i,7)=record3(j,2);
        z(i,8)=record3(j,3);
        z(i,9)=record3(j,4);
        %If we're at a matching timeslice, use "record" to contain

172

```matlab
        %difference information between actual and simulated. Divide by
        %sigma to account for uncertainty in the value.
        faa = (((z(i,1)/(z(i,1)+z(i,2)+z(i,3)))-(y(i,1)/(y(i,1)+y(i,2)+y(i,3))))^2)+faa;
        fab                    =                    (((z(i,2)/(z(i,1)+z(i,2)+z(i,3)))-
(y(i,2)/(y(i,1)+y(i,2)+y(i,3))))^2)+fab;%/(sigma(i,1)*sigma(i,2))+fab;    Currently
removing the sigma portion and seeing how the calculation responds.
        fac                    =                    (((z(i,3)/(z(i,1)+z(i,2)+z(i,3)))-
(y(i,3)/(y(i,1)+y(i,2)+y(i,3))))^2)+fac;%/(sigma(i,1)*sigma(i,3))+fac;
        fba                    =                    (((z(i,4)/(z(i,4)+z(i,5)+z(i,6)))-
(y(i,4)/(y(i,4)+y(i,5)+y(i,6))))^2)+fba;%/(sigma(i,4)*sigma(i,5))+fba;
        fbb                    =                    (((z(i,5)/(z(i,4)+z(i,5)+z(i,6)))-
(y(i,5)/(y(i,4)+y(i,5)+y(i,6))))^2)+fbb;
        fbc                    =                    (((z(i,6)/(z(i,4)+z(i,5)+z(i,6)))-
(y(i,6)/(y(i,4)+y(i,5)+y(i,6))))^2)+fbc;%/(sigma(i,5)*sigma(i,6))+fbc;
        fca                    =                    (((z(i,7)/(z(i,7)+z(i,8)+z(i,9)))-
(y(i,7)/(y(i,7)+y(i,8)+y(i,9))))^2)+fca;%/(sigma(i,7)*sigma(i,9))+fca;
        fcb                    =                    (((z(i,8)/(z(i,7)+z(i,8)+z(i,9)))-
(y(i,8)/(y(i,7)+y(i,8)+y(i,9))))^2)+fcb;%/(sigma(i,8)*sigma(i,9))+fcb;
        fcc = (((z(i,9)/(z(i,7)+z(i,8)+z(i,9)))-(y(i,9)/(y(i,7)+y(i,8)+y(i,9))))^2)+fcc;
    end
  end
end
faa = faa/lengthx;
fab = fab/lengthx;
fac = fac/lengthx;
fba = fba/lengthx;
fbb = fbb/lengthx;
fbc = fbc/lengthx;
fca = fca/lengthx;
fcb = fcb/lengthx;
fcc = fcc/lengthx;
%There are certain requirements, because these are probabilities. If the
%total probability for a curve deviates from 1, that means that we're
%dealing with an un-physical fit. Incorporate this into the quality of the fit.
PnetA = 1+((1-(Paa+Pab+Pac))^2);
PnetB = 1+((1-(Pba+Pbb+Pbc))^2);
PnetC = 1+((1-(Pca+Pcb+Pcc))^2);

%Combine together the deviations from constant probability with the quality
%of the fit to get a general description of how well we've fit this thing.
%simps() prefers that f and x be on the same order of magnitude.
f = 100000*((faa+fab+fac+fba+fbb+fbc+fca+fcb+fcc)/6)*PnetA*PnetB*PnetC;
%f=int16(ftest1);

%Feedback portion of function that tells you about the current state. This
%allows me to track how far simps() has gotten while it's running.
```

```matlab
%nmasterpasses=nmasterpasses+1;
%if mod(nmasterpasses,100)==0
%    tracker(length(tracker)+1)=f;
%      outstringer=strcat('Number of passes: ',num2str(nmasterpasses),'. f value:
',num2str(tracker(length(tracker))));
%    disp(outstringer);
%end
outputf = ['f: ' num2str(f)];
disp(outputf);


%Return G blank, as there is no point in contraints explicitly for this
%system.
G=[];
%Return the necessary components to plot the resulting fit.
out                                                                    =
{x,y(:,1)./(y(:,1)+y(:,2)+y(:,3)),z(:,1)./(z(:,1)+z(:,2)+z(:,3)),y(:,2)./(y(:,1)+y(:,2)+y(
:,3)),z(:,2)./(z(:,1)+z(:,2)+z(:,3)),y(:,3)./(y(:,1)+y(:,2)+y(:,3)),z(:,3)./(z(:,1)+z(:,2)
+z(:,3)),y(:,4)./(y(:,4)+y(:,5)+y(:,6)),z(:,4)./(z(:,4)+z(:,5)+z(:,6)),y(:,5)./(y(:,4)+y(
:,5)+y(:,6)),z(:,5)./(z(:,4)+z(:,5)+z(:,6)),y(:,6)./(y(:,4)+y(:,5)+y(:,6)),z(:,6)./(z(:,4)
+z(:,5)+z(:,6)),y(:,7)./(y(:,7)+y(:,8)+y(:,9)),z(:,7)./(z(:,7)+z(:,8)+z(:,9)),y(:,8)./(y(
:,7)+y(:,8)+y(:,9)),z(:,8)./(z(:,7)+z(:,8)+z(:,9)),y(:,9)./(y(:,7)+y(:,8)+y(:,9)),z(:,9).
/(z(:,7)+z(:,8)+z(:,9))};
```

C.2   SimFit_v4

This script uses the simps.m fitting algorithm (developed by Zeljko Bajzer (bajzer@mayo.edu) and Ivo Penzar (penzar@mayo.edu), Mayo Clinic and Foundation, Rochester, Minnesota, USA June, 1998/February, 1999) to iteratively adjust the simulation parameters of master3x3, ultimately finding the optimal set of parameters to describe the observed coupling. Limits for the search region, as well as initial guesses, are provided by the author. Given the large-dimensional search, intelligently choosing or permanently setting initial values results in significant time savings.

%This script uses master3x3.m and simps.m to determine the probability
%matrix and overall unimolecular reaction rate from a set of integrated
%kinetics.
%Version 2: Implements more accurate P's, and invariant initial
%intensities.

%This is prepared so that master3x3.m can give feedback mid-method.
%nmasterpasses=0;
%tracker=0;
%global tracker nmasterpasses;

%FITTING PARAMETERS---
fitP = zeros(2,27);
%Starting values:
%par =   [rate   Pab   Pab   Pac   Pba   Pbb   Pbc   Pca   Pcb
Pcc   Iaa   Iab   Iac   Iba   Ibb   Ibc   Ica   Icb   Icc
uB   uC   CorAC CorBC CorCC CorAB CorBB CorCB]
fitP(1,:)= [0.0002   0.028844 0.70755   0.15115 0.52779   0.37895   0.28505
0.22295 0.3646 0.38939 -6050.0274 -4199.9985 -1520.0031 -2800.0526 -
7750.1463 -1710.0049 -3150.0061 -3599.9907 -1949.998 1.33 0.896 1.2695
1.1878   2.1318 1.2743 1.4721 2.2234];
max =   [1e-2   1   1   1   1   1   1   1   1   1   -
6050.0271   -4199.9985   -1519.9937 -2800.0353   -7750.1463   -1710.0049 -
3150.0046 -3599.962 -1950.025 1.33 0.896 5   5   5   5   5   5];
min =   [1e-6   0   0   0   0   0   0   0   0   0   -
6050.0271   -4199.9985   -1519.9937 -2800.0353   -7750.1463   -1710.0049 -
3150.0046 -3599.962 -1950.025 1.33 0.896 0.5   0.5   0.5   0.5 0.5   1];
%--

%Use simps to fit the parameters listed above to the data in Volumes and
%times, within the error of QualValues.
[fitP(2,:), G] = simps('master3x3_paramore', fitP(1,:), (1:27), [], min, max,
Volumes, times, QualValues);

%Run those values through the master3x3 function to generate the data to

```
%plot the results of the fit above:
[f g out] = master3x3_paramore(fitP(2,:),Volumes,times,QualValues);

%Return the results:
disp(fitP(2,:));
figure(1);                                                      clf;
plot(out{1},out{2},'or',out{1},out{3},'r',out{1},out{4},'og',out{1},out{5},'g',out{1},
out{6},'ob',out{1},out{7},'b');
figure(2);                                                      clf;
plot(out{1},out{8},'or',out{1},out{9},'r',out{1},out{10},'og',out{1},out{11},'g',out{1
},out{12},'ob',out{1},out{13},'b');
figure(3);                                                      clf;
plot(out{1},out{14},'or',out{1},out{15},'r',out{1},out{16},'og',out{1},out{17},'g',out
{1},out{18},'ob',out{1},out{19},'b');
```
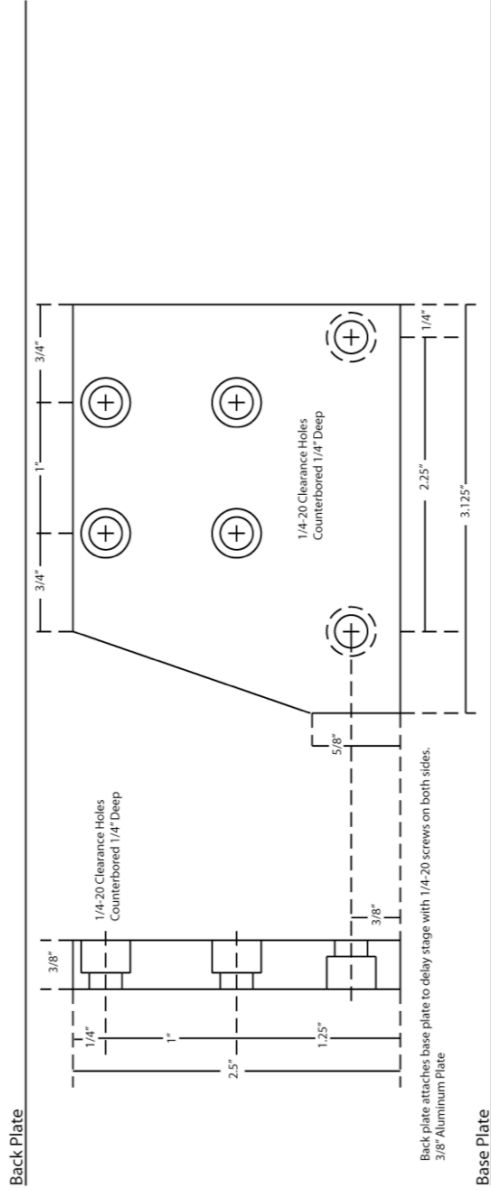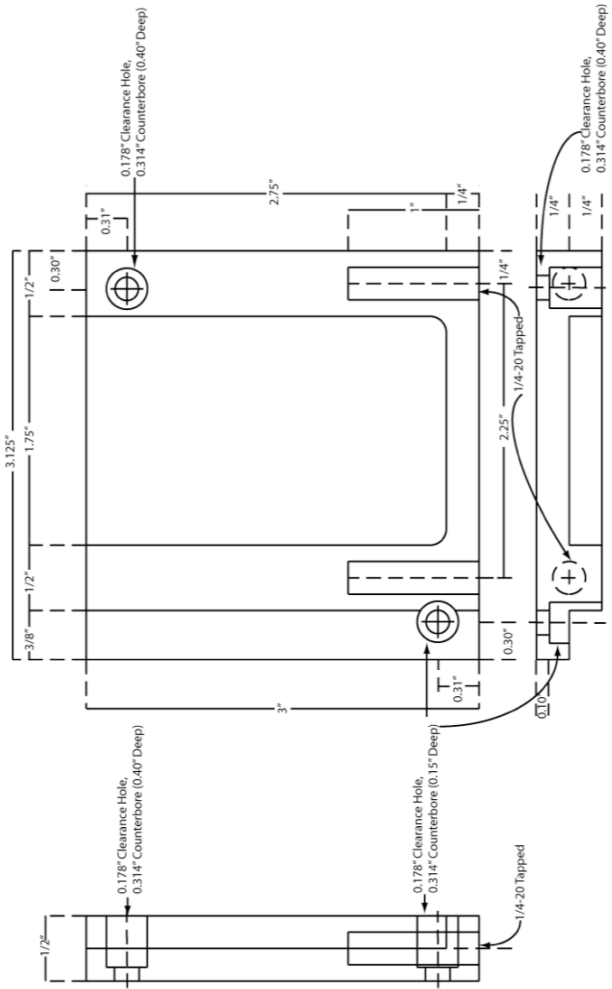
Appendix D   Machine drawings

Cryostat Mounting Bracket
Version 2

Material: Aluminum Plate

Adam Hill -- C.B. Harris Group, x2-6389
adhill@berkeley.edu